**Characterization of Butyrate Resistant Colorectal Cancer Spheroid Cells
and Its Response to Anticancer Drugs**

Kesara Nittayaboon

**A Thesis Submitted in Partial Fulfillment of the Requirements for the Degree of
Doctor of Philosophy in Biomedical Sciences
Prince of Songkla University
2023**

**Characterization of Butyrate Resistant Colorectal Cancer Spheroid Cells
and Its Response to Anticancer Drugs**

Kesara Nittayaboon

**A Thesis Submitted in Partial Fulfillment of the Requirements for the Degree of
Doctor of Philosophy in Biomedical Sciences
Prince of Songkla University
2023**

Thesis Title   Characterization of butyrate resistant colorectal cancer spheroid cells and its response to anticancer drugs

Author   Miss Kesara Nittayaboon

Major Program   Biomedical Sciences

Major Advisor

…………………………………

(Asst. Prof. Dr. Raphatphorn Navakanitworakul)

Examining Committee:

……………………………Chairperson

(Asst. Prof. Dr. Damratsamon Surangkul)

…………………………….Committee

(Dr. Kriengsak Lirdprapamongkol)

…………………………….Committee

(Prof. Dr. Surasak Sangkhathat)

…………………………….Committee

(Asst. Prof. Dr. Pasarat Khongkow)

……………………………Committee

(Asst. Prof. Dr. Raphatphorn Navakanitworakul)

The Graduate School, Prince of Songkla University, has approved this thesis as partial fulfillment of the requirements for the Doctor of Philosophy Degree in Biomedical Sciences

………………………………………

(Asst. Prof. Dr. Thakerng Wongsirichot)

Acting Dean of Graduate School

This is to certify that the work here submitted is the result of the candidate's own investigations. Due acknowledgement has been made of any assistance received.

....Signature

(Asst. Prof. Dr. Raphatphorn Navakanitworakul)

Major Advisor

....Signature

(Miss Kesara Nittayaboon)

Candidate

I hereby certify that this work has not been accepted in substance for any degree, and is not being currently submitted in candidature for any degree.

....Signature

(Miss Kesara Nittayaboon)

Candidate

ชื่อวิทยานิพนธ์	Characterization of butyrate resistant colorectal cancer spheroid cells and its response to anticancer drugs
ผู้เขียน	นางสาวเกศรา นิตยบูรณ์
สาขาวิชา	ชีวเวชศาสตร์
ปีการศึกษา	2565

บทคัดย่อ

        โรคมะเร็งลำไส้ใหญ่และไส้ตรง เป็นโรคมะเร็งที่พบได้ทั่วโลก รวมถึงประเทศไทย ปัจจัยเสี่ยงที่ทำให้เกิดโรคมีหลายปัจจัย โดยปัจจัยหลักที่ก่อให้เกิดมะเร็งลำไส้ คือ จุลินทรีย์ในลำไส้ ซึ่งจุลินทรีย์ในลำไส้มีบทบาทสำคัญต่อระบบนิเวศภายในลำไส้ ทั้งในด้านการรักษาความสมดุลภายในลำไส้ และการก่อให้เกิดการดำเนินของโรคมะเร็งลำไส้ บิวทิเรต เป็นกรดไขมันสายสั้น ผลิตจากจุลินทรีย์ในลำไส้ มีคุณสมบัติเป็นสารต้านมะเร็ง โดยบิวทิเรตสามารถยับยั้งการเจริญของเซลล์และกระตุ้นให้เซลล์เกิดการตายแบบอะพอพโทสิส อย่างไรก็ตาม การศึกษาการเปลี่ยนแปลงของจุลินทรีย์ในลำไส้พบว่า ผู้ป่วยมะเร็งลำไส้ที่มีภาวะดื้อต่อการรักษาด้วยยาเคมีบำบัดมีความชุกของจุลินทรีย์ที่สร้างบิวทิเรตในปริมาณสูง เมื่อเปรียบเทียบกับกลุ่มควบคุม เป็นที่น่าสนใจว่า สารบิวทิเรตอาจจะมีส่วนเกี่ยวข้องกับการเกิดมะเร็งลำไส้ และภาวะดื้อต่อการรักษาด้วยยาเคมีบำบัด การศึกษาในครั้งนี้ ผู้วิจัยได้ศึกษาลักษณะของเซลล์มะเร็งลำไส้ที่ถูกชักนำให้เกิดภาวะดื้อต่อสารบิวทิเรต เพื่อจำลองสภาวะการเกิดภาวะดื้อต่อสารบิวทิเรตภายในลำไส้ โดยใช้เซลล์มะเร็งลำไส้จำนวน 2 ชนิด คือ HCT-116 และ PMF-Ko14 นำมาบ่มด้วยสารบิวทิเรต ที่ความเข้มข้นสุดท้ายเป็น 3.2 mM เมื่อได้เซลล์ที่ดื้อต่อสารบิวทิเรต ทำการทดสอบเซลล์ดังกล่าวในแง่ของกลไกการเกิดภาวะดื้อต่อบิวทิเรต ได้แก่ การแสดงออกของยีนที่เกี่ยวข้องกับการนำสารเข้าและออกจากเซลล์ ซึ่งผลการทดสอบพบว่า เซลล์ที่ดื้อต่อสารบิวทิเรต (BR cell) มีการแสดงออกของยีนที่เกี่ยวข้องกับการนำสารเข้าและออกจากเซลล์เพิ่มขึ้น เมื่อเปรียบเทียบกับเซลล์ตั้งต้น (PT cell) นอกจากนั้น ผลของการวิเคราะห์โปรตีนพบว่า มีการแสดงออกของโปรตีนที่แตกต่างกันในเซลล์ทั้งสองชนิด ซึ่งสามารถจัดกลุ่มและระบุเซลล์แต่ละชนิดออกจากกันได้ การศึกษาครั้งนี้ ใช้วิธีทดสอบการเคลื่อนที่ของเซลล์ เพื่อวิเคราะห์ความรุนแรงของเซลล์ อีกทั้งยังพบว่า BR cell มีการดื้อต่อยาเคมีบำบัดด้วย โดยเซลล์ HCT-BR มีภาวะดื้อต่อยาเมทฟอร์มิน (MET) และยา oxaliplatin ในขณะที่เซลล์

PMF-BR มีภาวะดื้อต่อยา 5-fluorouracil จากผลข้างต้น สามารถยืนยันได้ว่า เซลล์ที่เกิดภาวะดื้อต่อสารบิวทิเรต จะมีภาวะดื้อต่อยาเคมีบำบัดร่วมด้วย ซึ่งภาวะเช่นนี้ มีความสำคัญต่อการดำเนินของโรคมะเร็งลำไส้ ส่งผลให้ไม่ตอบสนองต่อการรักษาและการกลับเป็นซ้ำของโรคได้ ผู้วิจัยจึงได้ทดสอบความเป็นพิษต่อเซลล์ของยา MET โดยยา MET เป็นยารักษาโรคเบาหวาน แต่ได้มีการศึกษาถึงฤทธิ์ต้านมะเร็งในมะเร็งหลายชนิด โดยผู้วิจัยได้ศึกษาเซลล์มะเร็ง PMF-ko14 ที่มีสภาวะดื้อและไม่ดื้อต่อสารบิวทิเรต ในรูปแบบ 3D spheroid ซึ่งพบว่า MET สามารถลดขนาดของ spheroid ยับยั้งการเจริญ และการเคลื่อนที่ของเซลล์ได้ นอกจากนั้น MET กระตุ้นให้เซลล์เกิดการตายแบบอะพอพโทสิส ผ่านทางกลไก caspase 3/7 ผู้วิจัยยังได้ศึกษากลไกของ MET โดยพบว่า MET กระตุ้นวิถีสัญญาณ AMP-activated protein kinase (AMPK) และ AKT serine/threonine kinase 1(Akt) อีกทั้งยับยั้งวิถีสัญญาณ Acetyl-CoA-carboxylase (ACC) และ mammalian target of rapamycin (mTOR) ซึ่งทั้งสองวิถีสัญญาณส่งผลให้มีการกระตุ้นกลไก caspase 3/7 ส่งผลให้เซลล์เกิดการตายได้ การศึกษาในครั้งนี้ แสดงให้เห็นว่า MET มีฤทธิ์ในการต้านเซลล์มะเร็ง โดยเฉพาะอย่างยิ่งเซลล์มะเร็งที่เกิดภาวะดื้อต่อยาเคมีบำบัด การใช้ยา MET ร่วมกับการใช้ยาเคมีบำบัด อาจเป็นทางเลือกในการรักษาโรคมะเร็งลำไส้ได้

คำสำคัญ : เซลล์มะเร็งลำไส้; ภาวะดื้อต่อบิวทิเรต; ยาเมทฟอร์มิน; การเพาะเลี้ยงเซลล์แบบ 3 มิติ

Thesis title   Characterization of butyrate resistant colorectal cancer spheroid cells and its response to anticancer drugs

Author   Miss Kesara Nittayaboon

Major Program Biomedical Sciences

Academic Year 2022

ABSTRACT

Colorectal cancer (CRC) is the most common cancer worldwide, including Thailand. There are several risk factors for CRC, especially microbiome. Gut-microbiota plays a critical role in homeostasis and carcinogenesis. Butyrate, a short-chain fatty acid-producing by gut-microbiota, plays a role in intestinal homeostasis. Butyrate acts as anti-cancer agent by growth inhibition and apoptosis induction. However, microbiota study reveals that butyrate-producing bacteria were found in CRC patients more than normal and correlated to chemoresistance feature. We characterized the butyrate resistance (BR) CRC cells by treating the HCT-116 and PMF-ko14 cells line with a maximum butyrate concentration of 3.2 mM. The butyrate 50% inhibitory concentration (IC_{50}) were increase in BR cells. The butyrate resistance mechanism was investigated with butyrate influx, and drug efflux genes expression. The increasing of influx and efflux gene expression in BR cells were found comparing to parental (PT) cells. Proteomic analysis was used to distinguish the normal and butyrate-resistant phenotype. Cell migration was used to evaluate the aggressive behavior of BR cells. The analysis reveal that HCT-BR cell show lower migration rate; however, the PMF-BR cell show higher migration rate than their PT cell. The cross-resistance to anti-cancer drugs was elucidated. We found the cross-resistance of metformin (MET) and oxaliplatin in HCT cells, and 5-fluorouracil was cross-resistance in PMF cells. Our study suggests that acquisition of resistance to butyrate induces chemoresistance in CRC cells, which may play an important role in CRC development, treatment, and metastasis. Moreover, we would like to further investigate the cytotoxicity of MET, an anti-diabetic drug with an anti-cancer activity, on PMF-BR -CRC cells in a 3D spheroid culture model. The results demonstrated that MET decreases spheroid size, viability, migration. Meanwhile, MET increases spheroid death through caspase 3/7 activity. The

molecular mechanism from western blotting revealed that AMP-activated protein kinase (AMPK) and AKT serine/threonine kinase 1(Akt) were significantly upregulated in MET treatment group, whereas Acetyl-CoA-carboxylase (ACC) and mammalian target of rapamycin (mTOR) were downregulated. This situation leads to caspase activation and apoptosis. Our results confirm that MET show a potential cytotoxicity especially on the BR cells. This finding suggest that MET is an effective strategy for drug-resistant CRC cells.

Key word: Colorectal cancer cell; Butyrate resistance; Metformin; Spheroid

ACKNOWLEDGEMENT

CONTENTS

CONTENTS (Continue)

Content	**Page**
Appendices	

LIST OF TABLES

LIST OF FIGURES

LIST OF FIGURES (Continue)

LIST OF ABBREVIATIONS

3D-model	3-Dimentional model
5-FU	5-fluorouracil
ACC	Acetyl-CoA-carboxylase
AKT	AKT serine/threonine kinase
AMPK	AMP-activated protein kinase
bp	Base pair
BR cell	Butyrate-resistant cell
CRC	Colorectal cancer
FuOX	A combination of 5-fluorouracil and oxaliplatin
HBR	HCT-116 resistant cell
HCT-BR	HCT-116 resistant cell
HCT	HCT-116 parental cell
HCT-PT	HCT-116 parental cell
HDAC	Histone deacetylase
IC_{50}	50% inhibitory concentration
MET	Metformin
mM	Millimolar
mTOR	Mammalian target of rapamycin
MTT	3-[4,5-dimethylazol-2-yl]-2,5-diphenyltetrazolium bromide
Oxa	Oxaliplatin
PBR	PMF-ko14 resistant cell

LIST OF ABBREVIATIONS (Continue)

PMF-BR   PMF-ko14 resistant cell

PMF   PMF-ko14 parental cell

PMF-PT   PMF-ko14 parental cell

PT cell   Parental cell

qRT-PCR   Real-Time Quantitative Reverse Transcription PCR

SCFA   Short-chain fatty acids

SD   Standard deviation

LIST OF PUBLICATION

1. **Nittayaboon K**, Leetanaporn K, Sangkhathat S, Roytrakul S, Navakanitworakul R. Characterization of Butyrate-Resistant Colorectal Cancer Cell Lines and the Cytotoxicity of Anticancer Drugs against These Cells., BioMed Res. Int. 2022. https://doi.org/10.1155/2022/6565300

2. **Nittayaboon K**, Leetanaporn K, Sangkhathat S, Roytrakul S, Navakanitworakul R. Cytotoxic effect of metformin on butyrate-resistant PMF-K014 colorectal cancer spheroid cells. Biomed. Pharmacother. 2022(151). https://doi.org/10.1016/j.biopha.2022.11321

Reprints were made with permission from the publisher

30 June 2022

Dear Dr. Nittayaboon,

I am delighted to inform you that the review of your Research Article 6565300 titled Characterization of butyrate-resistant colorectal cancer cell lines and the cytotoxicity of anti-cancer drugs against these cells has been completed and your article has been accepted for publication in BioMed Research International.

Please visit the manuscript details page to review the editorial notes and any comments from external reviewers. If you have deposited your manuscript on a preprint server, now would be a good time to update it with the accepted version. If you have not deposited your manuscript on a preprint server, you are free to do so.

We will now check that all of your files are complete before passing them over to our production team for processing. We will let you know soon should we require any further information.
As an open access journal, publication of articles in BioMed Research International are associated with Article Processing Charges. If applicable, you will receive a separate communication from our Editorial office in relation to this shortly. In regards to payments, we will:

Only ever contact you from @hindawi.com email addresses. If you receive communications that claim to be from us, or one of our journals, but do not come from an @hindawi.com email address, please contact us directly at help@hindawi.com
Only ever request payment through our own invoicing system.Any email requesting payment will always be from an @hindawi.com email address and will always direct you to our invoicing system with a link beginning https://invoicing.hindawi.com

If you receive payment requests or information in ways other than this, or have any questions about Article Processing Charges, please contact us at help@hindawi.com.

Finally, we have partnered with leading author service providers to offer our authors discounts on a wide range of post-publication services (including videos, posters and more) to help you enhance the visibility and impact of your academic paper. Please visit our author services page to learn more.

Thank you for choosing to publish with BioMed Research International.

Kind regards,
Richard Tucker

Reprints were made with permission from the publisher

27 May 2022

Dear Dr Nittayaboon,

Thank you for publishing your article in Biomedicine & Pharmacotherapy.
Dr Navakanitworakul completed the Rights and Access Form for your article Cytotoxic effect of metformin on butyrate-resistant PMF-K014 colorectal cancer spheroid cells on May 27, 2022.

The Order Summary is attached to this email. A copy of the Order Summary is also sent to all co-authors for whom we have contact details.
Your article will be free for everyone to read online as soon as it is published.

If you have any questions, please do not hesitate to contact us. To help us assist you, please quote our article reference BIOPHA_113214 in all correspondence.

Now that your article has been accepted, you will want to maximize the impact of your work. Elsevier facilitates and encourages authors to share their article responsibly. To learn about the many ways in which you can share your article whilst respecting copyright, visit: www.elsevier.com/sharing-articles.

Kind regards,
Elsevier Researcher Support

CHAPTER 1

INTRODUCTION

Based on the GLOBOCAN 2020 data, Colorectal cancer (CRC) is one of most common cancer worldwide. CRC was ranking in the fourth with 1.8 million in new cancer case, and in the second with 935,000 cases of mortality (1,2). In Thailand, CRC is still a leading cause of cancer-associated death. It is the third rank of new case with 20,748 cases in both male and female. Moreover, 11,331 cases is account to mortality rate (3). Previous report on colon and rectum cancer prediction showed that the number of death case is increase due to the increasing of population and ageing. The early diagnosis and treatment improvement are the key factor to reduce mortality rate of CRC (4). Presently, CRC treatment is surgery and chemoradiotherapy. Conventional chemotherapy targets cells with rapidly dividing and is the main treatment strategy for improving the mortality rate of patients with CRC. In Thailand, a combination of 5-fluorouracil (5-FU) and oxaliplatin (Oxa) or FuOx is the major chemotherapeutic treatment for CRC (5). However, 90% of failures in the chemotherapy during the invasion and metastasis of cancers are related to drug resistance (6). The risk factors of CRC are genetic and epigenetic alteration, dietary and exercise behavior, including microbial diversity in our intestinal as shown in Figure 1 (7–9). The accumulation of genetic alteration in host and environmental factors play an important role to contribute cancer progression. The microbiota plays a critical role in intestinal homeostasis and carcinogenesis. Microbial metabolites maintain the intestinal barrier and immune homeostasis. There are multi-step process of carcinogenesis driving by the influence of the microbiome. Imbalance of normal flora and pathogenic bacteria leads to cancer development. (10–12).
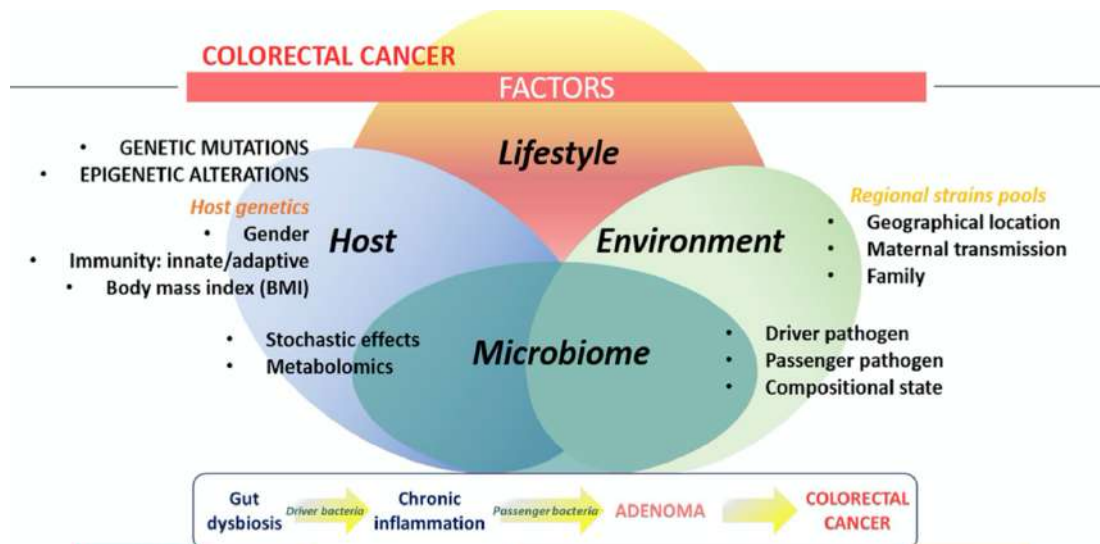
Figure 1. The figure illustrated a potential risk factor of colorectal cancer.

Butyrate is one of short-chain fatty acids (SCFAs) producing by human gut microbiota through fermentation of non-digestible carbohydrates. Butyrate plays an important role in homeostasis of gut. Butyrate at low-to-moderate concentration, which are present near the base of colonic crypts, are readily metabolized in the mitochondria to stimulate cell proliferation as an energy source. On the other hands, higher concentrations of butyrate presenting near the lumen exceed the metabolic capacity of the colonocyte. Unmetabolized butyrate enters to the nucleus and functions as a histone deacetylase (HDAC) inhibitor that epigenetically regulates gene expression to inhibit cell proliferation and induce apoptosis as the colonocytes exfoliate into the lumen (13). Additionally, glucose and aerobic glycolysis have been used for energy production instead of butyrate resulting in accumulation of butyrate in nucleus of the cancerous colonocyte. Then, butyrate competitively binds to the zinc sites of class I and II HDACs. This binding affects hyperacetylation of histones, resulting in a modified DNA conformation, which subsequently leads to the uncoiling or relaxing of chromatin leading to apoptosis of cancerous cells (14). Figure 2 show a mechanism of butyrate on normal and cancerous colonocyte.
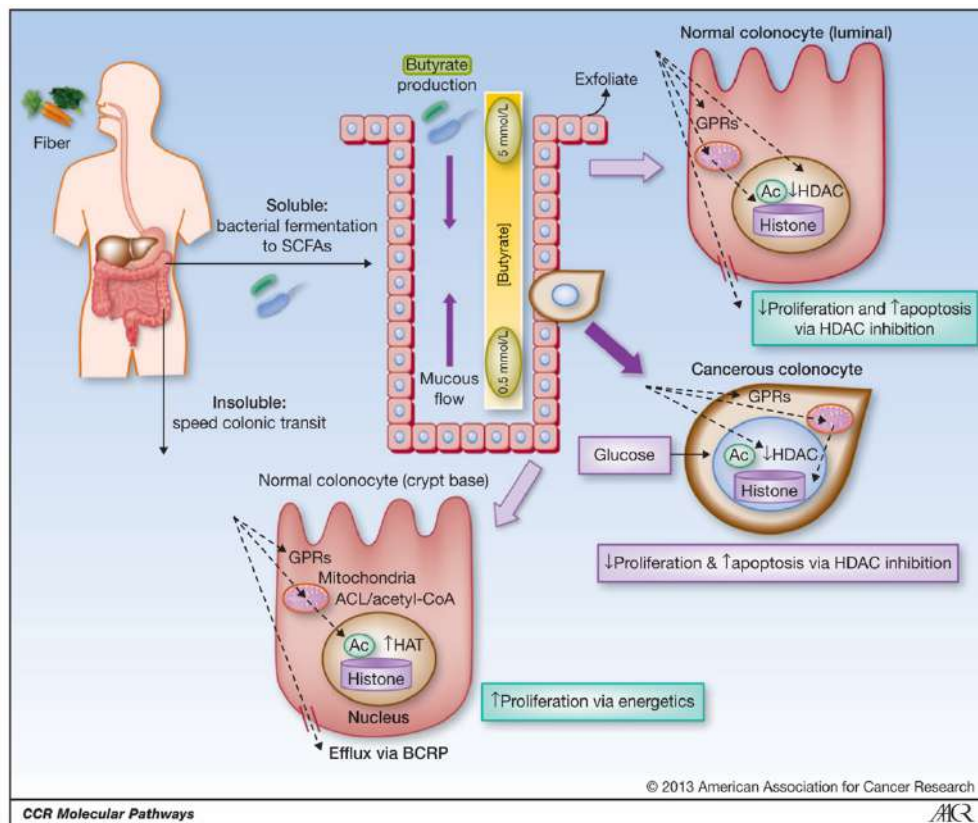
Figure 2. The action of butyrate on homeostasis. Butyrate at low-to-moderate concentration promote cell proliferation in normal colonocyte at base crypt. Butyrate at high concentration induce apoptosis in normal colonocyte at luminal site and cancerous colonocyte (13).

Butyrate also shows a controversy effect in CRC patients. On one hand, butyrate induces cancer cell to apoptosis. However, the microbiota study found that butyrate producing and inflammatory bacteria is higher in CRC patients than normal population (7). Long-term exposure of butyrate may transform cancer cell into butyrate-resistant cancer cell (BR cell) (15). The BR cells showed a malignant phenotype such as a survival in stress environment including glucose deprivation, and heat shock condition. Moreover, this BR cell has been considered as chemo-resistant cell which leading to treatment failure and cancer relapse (16,17).

In general, AMP-activated protein kinase (AMPK) is a crucial regulator for balancing energy supply and maintaining homeostasis, ultimately prevent cells from

stressful situations. AMPK is a metabolic sensor for various anabolic and catabolic signaling pathways (18). AMPK was induced by adiponectin and LKB1 signaling pathway resulting in phosphorylation and mTOR inhibition. The mTOR control various cancer cell activities including cell proliferation and invasion. Inhibition of mTOR leading to inhibit cell proliferation and invasion (19). Previous report suggested AMPK-activation drug or compound can sensitize these BR cells (20). Therefore, AMPK activation drugs seem to be a good candidate for CRC with BR cells. Metformin (MET) is one of anti-diabetic drugs with AMPK activation effect.

MET inhibits complex I (NADPH: ubiquinone oxidoreductase) of the mitochondrial respiratory chain, thereby increasing the cellular AMP to ATP ratio and leading to activation of AMPK and regulating AMPK-mediated transcription of target genes. This eventually prevents hepatic gluconeogenesis, enhances insulin sensitivity and fatty acid oxidation, and ultimately leads to a decrease in glucose levels. The drug show ability to decrease plasma insulin, reduce insulin resistance, and lower levels of circulating glucose in patients with type II DM (21). Previous retrospective study suggested that MET used is associated with lower cancer incidence in diabetic patients with endometrial, cervical, and lung cancer (22–24). MET showed a decreasing of brain tumor invasion through increasing of adhesion collagen (25). In CRC studies, MET is associated with metastasis inhibition in vivo and lower mortality rate in patients (26,27). Molecular mechanism of MET including growth and proliferation inhibition, migration and invasion suppression, and apoptosis induction. There are several actions of MET, for instant, activation of AMPK and caspase activity and downregulation of mTOR and Akt (25,28,29). Moreover, *in vitro* model shows an improvement of MET on chemotherapy (30–32). This information suggested the potential anticancer effect of MET. Figure 3 shows molecular mechanism of MET on cancer.
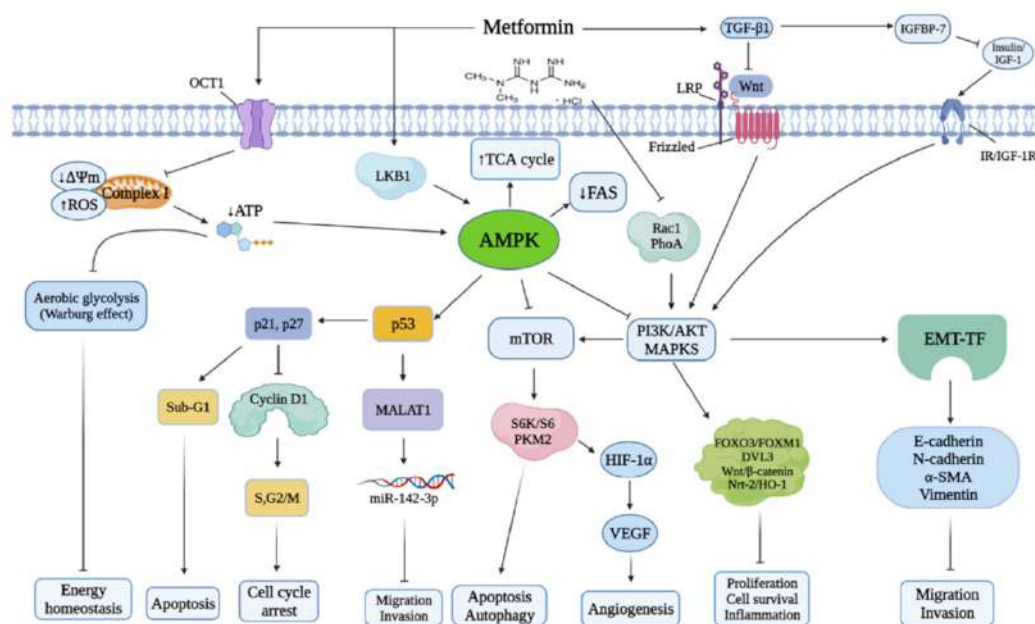
Figure 3. Molecular mechanisms of MET in cancer. MET generally modulates AMPK activation through mitochondria complex I inhibition and LKB1 leading to activates or inactivates downstream signaling target, including p21, p53, mTOR, PI3K/Akt, MAPKs. The activation or inactivation of these pathway resulting in inhibition of tumorigenesis, cell survival, migration, and invasion (Adapted from 28).

Taken together, we proposed the hypothesis that long-time-exposure of butyrate in CRC leads to butyrate-resistant phenotype or butyrate-resistant cell (BR cell) resulting in chemoresistant feature. To overcome their resistance to chemotherapy, we hypothesized that MET would show a potential cytotoxicity and therapeutic effect on those BR cell.

CHAPTER 2

OBJECTIVES

Part 1 Butyrate-resistant cell establishment and characterization

1. To establish butyrate-resistant (BR) cell lines using HCT-116 and PMF-ko14 colorectal cancer cells
2. To characterize the BR cells in view of cell morphology, butyrate sensitivity, expression of butyrate- and drug efflux-related genes, and migration rate.
3. To investigate the anti-cancer drug response of parental (PT) and BR cells.

Part 2 The effect of MET on BR spheroid cells

1. To construct spheroid model on PMF-PT and PMF-BR for anti-cancer drug response.
2. To determine the cytotoxic effect of MET on PMF spheroids.

CHAPTER 3

RESULTS AND DISCUSSION

Scope of study
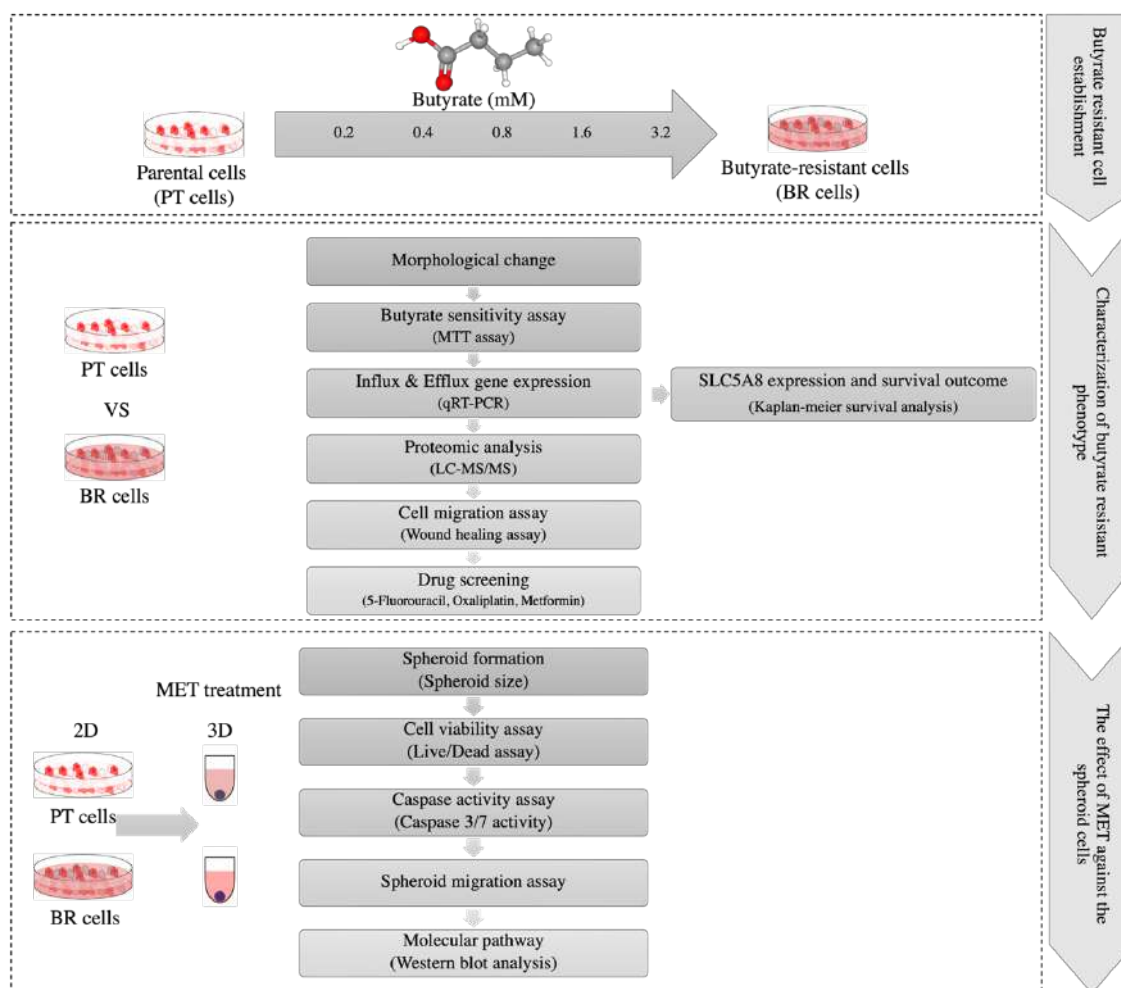
Figure 4. Research workflow.

Two types of colorectal cancer cells including HCT-116 and PMF-Ko14 were induced with Sodium butyrate. The characteristic of parental and butyrate-resistant cell (PT and BR cell) was investigated. Cell morphology was captured by inverted microscope. Butyrate sensitivity was determined by 3-[4,5-dimethylazol-2-yl]-2,5-diphenyltetrazolium bromide (MTT) assay. The expression of butyrate influx- and drug efflux- related genes were evaluated by Quantitative Reverse-Transcription polymerase chain reaction (qRT-PCR) and proteomic analysis were performed to determine their

difference. The aggressiveness of PT and BR cells were determined by wound healing assay and the anti-cancer drugs screening were evaluated by MTT assay. Next, spheroid formation was used as a 3-Dimentional (3D) model to investigate the drug testing. The cytotoxicity of MET was evaluated in term of spheroid formation, spheroid viability, and caspase activity. We firstly evaluated the effect of MET on spheroid size. Then, spheroid cell viability was evaluated by Live/dead assay. Caspase 3/7 activity were determined by Apo-live Glo assay kit. The aggressiveness of spheroid was evaluated by spheroid migration. Then, the expression level of protein in molecular pathway of spheroid were investigated after MET testing. The scope of study was shown in figure 4.

Part 1 Butyrate-resistant cell establishment and characterization

1. The difference of cellular morphology in PT and BR cells.

Colorectal cancer cell lines including HCT-116 and PMF-ko14 (PT cells) were used to established butyrate-resistant cells (BR cells) as HCT-BR and PMF-BR cells, respectively. The cells were exposed to butyrate for three months in a stepwise procedure up to 3.2 mM. Cell morphology of PT and BR cells were capture by inverted light microscope. Figure 5 showed a micrograph with a slightly difference between PT and BR cells. The HCT-116 show a sharp-point morphology, while HCT-BR show more rounded and expanded (16). The PMF-ko14 represent a polygonal epithelial cell structure with robust cell-to-cell interaction, while PMF-BR cell show a decreasing of cell-to-cell interaction. Both BR cells also showed the increasing of vacoularization and cellular volume. The results correlated to previous study in colorectal adenocarcinoma cell line; BCS-TC2.BR2 cell was showed an increasing of cellular volume and vacuolization (34).
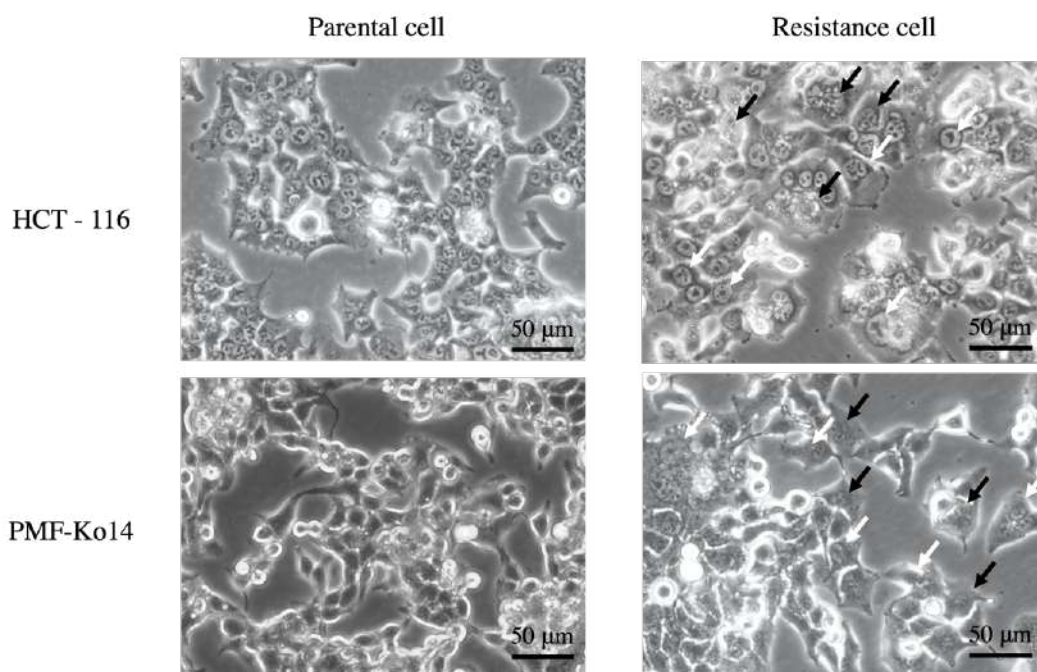
Figure 5. Micrographs represent HCT-116 and PMF-ko14 cell lines and their BR cells. Morphology of the cells were captured by inverted light microscope. The increasing of vacoularization (black arrow) and cellular volume (white arrow) werw observed as indicated in the picture. Scale bar = 50 μm

2. Butyrate sensitivity assay

Butyrate sensitivity of PT and BR cells were conducted by MTT assay. Cells were seeded in 96 well plate, then various concentration of butyrate was added. After 72 hours of incubation, MTT assay were performed. Formazan absorbance were detected by microplate spectrometer (SpectraMax 190, Molecular devices, San Jose, USA). The absorbance was analyzed by SoftMax Pro software (Version 2.2.1). The results are compared to control group and represented as the percentage of cell viability. Then, the 50% inhibitory concentration (IC_{50}) were calculated to evaluate the sensitivity of butyrate. The percentage of cell viability of PT and BR cells were shown in figure 6. The percent cell viability of BR cells was significantly higher than the PT cells. The results suggest that BR cells exhibit more resistant phenotype than those PT cells. Table 1 shows the IC_{50} value of the cells. The IC_{50} value of BR cells showed a significantly

higher than the PT cells. HCT-BR showed 5.38-fold higher than HCT-PT cell; similarly, PMF-BR showed 3.00-fold higher than PMF-PT cell. Previous studies on butyrate resistance cells showed that various colorectal cancer cell developed a resistance phenotype after chronic exposure of butyrate resulting in inferior response of anticancer drugs (20).
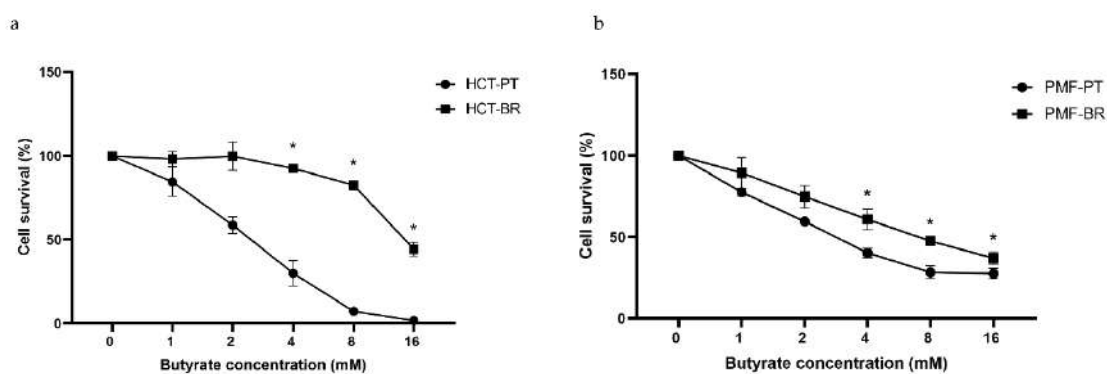
Figure 6. The percentage of cell survival of PT and BR cells from MTT assay.

Table 1. The IC$_{50}$ values of butyrate in PT and BR cells

Cell lines	Butyrate (mM, mean ± SD)	Fold	p-value (t-Test)
HCT-PT	2.76 ± 0.05	5.38	< 0.01
HCT-BR	14.85 ± 0.67		
PMF-PT	6.57 ± 0.80	3.00	< 0.01
PMF-BR	19.72 ± 1.62		

3. The butyrate-related and drug efflux pump gene expression

The expression of butyrate-related and drug efflux genes was evaluated by Quantitative Reverse-Transcription polymerase chain reaction (qRT-PCR). Table 2 showed a list of primers in our experiment. The relative expression of each gene was determined using an internal control; *GAPDH*. Figure 7 showed relative expression of *GPR109A*, a butyrate receptor, *GPR109B* the homolog of *GPR109A*, and *SLC5A8*, a sodium-couplet monocarboxylate transporter 1. The results showed significantly higher of *SLC5A8* in HCT-BR cell. In the same way, PMF-BR cell show a significantly higher of *GPR109A, GPR109B*, and *SLC5A8* than in PMF-PT cell. We also analyzed the correlation between butyrate-related gene expression and survival outcome of cancer patients with 5-FU and/or Oxa treatment using Kaplan-Meier survival analysis. The results showed in figure 8. We found the significantly correlated of *SLC5A8* gene expression and colorectal cancer patients. The result strongly suggests that high level of *SLC5A8* expression correlated with poor outcome in CRC patients. For the drug efflux genes, the expression level of each cell showed in figure 9. We found the difference expression pattern between two BR cells. The expression of *ABC-A5, ABC-C2,* and *ABC-C5* were found in both BR cells. The *ABC-B1, ABC-B6,* and ABC-F2 showed higher expression in HCT-BR cells, whereas PMF-BR cells showed higher expression of *ABC-C1, ABC-C3,* and *ABC-G2*. However, the expression of *ABC-B6* was not clear. Previous publication in chemoresistance-driving gene proposed that *ABC-C1* and *ABC-G2* are upregulated in Hep2-5-FU resistance cell (35). Paclitaxel-resistance cell show a higher level of *ABC-B6, ABC-C1, ABC-C3, ABC-C5, ABC-C10,* and *ABC-F2* (36). Moreover, in a doxorubicin-resistance cells showed the overexpression of ABC-C1 and ABC-F2 (37,38). The results suggested that the BR cells expressed more butyrate receptors and drug efflux to maintain their viability. Consequently, the BR cells with a higher expression of the genes may contribute to cell survival and drug resistance phenotypes. The mechanism of butyrate resistance was proposed in Figure 10.

Table 2. Primer sequences used for butyrate receptors and drug efflux pumps

Name	Sequence (5'-3')	Size (bp)	Note
GAPDH-F	ACG GAT TTG GTC GTA TTG G	207	Housekeeping gene
GAPDH-R	GGA AGA TGG TGA TGG GAT TT		
GPR109A-F	GGA CAA CTA TGT GAG GCG TTG G	650	Butyrate receptors
GPR109A-R	GGG CTG GAG AAG TAG TAC ACC		
GPR109B-F	CGT GAT GGA CTA CTA TGT GCG	280	
GPR109B-R	ATT TGC AGG GCC ATT CTG GAT		
SLC5A8-F	GGG TGG TCT GCA CAT TCT ACT	351	
SLC5A8-R	GCC CAC AAG GTT GAC ATA GAG		
ABC-A5-F	ATC ATG TGA GGC TGC TCA G	149	Drug efflux pumps
ABC-A5-R	ACA ACA GCA GTT TCT CCC ATA		
ABC-B1-F	GAA ACC AAC TGT CAG TGT ATT TTC	110	
ABC-B1-R	AGA GGA AGT CCA GCC CC		
ABC-B6-F	CCT GGT GTT CAA TGT CAT CC	168	
ABC-B6-R	CAT AGC ACG ACG AAA CTT GG		
ABC-C1-F	TCA GCC AGA AAA TCC TCC AC	196	
ABC-C1-R	GGC ACC ATG AGG ACC ATC		
ABC-C2-F	TCC TGG TTG ATG AAG GCT C	186	
ABC-C2-R	CAG TGA ATA AGA GGA TTG CAC A		
ABC-C3-F	GCC ACC CTG CTG ATA CAG T	141	
ABC-C3-R	AGA TCT CAC CCT CTG CCT TG		
ABC-C5-F	TGA GGG AGA GAA CCA GCA CT	229	
ABC-C5-R	AAG TAG TCC GGA TGG GCT TC		
ABC-F2-F	GTC TCC CAT TCC CAG GAT TT	182	
ABC-F2-R	CTG ATC TTG CTC CCA GTG AA		
ABC-G2-F	AGC AGC AGG TCA GAG TGT GG	280	
ABC-G2-R	GAT CGA TGC CCT GCT TTA CC		
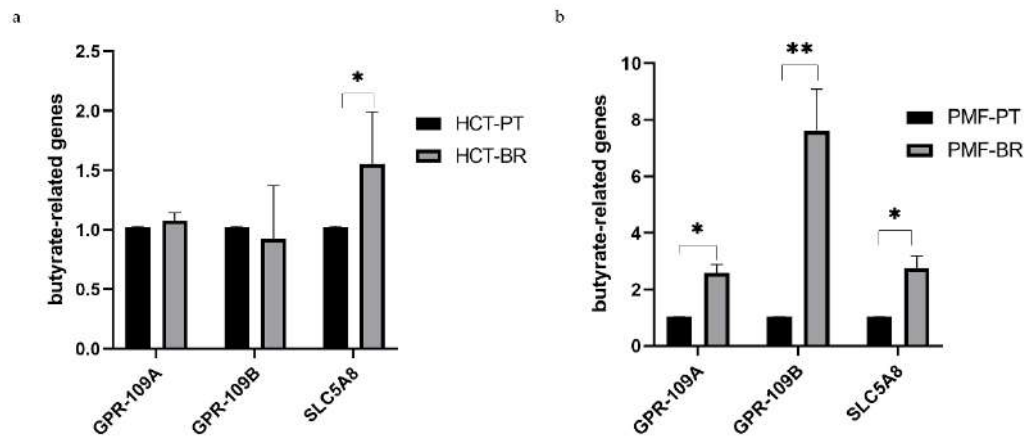
Figure 7. Butyrate-related gene relative expression of HCT (a) and PMF (b) cells. All genes are relative to *GAPDH*. The results are showed in a triplicated experiment with means ± SD. A Student's *t*-test was used to identify the statistically significant difference (* *p*-value < 0.05, ** *p*-value < 0.01).
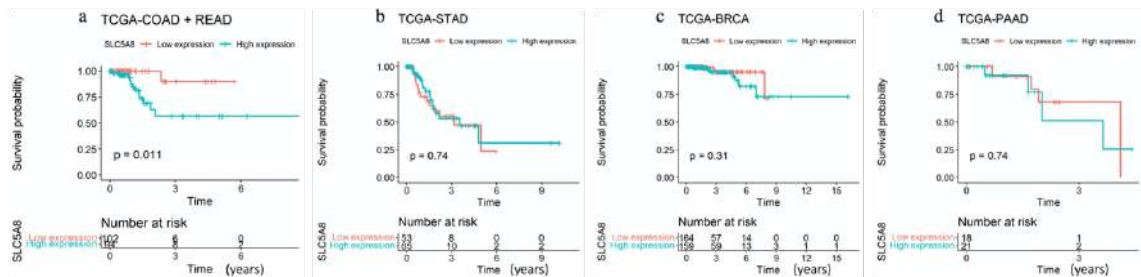
Figure 8. Kaplan-Meier survival analysis of cancer patients who treated with 5-FU, Oxa and Met. The survival probability curve of SLC5A8 gene expression in various cancer types such as colon adenocarcinoma and rectum adenocarcinoma (a), stomach adenocarcinoma (b), breast invasive carcinoma (c), and pancreatic adenocarcinoma (d).
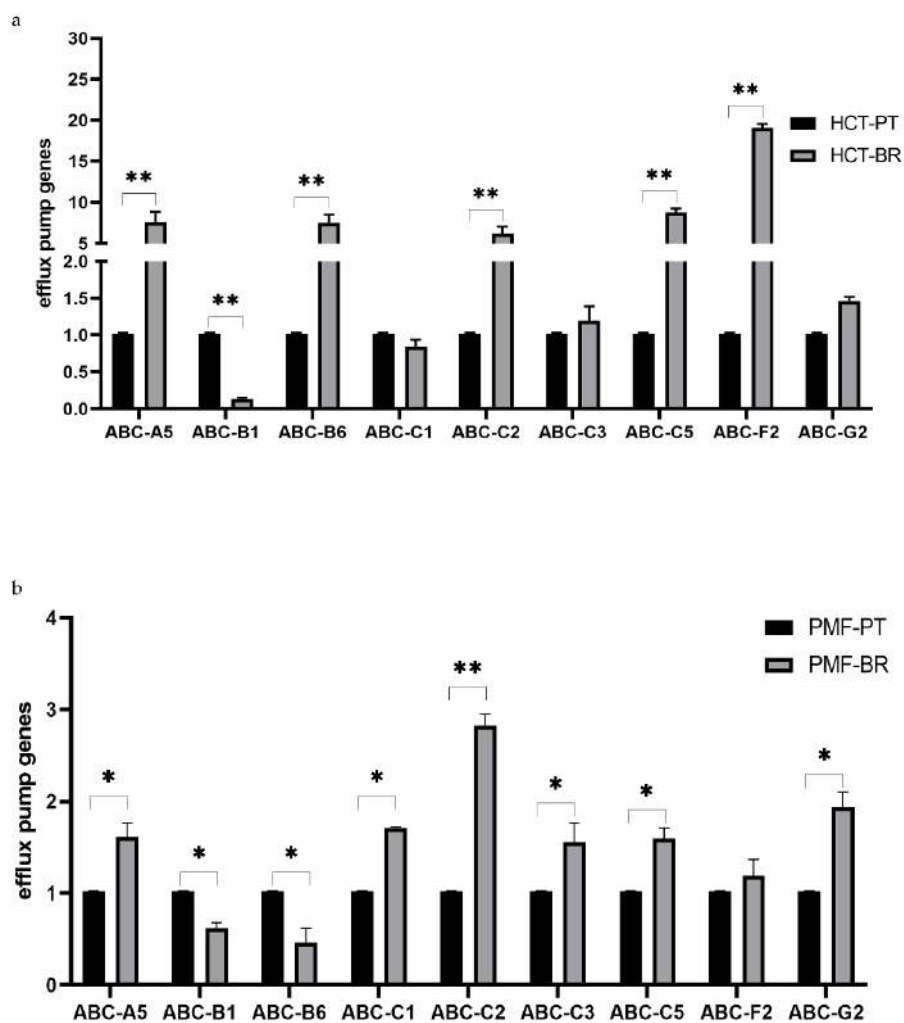
Figure 9. Drug efflux gene relative expression of HCT (a) and PMF (b) cells. All genes are relative to *GAPDH*. The results are showed in a triplicated experiment with means ± SD. A Student's *t*-test was used to identify the statistically significant difference (* *p*-value < 0.05, ** *p*-value < 0.01).
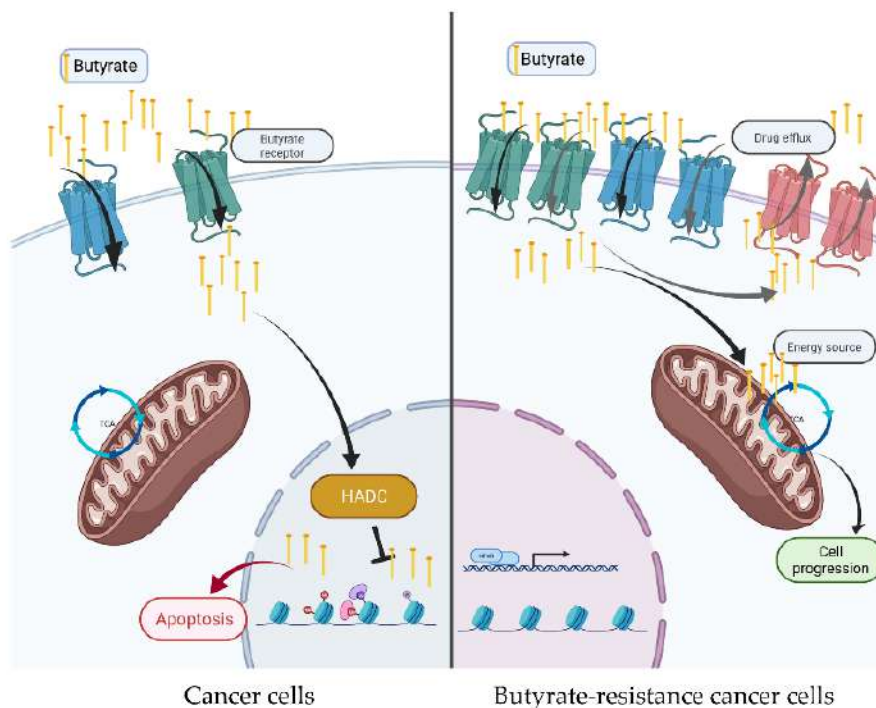
Figure 10. The proposed mechanism of butyrate-resistant cell development. Abbreviations: HDAC, histone deacetylase; TCA, tricarboxylic acid cycle. The schematic was created using BioRender.com.

4. The difference of protein pattern in PT and BR cells.

The characteristic of PT and BR cells were investigated by proteomic analysis. Figure 11 showed principal component analysis (PCA) of the cells. Proteome data showed that there is low dimensional variation among the cells. The unique proteins could be identified and distinguished PT and BR clusters in each cell types. The PC1 variation with 14.56% could be distinguished PMF-PT and PMF-BR; similarly, and PC2 variation with 11.86% could be distinguished HCT-PT and HCT-BR. The results suggest that there are some proteins sharing between PT and BR cells. We perform Venn diagram to confirm this finding. The Venn diagram illustrating the unique and share protein of each cell type showing in figure 12. The shared proteins are 90.60% (2,644 proteins) and 81.20% (2,285 proteins) in BR cell of HCT and PMF, respectively. We found that unique protein can be identified between PT and BR cells. In HCT cells, the unique proteins of PT cell showed 3.84% (112 proteins), while BR cell showed

5.56% (162 proteins). Additionally, there are 11.10% (313 proteins) unique protein of PMF-PT cell and 7.70% (217 proteins) unique proteins in PMF-BR cell. We further explored the differential protein expression in PT and BR cell from each cell were input. The bar graphs in figure 13 showed differential expression of protein and the gene listed in table 3 and 4 are top 10 upregulated and down regulated genes in HCT and PMF cells, respectively. Interestingly, the expression level of coatomer complex subunit beta 2 (COPB2) found to be decrease in both HCT-BR and PMF-BR cells. Previously, high expression of COPB2 has been reported to decrease overall survival in cancer patients including glioblastoma and hepatocellular carcinoma (39). According to UALCAN databased (University of Alabama at Birmingham cancer data analysis portal; http://ualcan.path.uab.edu/index.html), The COPB2 is related to vesicular budding and trafficking in Golgi apparatus. The COPB2 function in cancer showed in a controversial. Figure 14 represent the COPB2 expression in various type of cancer. We found the upregulation of the protein in tumor sample than in normal tissue. The protein expression showed higher in primary tumor of Colon cancer compared to normal. In contrast, the phosphorylation form of COPB2 is decreased in colon cancer stage comparing to normal. As a results, the function of COPB2 needs to be further addressed. We further investigated the biological processes of each cell. Figure 15 showed the biological process annotation pie chart. The results showed that HCT-BR and PMF-BR cells expressed the protein in response to stimulus which may imply to their response to butyrate. KEGG pathway enrichment were illustrated in figure 16. The bar graph showed that proteins in digestion and absorption, the phosphatidylinositol 3-kinase/Akt pathway, and pathways involved in cancers were enriched in PT cells. Meanwhile, the HCT-BR cell showed the enrichment of protein in homologous recombinant, mismatch repair, and DNA replication pathway. For the PMF-BR cell, adherent junction, cytokine, receptors, and protein in cancer were enriched.
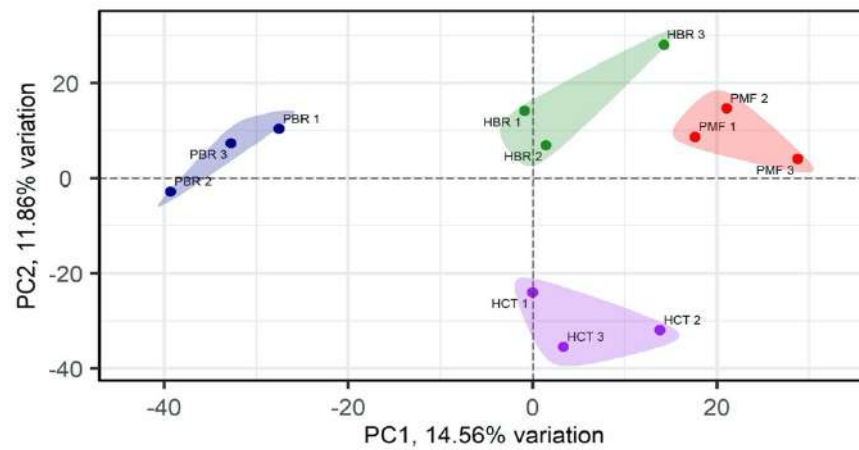
Figure 11. Proteomic data was plotted into Principal component analysis (PCA) using a biplot score of PC1 and PC2. The labeled dots and cell types as vectors for the parental (HCT and PMF) and resistant cells (HBR and PBR).
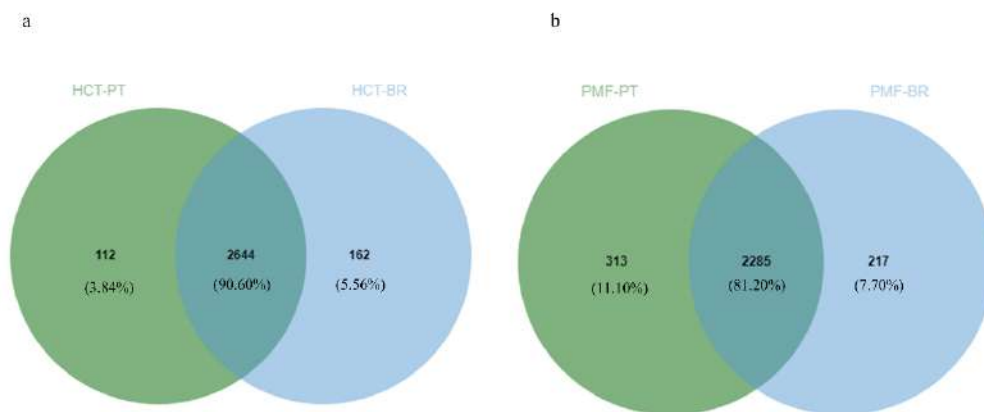
Figure 12. Venn diagram illustrating the relationship between HCT (a) and PMF (b) annotated genes.

(a)

(b)
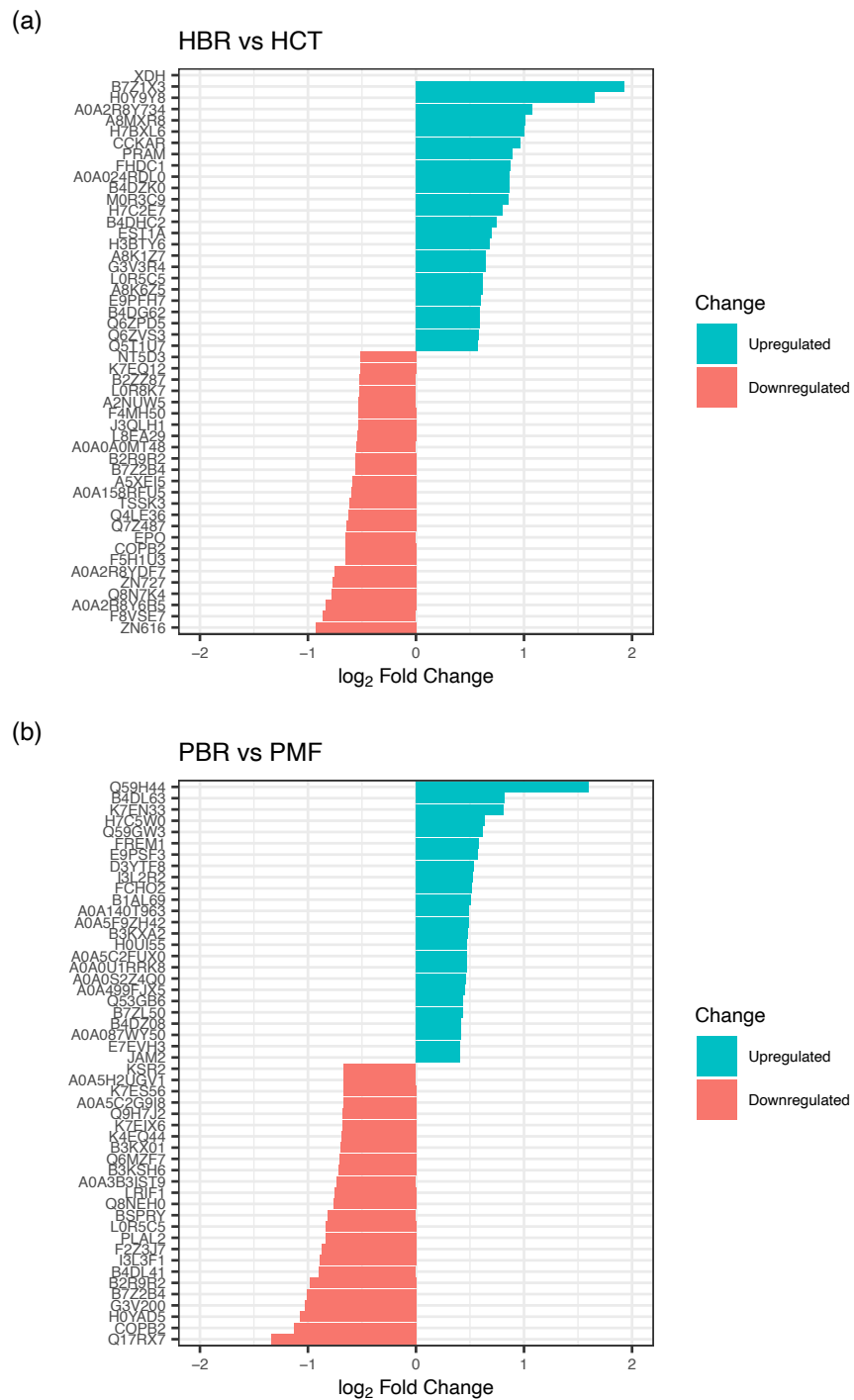
Figure 13. Bar graphs represent top 10 differential expression of proteins in HCT and PMF cells.
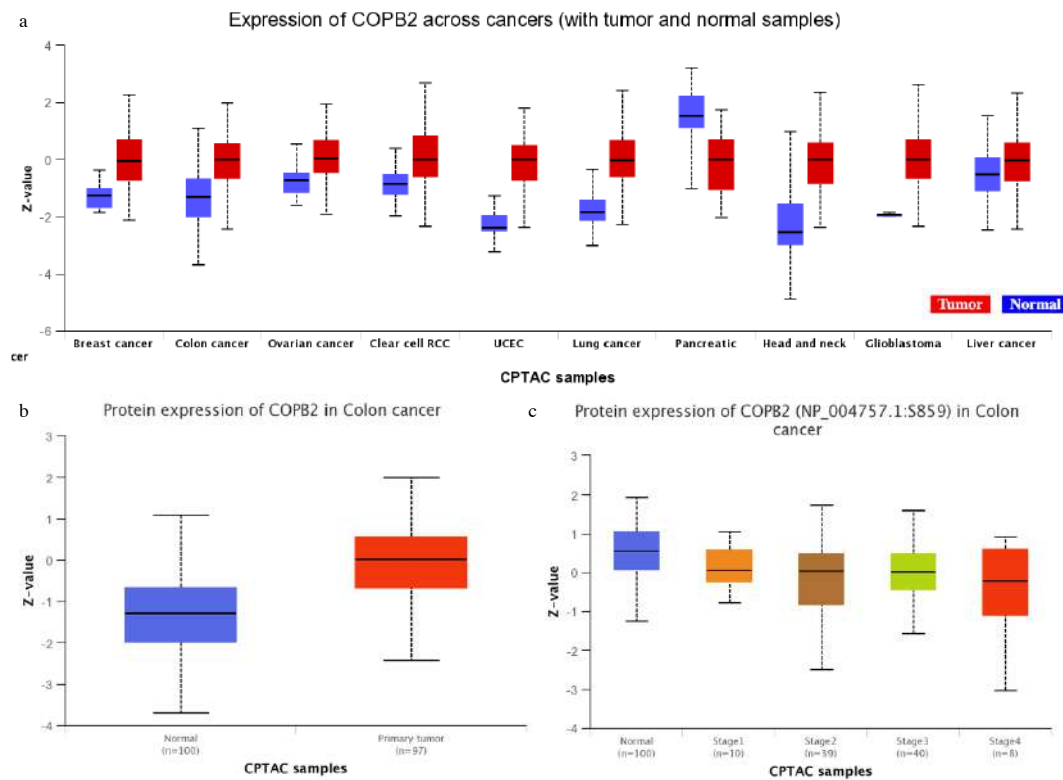
Figure 14. The expression level of COPB2 in various type of cancers. (a) COPB2 showed higher expression in cancer patients than normal tissue. (b) The expression of COPB2 in colorectal cancer comparing in normal and primary tumor. (c) The expression of phosphorylation form of COPB2 in each stage of cancer. Z-values represent standard deviations from the median across samples for the given cancer type.

Table 3. Top 10 upregulated and downregulated proteins in HCT cells.

HBR vs. HCT	ENTRY	Protein	Function
Up	XDH	Xanthine dehydrogenase/oxidase	Key enzyme in purine degradation.
	B7Z1X3	Dynein regulatory complex subunit 4	Microtubule binding, small GTPase binding
	H0Y9Y8	RUN and FYVE domain-containing protein 1	Binds phospholipid vesicles containing phosphatidylinositol 3-phosphate and participates in early endosomal trafficking.
	A0A2R8Y734	Thrombopoietin	Lineage-specific cytokine affecting the proliferation and maturation of megakaryocytes from their committed progenitor cells.
	A8MXR8	PHD finger protein 20-like protein 1	Regulation of transcription, DNA-templated.
	H7BXL6	Otogelin-like protein	Extracellular region.
	CCKAR	Cholecystokinin receptor type A	Receptor for cholecystokinin. Mediates pancreatic growth and enzyme secretion, and smooth muscle contraction of the gall bladder and stomach.
	PRAM	PML-RARA-regulated adapter molecule 1	Lipid binding, protein kinase binding, and integrin-mediated signaling pathway.
	FHDC1	FH2 domain-containing protein 1	Protein localization to plasma membrane
	A0A024RDL0	DNA-directed RNA polymerase III subunit RPC9	Microtubule-associated formin which regulates both actin and microtubule dynamics.
Down	Q7Z487	Transforming growth factor beta 1	DNA-directed 5'-3' RNA polymerase activity and nucleotide binding.
	EPO	Erythropoietin receptor	Growth factor activity.
	COPB2	Coatomer subunit beta'	Receptor for erythropoietin. Mediates erythropoietin-induced erythroblast proliferation and differentiation. Upon EPO stimulation, EPOR dimerizes triggering the JAK2/STAT5 signaling cascade.
	F5H1U3	Peptidylprolyl isomerase	The coatomer is a cytosolic protein complex that binds to dilysine motifs and reversibly associates with Golgi non-clathrin-coated vesicles, which further mediate biosynthetic protein transport from the ER, via the Golgi up to the trans Golgi network.

A0A2R8YDF7	Lysine-specific demethylase 4A	FK506 binding.
ZN727	Putative zinc finger protein 727	Heat shock protein binding.
Q8N7A4	cDNA FLJ25865 cis, clone CBR01927	Peptidyl-prolyl cis-trans isomerase activity.
A0A2R8Y6R5	Caseinolytic peptidase B protein homolog	Histone demethylase that specifically demethylates 'Lys-9' and 'Lys-36' residues of histone H3, thereby playing a central role in the histone code.
F8VSE7	Transcription factor E2F7	DNA-binding transcription factor activity, RNA polymerase II-specific.
ZN616	Zinc finger protein 616	Uncharacterized protein.

Abbreviations: HCT, HCT parental cells; HBR, butyrate resistant HCT cells.

Table 4. Top 10 upregulated and downregulated proteins in PMF cells.

PBR vs. PMF	ENTRY	Protein	Function
Up	Q59H44	Lymphocyte antigen 75 variant	Integral component of membrane
	B4DL63	cDNA FLJ51231, highly similar to Mitochondrial ornithine transporter 1	Integral component of membrane
	K7EN33	Notchless protein homolog 1	Plays a role in regulating Notch activity. Plays a role in regulating the expression of CDKN1A and several members of the Wnt pathway, probably via its effects on Notch activity.
	H7C5W0	DnaJ homolog subfamily B member 5	Chaperone binding, unfolded protein binding
	Q59GW3	ST8 alpha-N-acetyl-neuraminide alpha-2,8-sialyltransferase 3 variant	Sialyltransferase activity, protein glycosylation
	FREM1	FRAS1-related extracellular matrix protein 1	Extracellular matrix protein that plays a role in epidermal differentiation and is required for epidermal adhesion during embryonic development.
	E9PSF3	Bromodomain and PHD finger-containing protein 3	Metal ion binding
	D3YTF8	Thioredoxin-disulfide reductase	Protein has several cofactor bindings sites
	I3L2R2	Protein PIMREG	During mitosis, may play a role in the control of metaphase-to-anaphase transition.

	FCHO2	F-BAR domain only protein 2	Functions in an early step of clathrin-mediated endocytosis. Has both a membrane binding/bending activity and the ability to recruit proteins essential to the formation of functional clathrin-coated pits.
	PLAL2	Zinc finger protein PLAGL2	DNA-binding transcription activator activity, RNA polymerase II-specific, lipid metabolic process, positive regulation of intrinsic apoptotic signaling pathway
	F2Z3J7	Rab-like protein 2B	GTPase activity, GTP binding
	I3L3F1	Caspase recruitment domain-containing protein 14	Acts as a scaffolding protein that can activate the inflammatory transcription factor NF-kappa-B and p38/JNK MAP kinase signaling pathways.
	B4DL41	cDNA FLJ57825, highly similar to DNA-dependent protein kinase catalytic subunit	Kinase activity, Molecular function: Kinase, Transferase
Down	B2R9R2	cDNA, FLJ94517, highly similar to Homo sapiens baculoviral IAP repeat-containing 4 (BIRC4), mRNA	Metal ion binding
	B7Z2B4	cDNA FLJ53389, highly similar to Homo sapiens RAB GTPase activating protein 1 (RABGAP1), mRNA	GTPase activator activity
	G3V200	Liprin-alpha-2	Alters PTPRF cellular localization and induces PTPRF clustering. May regulate the disassembly of focal adhesions. May localize receptor-like tyrosine phosphatases type 2A at specific sites on the plasma membrane
	H0YAD5	Probable ATP-dependent RNA helicase DDX46	Protein predicted

COPB2	Coatomer subunit beta 2	The coatomer is a cytosolic protein complex that binds to dilysine motifs and reversibly associates with Golgi non-clathrin-coated vesicles, which further mediate biosynthetic protein transport from the ER, via the Golgi up to the trans Golgi network.
Q17RX7	Ras association (RalGDS/AF-6) domain family member 1	Intracellular signal transduction

Abbreviations: PMF, PMF parental cells; PBR, butyrate resistant PMF cells.

Figure 15. Pie chart illustrations the biological process of HCT-PT (a), HCT-BR (b), PMF-PT (c), and PMF-BR (d). HCT-PT, HCT parental cell, HCT-BR, butyrate-resistant HCT cell, PMF-PT, PMF parental cell; PMF-BR, butyrate-resistant PMF cell.

(a)

(b)
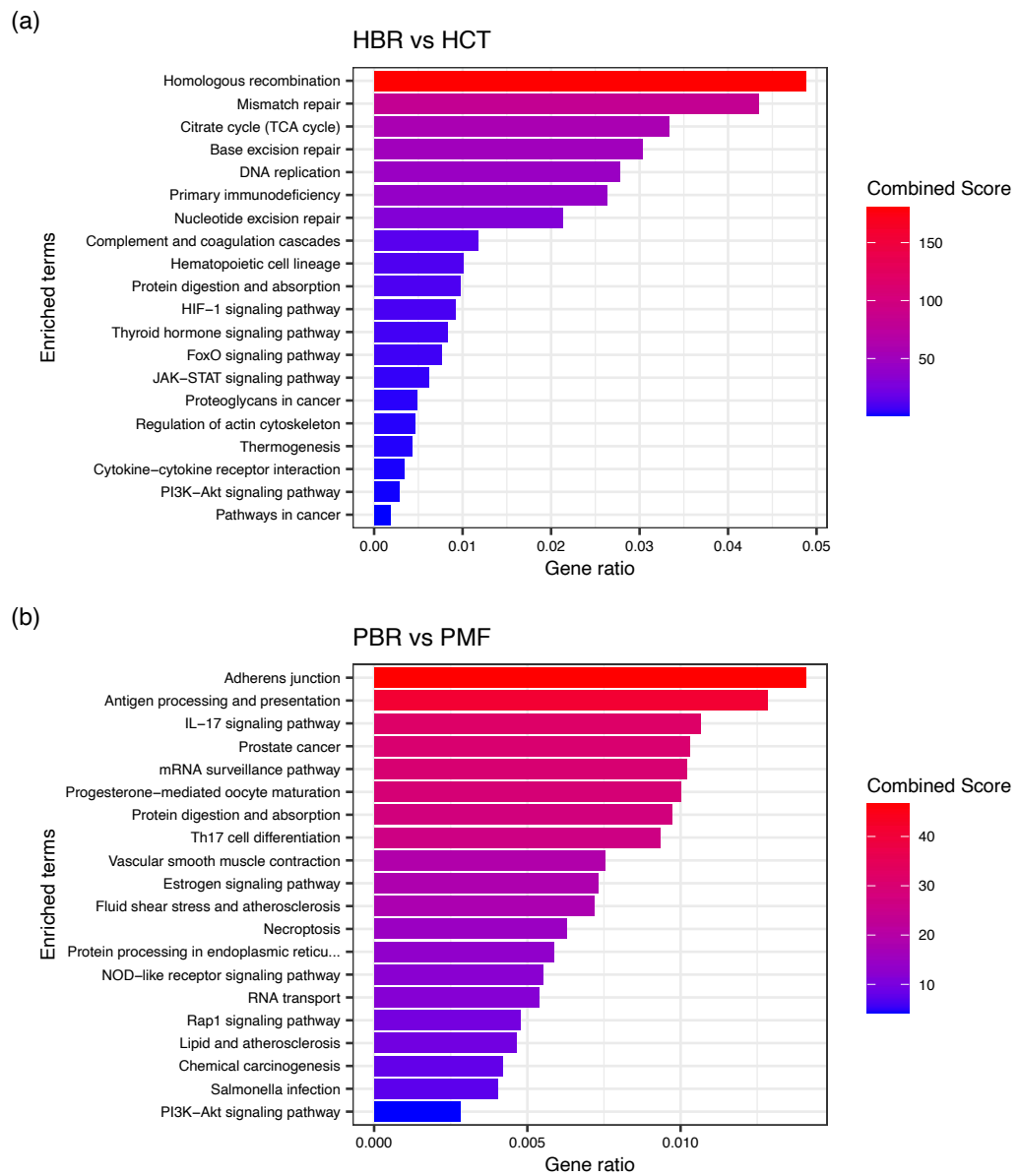
Figure 16. Bar graph showing top 20 KEGG pathway enrichment of HCT (a), and PMF (b) cells.

5. The migration capacity of PT and BR cells.

Wound healing assay were used to examine the migration capacity of PT and BR cells. The wound field were observed for 24 hours. Figure 17 showed cell migration of the cells. We found a significant difference of cell migration between cells. The migration rate of HCT cells is 45.18%, and 33.29% in HCT-PT, and HCT-BR cells, respectively. The HCT-BR cells showed significantly lower than HCT-PT cell. This may correlated to the down regulation of JAK2/STAT5 signaling pathway (40,41). On the contrary, the migration rate of PMF cell is 25.39% and 33.29% in PMF-PT, and PMF-BR, respectively. We found the significantly higher migration rate of PMF-BR cell. This result correlated to Notchless protein homolog 1 upregulation. This protein plays a role in Notch activity leading to cell migration and invasion in brain cancer (42).
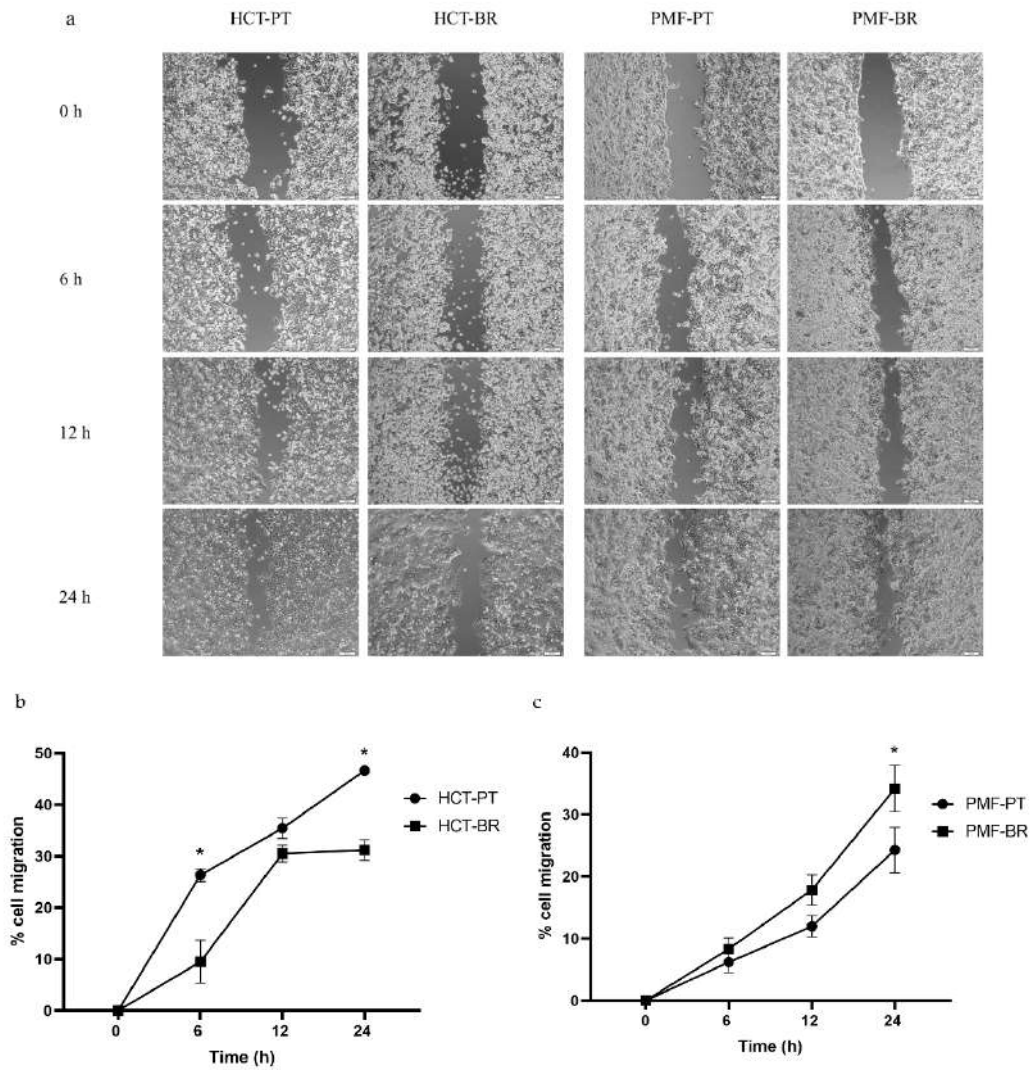
Figure 17. Micrograph illustration of cell migration capacity by wound healing assay. The cells were capture after 24 h wound field generation (a). The wound field were captured by inverted microscope with 10x magnification. Scale bar = 100 μm. Line graph represent the migration capacity (%) of HCT (b) and PMF (c) cells. Significant differences were determined using Student's *t*-test (*p*-value <0.05).

6. The sensitivity of anticancer drugs

To test the drugs sensitivity of PT and BR cells, MTT assay and IC_{50} were performed. We evaluated the IC_{50} then compared between PT and BR cells in each cell type. The results shown in table 5. We found the higher IC_{50} in BR cells. The HCT-BR cell showed 13.50-fold and 3.66-fold higher than HCT-PT against Oxaliplatin and MET, respectively. Likewise, PMF-BR cell showed 1.73-fold higher than PMF-PT cell against 5-Fluorouracil. The result suggested that butyrate-resistance phenotype correlated to chemotherapy resistance in BR cells. Consequently, the cross-resistance was found in the BR cells including Oxaliplatin and MET in HCT-BR cell, and 5-Fluorouracil in PMF-BR cell. From these results, we select PMF cells for further MET experiment. Previous studies on butyrate-resistance colon cancer cell also showed a cross-resistance of chemotherapy phenotype (16,20). Our results confirm the cross-resistance hypothesis.

Table 5. The cytotoxicity values (IC_{50}) of the anti-cancer agents against the HCT and PMF cell lines.

Cell lines	5-Fluorouracil (μM, mean ± SD)	Oxaliplatin (μM, mean ± SD)	Metformin (mM, mean ± SD)
HCT-PT	9.70 ± 0.09	2.13±0.13	1.75 ± 0.07
HCT-BR	9.45 ± 0.27	**28.76±3.43****	**6.41 ± 0.18****
PMF-PT	15.07 ± 1.74	28.15±3.90	1.67 ± 0.28
PMF-BR	**26.18 ± 4.37***	26.92±4.82	1.58 ± 0.15

* *p*-value < 0.05, ** *p*-value < 0.01

Part 2 The effect of MET on BR spheroid cells

7. Spheroid formation and characterization of spheroids.

Spheroid cells were grown in a poly-(2-hydroxyethyl methacrylate) or Poly-HEMA coated plate. First, stock solution with 120 mg/ml were prepared in 95% ethanol by stirring at a room temperature. A working solution with 5 mg/ml was then prepared in a same procedure. An aliquot of 20 μl was transfer into a single well of 96-well U-bottom plate, then the plates were dried in an incubator for 3 days. PMF cells were seeded into the plate to generate 200-300 μm spheroid cells.

The characterization of spheroid was evaluated including, spheroid morphology, CD44 and stemness gene expression. Initially, the morphology of spheroid was investigated. We found that both cells formed spheroids with a round-shape structure, compact morphology, and smooth surface. Our result correlated with previous results on BCS-TC2.BR2 colorectal cancer spheroids (34). The size of PMF-PT spheroids was slightly larger than that of PMF-BR spheroids (Figure 18A). The average diameter of the PT spheroid was 208.29 ± 7.94 μm, whereas that of the BR spheroid was 196.41 ± 9.43 μm. The stemness protein marker, CD44, was detected in both spheroid cells. We further investigated the stemness gene marker, including, *SOX2, OCY4, KLF4,* and *CXCR4* using qRT-PCR assay comparing between monolayer (2D) and spheroid (3D) cells. The expression level showed in figure 18 B and C. We found the significantly upregulated in stemness gene including SOX2 and OCT4 in both spheroid cells. The result correlated with previous study which showed the upregulation of stem cell marker in spheroid cell compared to their monolayer cell (43).

We further investigated the butyrate and 5-FU sensitivity of the spheroid cells. Butyrate and 5-Fluorouracil at various concentration were incubated, then IC_{50} value were determined using ApoLive-Glo assay. The results showed in figure 19. We found that the IC_{50} value of butyrate and 5-Fluorouracil in PMF-BR spheroid cell showed 2.7- and 2.65-fold higher than PMF-PT spheroid cell. The results suggested that PMF-BR spheroid cell still present a butyrate-resistance phenotype and cross-resistance to chemotherapy.
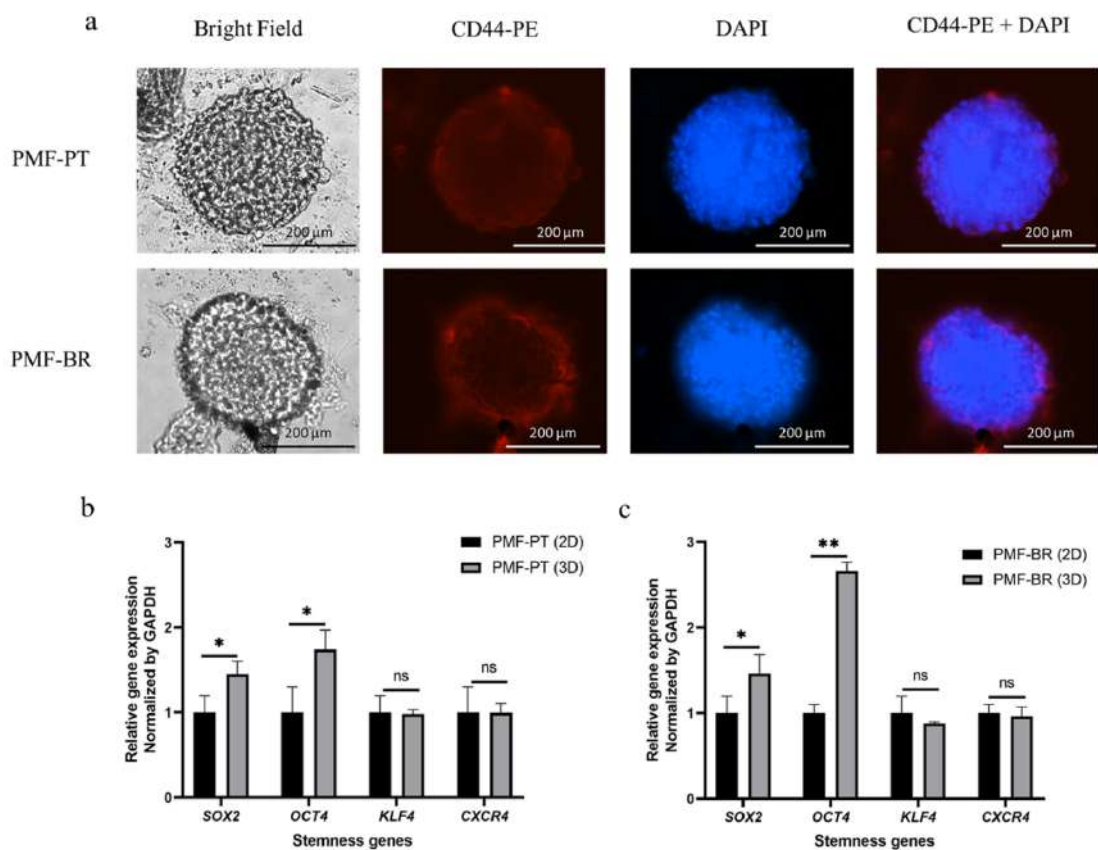
Figure 18. Spheroid morphology of PMF-PT and PMF-BR and their characteristics. Spheroid cells were formed by seeding the cells on poly-HEMA coated plates for 72 h, then stained with CD44-PE (red) and DAPI (blue). The images were capture using an inverted microscope with 10x magnification (scale bar = 100 μm) (A). Expression of stemness genes including *SOX2*, *OCT4*, *KLF4* and *CXCR4* were performed using RT-qPCR in PMF-PT (B) and PMF-BR (C) in comparison of 2D monolayers and 3D spheroids. Data are shown as mean ± SD of triplicate experiments, * *p-value* < 0.05 and ** *p-value* < 0.01; the mean difference is significant at the 0.05 and 0.01 level, respectively compared between 2D and 3D via Student's *t*-test.
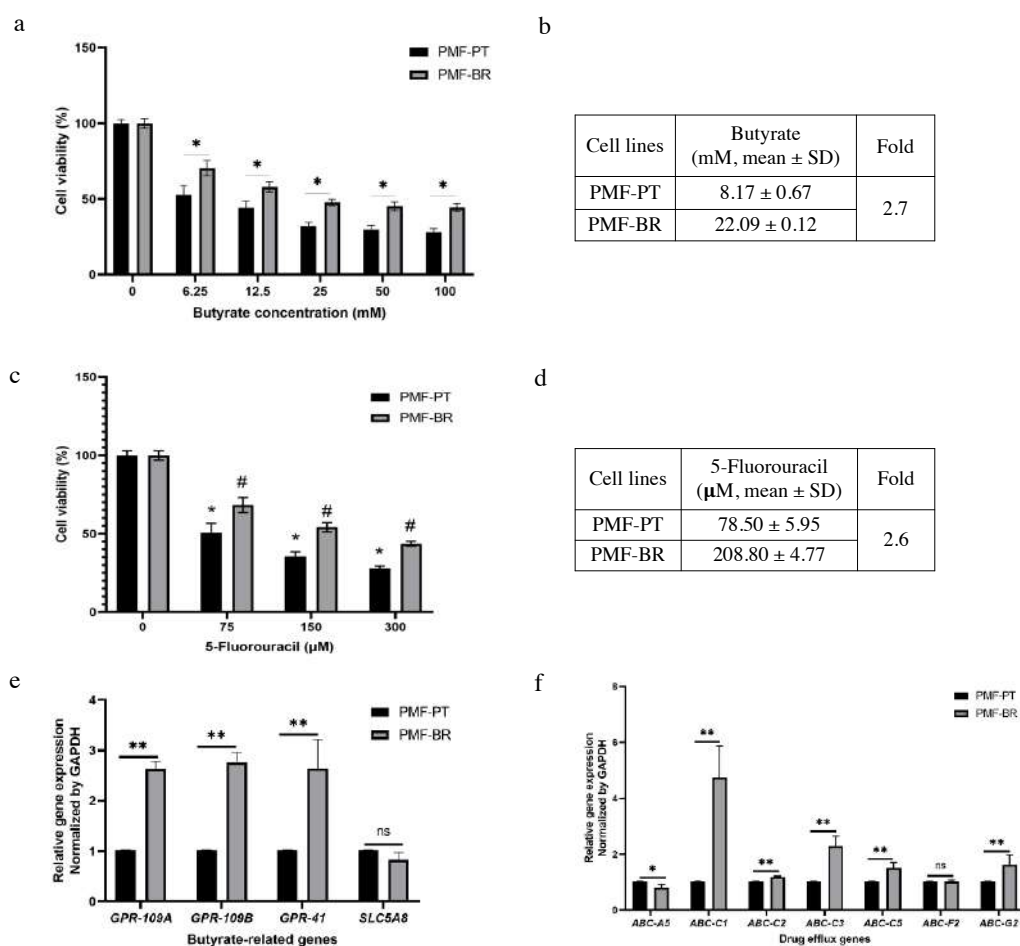
Figure 19. Characterization of butyrate resistance spheroids. Effect of butyrate and 5-FU on PMF-PT and PMF-BR spheroids for 72 h represented as percentage of cell viability (a and c). The IC_{50} value of butyrate and 5-FU after the 72-h treatment was estimated from dose response curves (b and d). Relative expression of butyrate-related genes (e) and drug efflux genes (f) in the spheroids. Gene expression levels are shown relative to those of GAPDH. Data are shown as mean ± SD of triplicate experiments. For figure a, e, and f * *p-value* < 0.05 and ** *p-value* < 0.01 compared between PMF-PT and PMF-BR spheroids via Student's *t*-test. For figure c * *p*-value < 0.05 compared with PMF-PT control; MET 0 mM, # *p*-value < 0.05 compared with PMF-BR control; MET 0 mM via Student's *t*-test.

8. MET decrease spheroids size on PMF-PT and PMF-BR spheroid cells

The size of spheroid after MET treatment was evaluated. Diameter of spheroid was calculated by ImageJ analysis software. In brief, spheroid at day 3 after treatment were capture, then the photos were import to ImageJ software. The scale bar was calibrated in a micrometer unit. The diameter was then measure using a 5-linear line across the edge of spheroid. The software converted pixels of linear line into real micrometer, the average of each line was then calculated and compared among concentration. Figure 20 showed the decreasing of spheroid size in a dose-dependent manner. It is noticeable that the spheroid at 100 mM showed an increasing of the size, resulting from cell death and disaggregation (44).
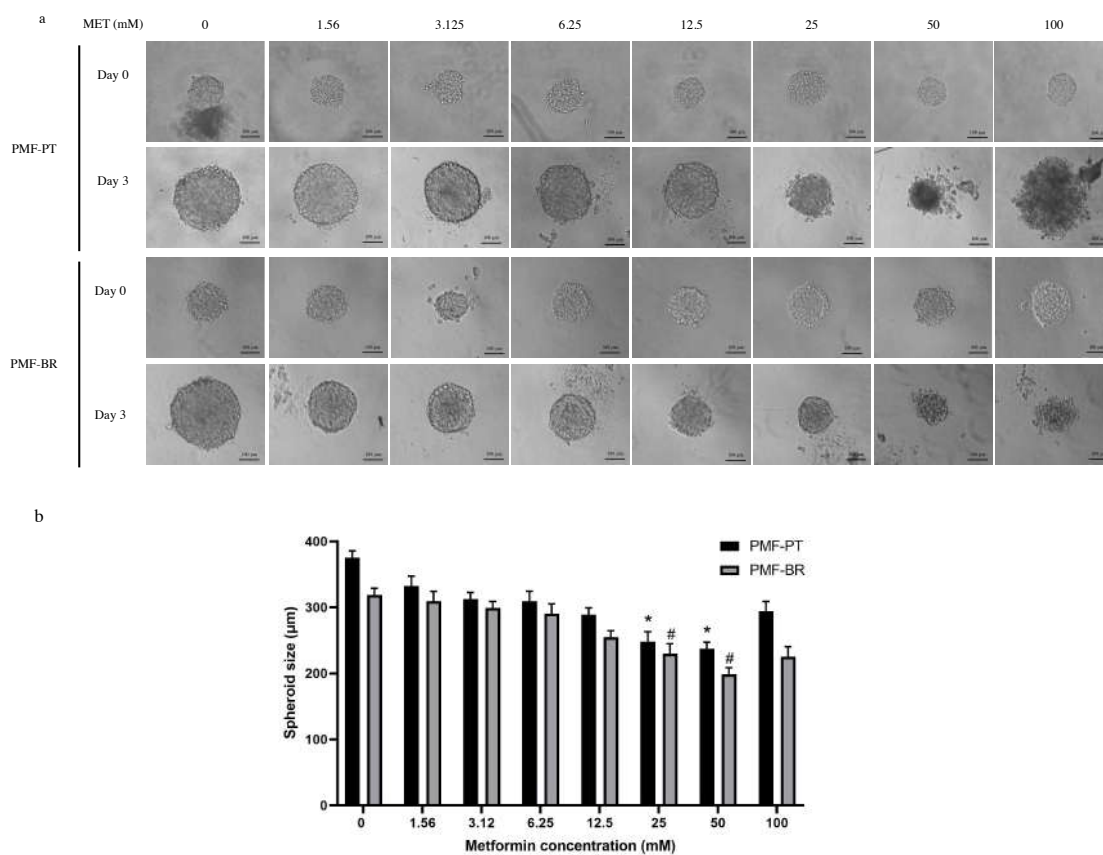
Figure 20. Effect of MET on the size of PMF-PT and PMF-BR spheroids. The spheroids were incubated with various concentrations of MET for 72 h. Spheroids were imaged by inverted microscopy (10x magnification) (A). The bar graphs show the size of the spheroids. Scale bar=100 μm. Significance: * p-value < 0.05 compared with PMF-PT control; MET 0 mM, # p-value < 0.05 compared with PMF-BR control; MET 0 mM.

9. MET induce spheroid death on PMF-PT and PMF-BR spheroid cells

Cell viability of spheroid after 72 h of treatment with MET were conducted by LIVE/DEAD cell imaging kit. Viable cell was probed by calcein AM - a cell-permeant dye using to determine cell viability through intracellular esterase activity, while BOBO-3- a cell-impermeant nucleic acid stain- were used for death cells. Figure 21 showed the cytotoxic effect of MET on spheroid cells. The result demonstrated that a green-fluorescent signal is decrease and red fluorescent signal is increase indicating to cell death in MET treatment group compared to control.
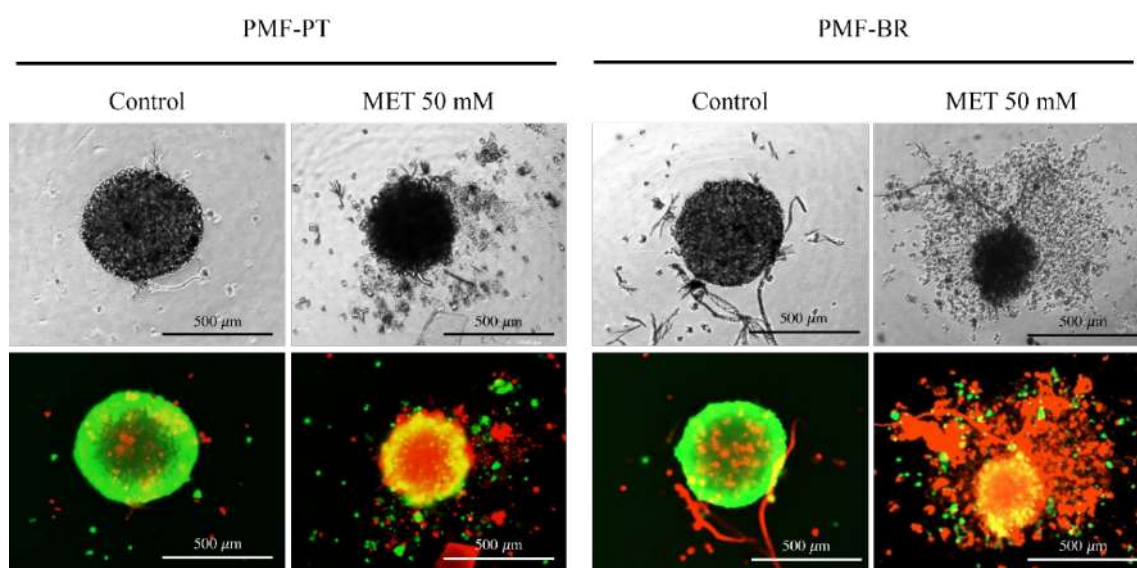
Figure 21. Cytotoxic effect of MET on PMF-PT and PMF-BR spheroids. After being treated with MET at 50 mM for 72 h, the live/dead staining (live = green and dead = red) of the spheroids was imaged with a LionheartFX live cell imager (10x magnification). Scale bar = 500 μm.

10. MET decrease cell viability and increase caspase activity on PMF-PT and PMF-BR spheroid cells

The mode of cell death was investigated by ApoLive-Glo assay. In brief, enzyme activity of viable cells and caspase 3/7 activity of apoptotic cells were evaluated. Spheroid cells were incubated with MET at various concentration for 3 days, then ApoLive-assay were performed. The results showed in figure 22. The results indicated that MET decreased spheroid viability and increase caspase 3/7 activity. These results suggested that MET induce spheroid apoptosis through activation of caspase activity. It is noticeable that the caspase activity of PMF-BR spheroid cell showed higher than in PMF-PT spheroid. This result suggested that PMF-BR spheroid are more sensitive to MET than PMF-PT spheroid cell.
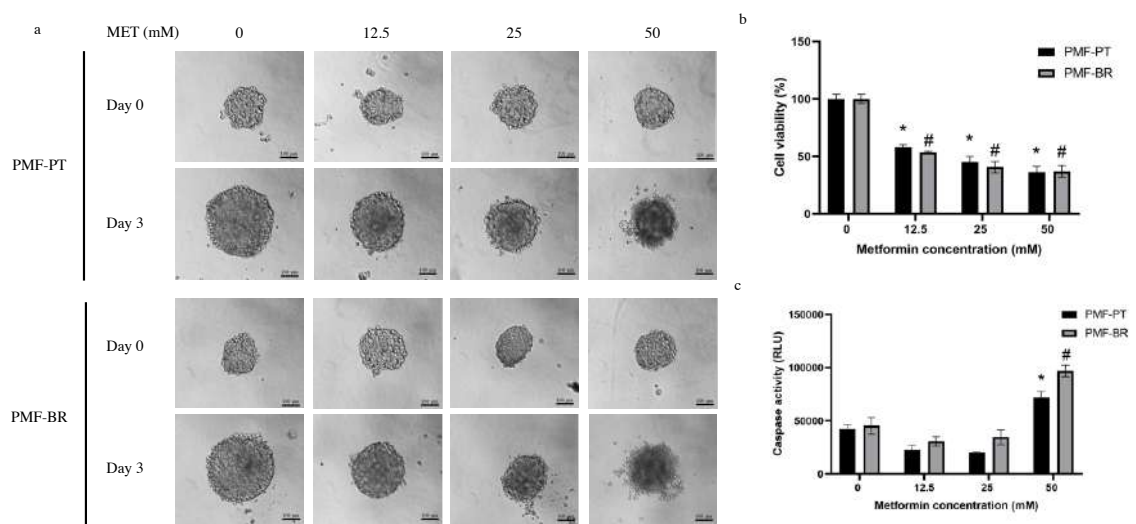
Figure 22. MET induced apoptosis in PMF-PT and PMF-BR spheroids. The morphology of the spheroids after MET treatment at 0, 12.5, 25, and 50 mM for 72 h was captured using an inverted microscope (10x magnification) (A). Scale bar = 100 μm. The ApoLive-Glo assay was used to determine cell viability (B) and caspase-3/7 activity (C). Statistical analysis was performed using the student's *t*-test. Significance: * *p*-value < 0.05 compared with PMF-PT control; MET 0 mM, # *p*-value < 0.05 compared with PMF-BR control; MET 0 mM.

11. MET decrease migration on PMF-PT and PMF-BR spheroid cells

The anti-migration potential of MET was examined using tumor spheroid-based migration assay. Shortly, spheroids were treated with various concentration of MET for 72 h, then the spheroids were transferred to a flat-bottom plate with a fresh completed media. The spheroids were allowed to incubate for another 72 h, the migration area was then evaluated using ImageJ software. Spheroid size at day 3 after MET treatment (Day 3) and migration area were calculated into a percentage of spheroid migration. Figure 23 showed the migration area and the percentage of spheroid migration in each cell type. We found the significantly decreased of spheroid migration at 25 and 50 mM in PMF-PT cell and at 50 mM in PMF-BR cell. The result suggested that MET showed an anti-migration property in both spheroids. The results correlated to previous publication in cervical study. MET decreased invasion and migration in various type of cervical cancer (33). Moreover, the results from cholangiocarcinoma and pancreatic cancer supported anti-migration and anti-invasion properties of MET (30,45).
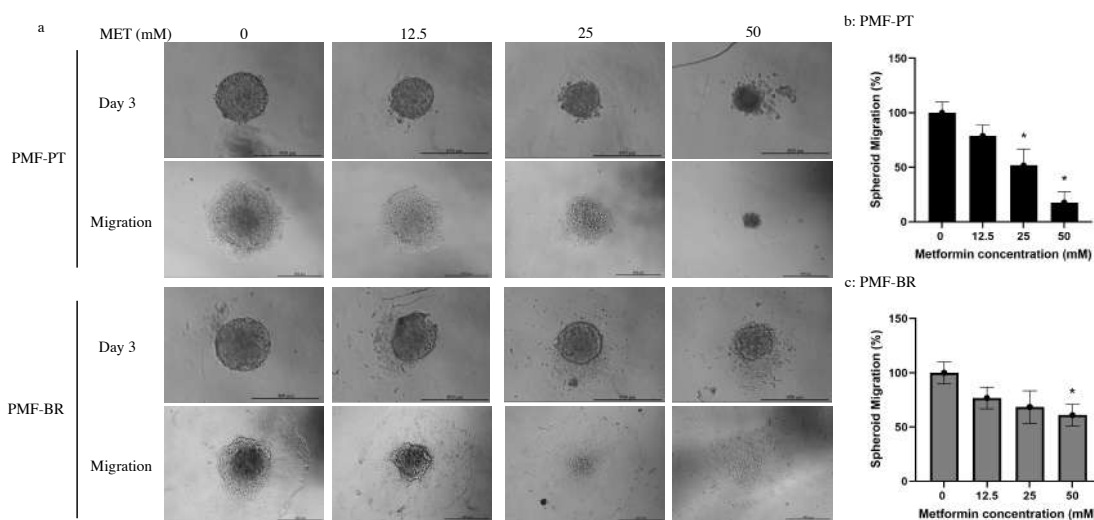
Figure 23. Effect of MET on the cell migration of PMF-PT and PMF-BR spheroids. The spheroids treated with 0, 12.5, 25, and 50 mM of MET for 72 h were transferred to a flat-bottom plate and were incubated for further 72 h. The representative images were capture using an inverted microscopy (10x magnification) (a). The bar graphs show the average percentage of the migration of PMF-PT (b) and PMF-BR (c) spheroids compared with the control value obtained from three independent experiments $\pm$ SD (n = 3). Scale bar = 400 μm. Statistical analysis was performed using the student's *t*-test. Significance: * *p*-value < 0.05 compared with the control; MET 0 mM.

12. Molecular mechanism of MET on PMF-PT and PMF-BR spheroid cells

The molecular mechanism of MET was previously proposed. The main mechanism is AMPK activation and mTOR inhibition (28,33,46). These two pathways also showed an essential role in cancer including proliferation inhibition and apoptosis induction. We therefore investigated the proteins in these pathways. Western blot analysis was used to determine the protein expression. After MET treatment, spheroids were collected, the protein were then extracted. The 30 μg of protein were run into SDS-polyacrylamide gel electrophoresis (SDS-PAGE) followed by transfer to polyvinylidene difluoride (PVDF) membranes (Amersham Pharmacia Biotech, USA). The membranes were blocked in 5% non-fat milk in Tris-buffer saline with 0.1% (v/v) Tween-20 (TBS-T) for 1 h at room temperature. The membrane was then washed twice with TBS-T. Each membrane was incubated overnight at 4ºC, shaking continuously with primary antibodies (1:1000 diluted with 1% non-fat milk in TBS-T) specific to primary antibody listed in table 5 and β-actin was used as internal control. After overnight incubation, the membranes were washed with TBS-T and were incubated for 2 h with a secondary diluted in 1% non-fat milk in TBS-T. Then, the membranes were washed again with TBS-T and the last washing was performed using TBS for 10 min. The protein expressions were visualized using an enhanced chemiluminescence reagent (Pierce™ ECL Western Blotting Substrate, Thermo Fisher scientific, USA). Densitometry was performed using a Chemiluminescence & Epi Fluorescence Alliance Q9 Advanced (Uvitec, UK) imager. The results showed in figure 24. Phospho-AMPK and p-Akt were significantly upregulated in the MET-treated group in both PT and BR spheroids. In addition, acetyl-CoA-carboxylase (ACC) was significantly reduced in the MET-treated group. We also found that p-mTOR exhibited lower expression in the MET-treated group; however, we found no significant difference in ratio of mTOR/p-mTOR expression. We also examined other molecules in the mTOR pathway. The expression of Raptor and Rictor were not different. The binding molecule of mTOR, Raptor, and Rictor is GβL. We found a significant decrease in GβL expression following MET treatment. Finally, c-Raf showed a significant decrease in MET-treated BR spheroids. Altogether, these results suggested that MET could inhibit the cell viability of both PMF-PT and PMF-BR spheroids by activating the AMPK and Akt

pathways and caspase activity and inhibiting the ACC and mTOR pathways. Our study confirmed MET action on AMPK activation. The mechanism of MET on our cells was proposed in Figure 25.

Table 6. List of antibodies used in Western blot analysis.

List of antibody	Dilution	Antibody	Cat. No.
1	1:1000	Phospho-AMPKα (Thr172) Rabbit mAb	2535
2	1:1000	AMPKα (D5A2) Rabbit mAb	5831
3	1:1000	Phospho-Acetyl-CoA Carboxylase (Ser79) (D7D11) Rabbit mAb	11818
4	1:1000	Acetyl-CoA Carboxylase (C83B10) Rabbit mAb	3676
5	1:1000	Phospho-Akt (Ser473) (D9E) XP®Rabbit mAb	4060
6	1:1000	Akt (pan) (C67E7) Rabbit mAb	4691
7	1:1000	Phospho-c-Raf (Ser259) Antibody	9421
8	1:1000	Phospho-mTOR (Ser2448) Antibody	2971
9	1:1000	mTOR (7C10) Rabbit mAb	2983
10	1:1000	Raptor (24C12) Rabbit mAb	2280
11	1:1000	Rictor (53A2) Rabbit mAb	2114
12	1:1000	GβL (86B8) Rabbit mAb	3274
13	1:1000	β-Actin antibody	4967
14	1:1000	Anti-rabbit IgG, HRP-linked Antibody	7074
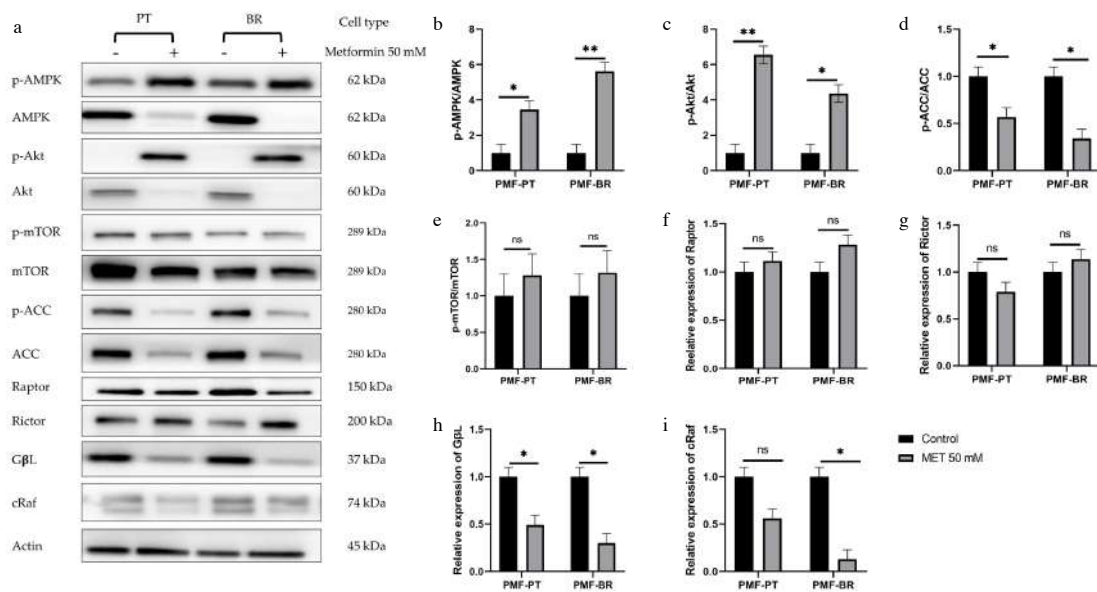
Figure 24. Effect of MET on the AMPK/ACC/mTOR pathway and its binding proteins. Both PMF spheroids were treated with and without MET (50 mM) for 72 h. After incubation, the spheroids were collected and lysed. The proteins were loaded on SDS-PAGE, and those of interest were examined by Western blot analysis. Actin was used as internal control (a). The quantitative proteins of interest, including p-AMPK/AMPK (b), p-Akt/Akt (c), p-ACC/ACC (d), p-mTOR/mTOR (e), Raptor (f), Rictor (g), GβL (h), and c-Raf (i), were normalized to actin band intensity. Data are shown as the mean ± SD of triplicate experiments. Statistical analysis was performed using Student's *t*-test. Significance: * *p*-value < 0.05 compared with the control; MET 0 mM. ** *p*-value < 0.01 compared with the control; MET 0 mM.
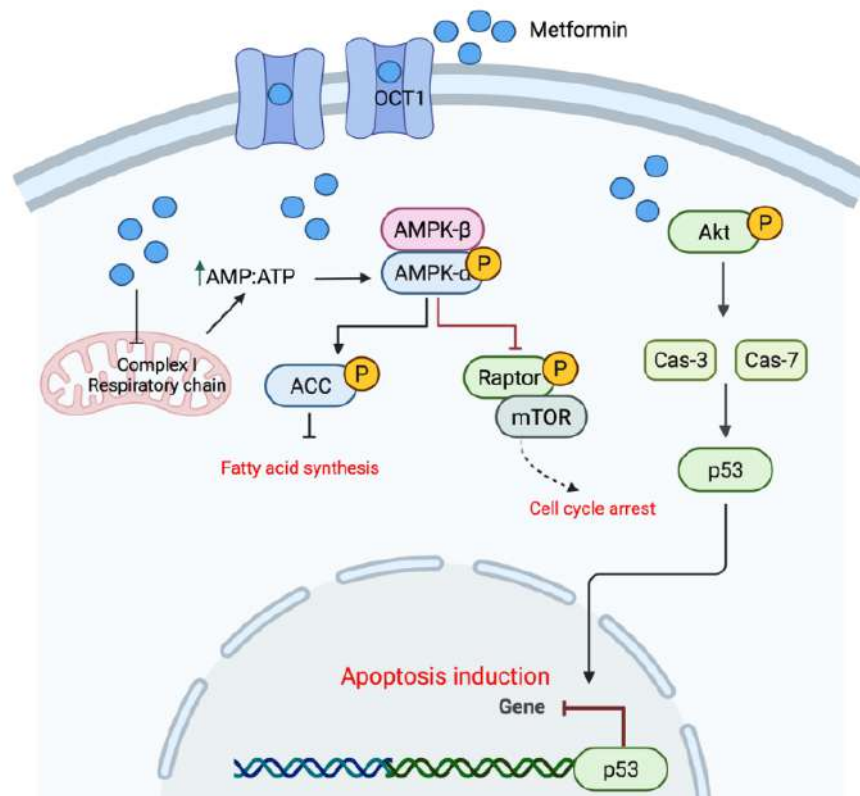
Figure 25. The proposed mechanism of MET on AMPK/Akt/mTOR pathway in spheroid cells.

CHAPTER 4

CONCLUDING REMARK

1. Butyrate-resistance cell showed a malignant characteristic including upregulation of drug efflux pump genes, the migration capacity and cross-resistant to anti-cancer drugs.

2. The HCT-BR cells, represented to primary tumor, showed a cross-resistance to Oxa and MET. Meanwhile, PMF-BRmet cells, represented to metastatic tumor, showed a cross-resistance to 5-FU. This finding showed a potential of MET on PMF cells.

3. MET showed a potential cytotoxicity including spheroid size reduction, and increasing of cell death on both PT and BR spheroid cells through the activation of AMPKα and Akt and inhibition of ACC and GβL.

LIMITATION

1. The 3D spheroid culture was used in present study. This system uses only one cell type to investigate all experiment. It cannot reflex the heterogeneity of tumor bulk which compose of a various type of cells.

FURTHER STUDY

1. The effect of metformin should be validated in mouse model.

2. Since the potential anticancer effect of butyrate and metformin, the combination of these two compounds should be further investigated.

3. Specificity of drug influx/efflux protein to butyrate and interested drug should be explored.

4. Secretome of BR cells should be addressed in term of molecular role in gut mucrobiome as an *in vitro* model.

5. Genetic alteration of butyrate resistant cells in view of characterization and its underlying mechanism on drug influx/efflux should be considered.

REFERENCES

1. Deo SVS, Sharma J, Kumar S. GLOBOCAN 2020 Report on Global Cancer Burden: Challenges and Opportunities for Surgical Oncologists. Ann Surg Oncol. 2022;1–4.

2. Li N, Lu B, Luo C, Cai J, Lu M, Zhang Y, et al. Incidence, mortality, survival, risk factor and screening of colorectal cancer: A comparison among China, Europe, and northern America. Cancer Lett. 2021;522:255–68.

3. Sung H, Ferlay J, Siegel RL, Laversanne M, Soerjomataram I, Jemal A, et al. Global cancer statistics 2020: GLOBOCAN estimates of incidence and mortality worldwide for 36 cancers in 185 countries. CA Cancer J Clin. 2021;71(3):209–49.

4. Araghi M, Soerjomataram I, Jenkins M, Brierley J, Morris E, Bray F, et al. Global trends in colorectal cancer mortality: projections to the year 2035. Int J Cancer. 2019;144(12):2992–3000.

5. Sermsri N, Boonpipattanapong T, Prechawittayakul P, Sangkhathat S. Influence of payer source on treatment and outcomes in colorectal cancer patients in a university hospital in Thailand. Asian Pacific Journal of Cancer Prevention. 2014;15(20):9015–9.

6. Mansoori B, Mohammadi A, Davudian S, Shirjang S, Baradaran B. The different mechanisms of cancer drug resistance: A brief review. Adv Pharm Bull. 2017;7(3):339–48.

7. Saus E, Iraola-Guzmán S, Willis JR, Brunet-Vega A, Gabaldón T. Microbiome and colorectal cancer: Roles in carcinogenesis and clinical potential. Mol Aspects Med. 2019;69(March):93–106.

8. Song M, Chan AT. Diet, Gut Microbiota, and Colorectal Cancer Prevention: a Review of Potential Mechanisms and Promising Targets for Future Research. Curr Colorectal Cancer Rep. 2017;13(6):429–39.

9. Koh A, De Vadder F, Kovatcheva-Datchary P, Bäckhed F. From dietary fiber to host physiology: Short-chain fatty acids as key bacterial metabolites. Cell. 2016;165(6):1332–45.

10. Louis P, Flint HJ. Diversity, metabolism and microbial ecology of butyrate-producing bacteria from the human large intestine. FEMS Microbiol Lett. 2009;294(1):1–8.

11. Jahani-Sherafat S, Alebouyeh M, Moghim S, Amoli HA, Ghasemian-Safaei H. Role of gut microbiota in the pathogenesis of colorectal cancer; a review article. Hepatol Bed Bench. 2018;11(2):101–9.

12. Gagnière J, Raisch J, Veziant J, Barnich N, Bonnet R, Buc E, et al. Gut microbiota imbalance and colorectal cancer. World J Gastroenterol. 2016;22(2):501–18.

13. Bultman SJ. Molecular pathways: Gene-environment interactions regulating dietary fiber induction of proliferation and apoptosis via butyrate for cancer prevention. Clinical Cancer Research. 2014;20(4):799–803.

14. Donohoe DR, Collins LB, Wali A, Bigler R, Sun W, Bultman SJ. The Warburg Effect Dictates the Mechanism of Butyrate-Mediated Histone Acetylation and Cell Proliferation. Mol Cell. 2012;48(4):612–26.

15. De Silanes IL, Olmo N, Turnay J, González De Buitrago G, Pérez-Ramos P, Guzmán-Aránguez A, et al. Acquisition of resistance to butyrate enhances survival after stress and induces malignancy of human colon carcinoma cells. Cancer Res. 2004;64(13):4593–600.

16. Kang HR, Choi HG, Jeon CK, Lim SJ, Kim SH. Butyrate-mediated acquisition of chemoresistance by human colon cancer cells. Oncol Rep. 2016;36(2):1119–26.

17. Yoo HY, Park SY, Chang SY, Kim SH. Regulation of Butyrate-Induced Resistance through AMPK Signaling Pathway in Human Colon Cancer Cells. Biomedicines. 2021;9(11).

18. Sinnett SE, Brenman JE. Past strategies and future directions for identifying AMP-activated protein kinase (AMPK) modulators. Pharmacol Ther. 2014;143(1):111–8.

19. Gutierrez-Salmeron M, Chocarro-Calvo A, García-Martínez JM, de la Vieja A, Garcia-Jimenez C. Epidemiological bases and molecular mechanisms linking obesity, diabetes, and cancer. Endocrinología, Diabetes y Nutrición (English ed). 2017;64(2):109–17.

20. Yoo HY, Park SY, Chang SY, Kim SH. Regulation of Butyrate-Induced Resistance through AMPK Signaling Pathway in Human Colon Cancer Cells. Vol. 9, Biomedicines. 2021.

21. Viollet B, Guigas B, Sanz Garcia N, Leclerc J, Foretz M, Andreelli F. Cellular and molecular mechanisms of metformin: an overview. Clin Sci (Lond). 2012 Mar;122(6):253–70.

22. Tang YL, Zhu LY, Li Y, Yu J, Wang J, Zeng XX, et al. Metformin Use Is Associated with Reduced Incidence and Improved Survival of Endometrial Cancer: A Meta-Analysis. Biomed Res Int. 2017;2017:1–9.

23. Gandini S, Puntoni M, Heckman-Stoddard BM, Dunn BK, Ford L, DeCensi A, et al. Metformin and cancer risk and mortality: A systematic review and meta-analysis taking into account biases and confounders. Cancer Prevention Research. 2014;7(9):867–85.

24. Chu D, Wu J, Wang K, Zhao M, Wang C, Li L, et al. Effect of metformin use on the risk and prognosis of endometrial cancer: A systematic review and meta-analysis. BMC Cancer. 2018;18(1):1–11.

25. Al Hassan M, Fakhoury I, El Masri Z, Ghazale N, Dennaoui R, El Atat O, et al. Metformin Treatment Inhibits Motility and Invasion of Glioblastoma Cancer Cells. Anal Cell Pathol (Amst). 2018;2018:5917470.

26. Sugiura K, Okabayashi K, Seishima R, Ishida T, Shigeta K, Tsuruta M, et al. Metformin inhibits the development and metastasis of colorectal cancer. Medical Oncology. 2022;39(9):136.

27. Lee JH, Kim T Il, Jeon SM, Hong SP, Cheon JH, Kim WH. The effects of metformin on the survival of colorectal cancer patients with diabetes mellitus. Int J Cancer. 2012;131(3):752–9.

28. Kwan HT, Chan DW, Cai PCH, Mak CSL, Yung MMH, Leung THY, et al. AMPK Activators Suppress Cervical Cancer Cell Growth through Inhibition of DVL3 Mediated Wnt/β-Catenin Signaling Activity. PLoS One. 2013;8(1):1–10.

29. Mu Q, Jiang M, Zhang Y, Wu F, Li H, Zhang W, et al. Metformin inhibits proliferation and cytotoxicity and induces apoptosis via AMPK pathway in CD19-chimeric antigen receptor-modified T cells. Onco Targets Ther. 2018;11:1767.

30. Wandee J, Prawan A, Senggunprai L, Kongpetch S, Kukongviriyapan V. Metformin sensitizes cholangiocarcinoma cell to cisplatin-induced cytotoxicity through oxidative stress mediated mitochondrial pathway. Life Sci. 2019;217:155–63.

31. Hirsch HA, Iliopoulos D, Struhl K. Metformin inhibits the inflammatory response associated with cellular transformation and cancer stem cell growth. Proceedings of the National Academy of Sciences. 2013;110(3):972–7.

32. Sun S, Gong F, Liu P, Miao Q. Metformin combined with quercetin synergistically repressed prostate cancer cells via inhibition of VEGF/PI3K/Akt signaling pathway. Gene. 2018;664:50–7.

33. Chen YH, Wang PH, Chen PN, Yang SF, Hsiao YH. Molecular and Cellular Mechanisms of Metformin in Cervical Cancer. Vol. 13, Cancers . 2021.

34. Olmo N, Turnay J, Lecona E, García-Díez M, Llorente B, Santiago-Gómez A, et al. Acquisition of resistance to butyrate induces resistance to luminal components and other types of stress in human colon adenocarcinoma cells. Toxicology in Vitro. 2007;21(2):254–61.

35. Duz MB, Karatas OF. Expression profile of stem cell markers and ABC transporters in 5-fluorouracil resistant Hep-2 cells. Mol Biol Rep. 2020;47(7):5431–8.

36. Duz MB, Karatas OF. Differential expression of ABCB1, ABCG2, and KLF4 as putative indicators for paclitaxel resistance in human epithelial type 2 cells. Mol Biol Rep. 2021;48(2):1393–400.

37. Gillet JP, Efferth T, Steinbach D, Hamels J, De Longueville F, Bertholet V, et al. Microarray-based detection of multidrug resistance in human tumor cells by expression profiling of ATP-binding cassette transporter genes. Cancer Res. 2004;64(24):8987–93.

38. Thorn CF, Oshiro C, Marsh S, Hernandez-Boussard T, McLeod H, Klein TE, et al. Doxorubicin pathways. Pharmacogenet Genomics. 2011;21(7):440–6.

39. Zhou Y, Wang X, Huang X, Li X, Cheng K, Yu H, et al. High expression of COPB2 predicts adverse outcomes: A potential therapeutic target for glioma. CNS Neurosci Ther. 2020;26(3):309–18.

40. Rawlings JS, Rosler KM, Harrison DA. The JAK/STAT signaling pathway. J Cell Sci. 2004;117(8):1281–3.

41. Chang JC. Cancer stem cells: Role in tumor growth, recurrence, metastasis, and treatment resistance. Medicine (United States). 2016;95(1):S20–5.

42. Allenspach EJ, Maillard I, Aster JC, Pear WS. Notch signaling in cancer. Cancer Biol Ther. 2002;1(5):466–76.

43. Gheytanchi E, Naseri M, Karimi-Busheri F, Atyabi F, Mirsharif ES, Bozorgmehr M, et al. Morphological and molecular characteristics of spheroid formation in HT-29 and Caco-2 colorectal cancer cell lines. Cancer Cell Int. 2021;21(1):1–16.

44. Zanoni M, Pignatta S, Arienti C, Bonafè M, Tesei A. Anticancer drug discovery using multicellular tumor spheroid models. Expert Opin Drug Discov. 2019;14(3):289–301.

45. Bao B, Wang Z, Ali S, Ahmad A, Azmi AS, Sarkar SH, et al. Metformin inhibits cell proliferation, migration and invasion by attenuating CSC function mediated by deregulating miRNAs in pancreatic cancer cells. Cancer Prevention Research. 2012;5(3):355–64.

46. LaMoia TE, Shulman GI. Cellular and Molecular Mechanisms of Metformin Action. Endocr Rev. 2021 Feb 1;42(1):77–96.

APPENDIX A

Additional data

Additional Table 1. Primer sequences used for stemness genes, butyrate receptors and drug efflux genes.

Name	Sequence (5'-3')	Gene groups
GAPDH-F	ACG GAT TTG GTC GTA TTG G	Housekeeping gene
GAPDH-R	GGA AGA TGG TGA TGG GAT TT	
GPR109A-F	GGA CAA CTA TGT GAG GCG TTG G	Butyrate receptors
GPR109A-R	GGG CTG GAG AAG TAG TAC ACC	
GPR109B-F	CGT GAT GGA CTA CTA TGT GCG	
GPR109B-R	ATT TGC AGG GCC ATT CTG GAT	
GPR-41-F	CCG GAT ATC ACC ATG GAT ACA GGC CCC GAC	
GPR-41-R	CTT GTC TAG ACT AGC TTT CAG CAC AGG C	
SLC5A8-F	GGG TGG TCT GCA CAT TCT ACT	
SLC5A8-R	GCC CAC AAG GTT GAC ATA GAG	
ABC-A5-F	ATC ATG TGA GGC TGC TCA G	Drug efflux pumps
ABC-A5-R	ACA ACA GCA GTT TCT CCC ATA	
ABC-C1-F	TCA GCC AGA AAA TCC TCC AC	
ABC-C1-R	GGC ACC ATG AGG ACC ATC	
ABC-C2-F	TCC TGG TTG ATG AAG GCT C	
ABC-C2-R	CAG TGA ATA AGA GGA TTG CAC A	
ABC-C3-F	GCC ACC CTG CTG ATA CAG T	
ABC-C3-R	AGA TCT CAC CCT CTG CCT TG	
ABC-C5-F	TGA GGG AGA GAA CCA GCA CT	
ABC-C5-R	AAG TAG TCC GGA TGG GCT TC	
ABC-F2-F	GTC TCC CAT TCC CAG GAT TT	
ABC-F2-R	CTG ATC TTG CTC CCA GTG AA	
ABC-G2-F	AGC AGC AGG TCA GAG TGT GG	
ABC-G2-R	GAT CGA TGC CCT GCT TTA CC	
SOX2-F	CTC CGG GAC ATG ATC AGC	Stemness markers
SOX2-R	GGT AGT GCT GGG ACA TGT G	
OCT4-F	CCC AAT TAC CCA TCC TTC CTG	
OCT4-R	GTC TTC CCC TCT TTG GCT TG	
KLF4-F	CTG GAG AAG GAG AAG CTG GA	
KLF4-R	CAA ATT GCT CGA GTT CTT TCT G	
CXCR4-F	CCC TCA AGA CCA CAG TCA TCC	
CXCR4-R	GTT CTC AAA CTC ACA CCC TTG C	

Additional data (Continue)

Chemical Reagents for cell culture

10X Tris buffer saline (TBS) pH7.6

Tris base	24.2 g
NaCl	8.0 g
dH$_2$O	1000 ml

Adjust pH to 7.6 with conc. HCl

Autoclave and store at 4°C

1X PBS vol 1 L

C$_1$V$_1$	=	C$_2$V$_2$
10X *V$_1$	=	1X *1000ml
V$_1$	=	100 ml

Total volume 1000 ml   Add 10X PBS 100 ml + DW 900 ml

Sterile by autoclave

Dulbecco's Modified Eagle's medium+10% Fetal bovine serum (DNEM+10%FBS , pH 7.4) volume 1 L

DMEM (Dulbecco's Modified Eagle Medium, powder)	1 bag
sodium bicarbonate	3.7 g
dH$_2$O	1000 ml
Fetal bovine serum	100 ml
Adjust pH to 7.4 with 1 N HCl	
Penstrep (10000 U/ml Penicillium and 10000 μg/ml streptomycin)	10 ml
L-glutamine (200 mM)	10 ml

Filtered with 0.2 μm nitrocellulose filter membrane

Store at 4°C

Dulbecco's Modified Eagle's medium (DEME serum-free medium, pH 7.4) volume 1 L

DMEM (Dulbecco's Modified Eagle Medium, powder)	1 bag
sodium bicarbonate	3.7 g
Adjust pH to 7.4 with 1 N HCl	1 ml
Filtered with 0.2 μm nitrocellulose filter membrane	
Store at 4°C	
Penstrep (10000 U/ml Penicillium and 10000 μg/ml streptomycin)	10 ml
L-glutamine (200 mM)	10 ml

MTT (3-(4,5-Dimethylthiazol-2-yl)-2,5-Diphenyltetrazolim Bromide) solution 5 mg/ml

MTT (powder)	50 g
1X PBS	10 ml
Dissolve by vortex	
Wrapped with foil and store at 4 °C	
Working 0.5 mg/ml ; 5 mg/ml MTT solution stock 1 ml + 1X PBS 9 ml	

Chemical Reagents for Western blot analysis

1.5 M Tris HCl pH 8.8

Tris base	18.17 g
dH$_2$O	100 ml
Adjust pH to 8.8 with conc. HCl	
Autoclave and store at 4°C	

1.0 M Tris HCl pH6.8

Tris base	12.19 g
dH$_2$O	100 ml

Adjust pH to 6.8 with conc. HCl

Autoclave and store at 4°C

10 % Ammonium persulfate (APS) (W/V)

APS	0.1 g
dH$_2$O	1 ml

Keep in aluminium foil (Dark)

Fresh before use and store at 4°C

1 N NaOH

NaOH	40 g
dH$_2$O	1 L

1N HCl

HCl	82.84 ml
dH$_2$O	917.66 ml

10 % SDS (W/V)

SDS	100 g
dH$_2$O	1 L

4X SDS loading buffer

		Final concentration
100% glycerol	10 ml	40%
1M Tris HCl pH6.8	5 ml	200 mM
DTT	1.54 g	400 mM
SDS	2.0 g	8%
Beta-mercapto	1.79 g	8%
Bromophenol blue	0.1 g	0.4%
dH$_2$O	8.21 ml	

Coomassie brilliant blue solution

		Final concentration
Coomassie brilliant blue R/G	0.2 g	0.1%
Methanol (v/v)	400 ml	4%
Acetic acid (v/v)	100 ml	10%
dH$_2$O	500 ml	50%

Ponceau S solution

		Final concentration
Ponceau S	1 g	0.1 %
Acetic acid	5 ml	5.0 %
dH$_2$O	950 ml	

Storage at room temp

10X Running Buffer

Tris base	30.3 g
Glycine	144.2 g
SDS	10.0 g
dH$_2$O	1000 ml

Autoclave and store at 4°C

1x Running buffer

Tris base	3.03 g
Glycine	14.42 g
SDS	1.0 g
dH$_2$O	1,000 ml

10X Transfer Buffer

		Final Concentration
Tris base	30.3 g	12 mM
Glycine	144.2 g	9.6 mM
dH$_2$O	1000 ml	

Autoclave and store at 4°C

1X Transfer buffer

C_1V_1	=	C_2V_2
10X *V_1	=	1X *1000ml
V_1	=	100 ml

		Final concentration
10X Transfer Buffer	100 ml	1X
Methanol	200 ml	20 %
dH$_2$O	700 ml	

Prepare Fresh before use and store at 4°C

10X Tris buffer saline (TBS) pH7.6

Tris base	24.2 g
NaCl	8.0 g
dH$_2$O	1000 ml

Adjust pH to 7.6 with conc. HCl

Autoclave and store at 4°C

1X TBS

10X TBS pH7.6	100 ml
dH$_2$O	900 ml

1X TBS-T

10X TBS pH7.6	100 ml
dH$_2$O	900 ml
Tween 20	1 ml

5% Non-Fat Milk (NFM) in 1X TBS-T

NFM	5 g
1 TBS-T	100 ml

1% Non-Fat Milk (NFM) in 1X TBS-T

NFM	1 g
1 TBS-T	100 ml

Reagents for RNA extraction

DEPC-H$_2$O (Diethylpyrocarbonate treated water)

DEPC reagent	1 ml
dH$_2$O	1,000 ml

     Starrier in fume hood for 1 h.

     Sterile by autoclave

     Storage: Working 4°C, stock -20°C

70% ethanol (volume 200 ml)

Absolute Ethanol	140 ml
DEPC-H$_2$O	60 ml
Total Vol	100 ml

Mix with autoclaved cylinder

Storage at 4°C

10x TAE

Tris-base	48.4 g
Glacial acetic acid	11.42 ml
0.5 M EDTA, pH 8.0	20 ml
Total Vol	1,000 ml

     Adjust volume 1,000 ml with Deionized water (DI)

     Filter by what-man, Sterile by autoclave, Store at room temp.

0.5x TAE vol 1 L

C1V1	=	C2V2
10x * V1	=	0.5X * 1,000 ml
V1	=	(0.5X * 1,000 ml) / 10X
	=	50ml

		Final concentration
10X TAE	50 ml	1X
dH$_2$O	950 ml	
Total Vol	1,000 ml	

Store at Room Temperature

APPENDIX B

Publications

1. **Nittayaboon K**, Leetanaporn K, Sangkhathat S, Roytrakul S, Navakanitworakul R. Characterization of Butyrate-Resistant Colorectal Cancer Cell Lines and the Cytotoxicity of Anticancer Drugs against These Cells., BioMed Res. Int. 2022. https://doi.org/10.1155/2022/6565300

2. **Nittayaboon K**, Leetanaporn K, Sangkhathat S, Roytrakul S, Navakanitworakul R. Cytotoxic effect of metformin on butyrate-resistant PMF-K014 colorectal cancer spheroid cells. Biomed. Pharmacother. 2022(151). https://doi.org/10.1016/j.biopha.2022.113214

Oral presentation

1. **Nittayaboon K**, Sangkhathat S, and Navakanitworakul R. Effect of Metformin on AMPK/AKT/MTOR Pathway Against Butyrate-Resistant Colorectal Cancer Spheroid Cells. IBSC2021. November 25-26, 2021. Novi Sad, Serbia.

REPRINT OF ARTICLES

First article

Characterization of Butyrate-Resistant Colorectal Cancer Cell Lines and the

Cytotoxicity of Anticancer Drugs against These Cells

Hindawi

Research Article

Characterization of Butyrate-Resistant Colorectal Cancer Cell Lines and the Cytotoxicity of Anticancer Drugs against These Cells

Kesara Nittayaboon [D],[1] **Kittinun Leetanaporn** [D],[1] **Surasak Sangkhathat** [D],[1] **Sittiruk Roytrakul** [D],[2] **and Raphatphorn Navakanitworakul** [D][1]

[1]Department of Biomedical Sciences and Biomedical Engineering, Faculty of Medicine, Prince of Songkla University, Hat Yai, Songkhla, Thailand 90110
[2]Functional Ingredients and Food Innovation Research Group, National Center for Genetic Engineering and Biotechnology (BIOTEC), National Science and Technology Development Agency, Pathumthani 12120, Thailand

Correspondence should be addressed to Raphatphorn Navakanitworakul; nraphatp@medicine.psu.ac.th

Colorectal cancer (CRC) is the third most common cancer worldwide. The gut microbiota plays a critical role in homeostasis and carcinogenesis. Butyrate, a short-chain fatty acid produced by the gut microbiota, plays a role in intestinal homeostasis and acts as an anticancer agent by inhibiting growth and inducing apoptosis. However, microbiota studies have revealed an abnormally high abundance of butyrate-producing bacteria in patients with CRC and indicated that it leads to chemoresistance. We characterized butyrate resistance in HCT-116 and PMF-K014 CRC cells after treatment with a maximum butyrate concentration of 3.2 mM. The 50% inhibitory concentration of butyrate was increased in butyrate-resistant (BR) cells compared with that in parental (PT) cells. The mechanism of butyrate resistance was initially investigated by determining the expression of butyrate influx- and drug efflux-related genes. We found the increased expression of influx- and efflux-related genes in BR cells compared with that in PT cells. Proteomic data showed both identical and different proteins in PT and BR cells. Further analysis revealed the crossresistance of HCT-116 cells to metformin and oxaliplatin and that of PMF-K014 cells to 5-fluorouracil. Our findings suggest that the acquisition of butyrate resistance induces the development of chemoresistance in CRC cells, which may play an important role in CRC development, treatment, and metastasis.

1. Introduction

Colorectal cancer (CRC) is the third most common cancer and second leading cause of cancer-related deaths worldwide. In Thailand, CRC is the third most common cancer, and 11% of the cancer-related deaths are attributed to CRC [1]. According to a World Health Organization report in 2020, the death rate associated with CRC accounted for 9% of the incidence. Several risk factors are associated with CRC, including host genetic and epigenetic alterations, dietary lifestyle, environment, and microbial community imbalance [2–5]. The gut microbiota plays a key role in homeostasis and carcinogenesis, producing metabolites to maintain intestinal barrier integrity and immune homeostasis. An imbalance in the microbiome leads to carcinogenesis [6–8]. Currently, CRC is treated using surgery and chemoradiotherapy. Conventional chemotherapy targets rapidly dividing cells and is the main treatment strategy for improving the mortality rate of patients with CRC. In Thailand, a combination of 5-fluorouracil (5-FU) and oxaliplatin (Oxa) (FuOx) is the chemotherapeutic treatment of choice for CRC [9]. The main mechanism of action of 5-FU is the inhibition of thymidylate synthase [10]. Oxa covalently binds DNA, leading to the formation of platinum-DNA adducts that induce a prolonged G2 arrest and inhibit growth, resulting in apoptotic cell death [11]. Metformin (Met) is typically
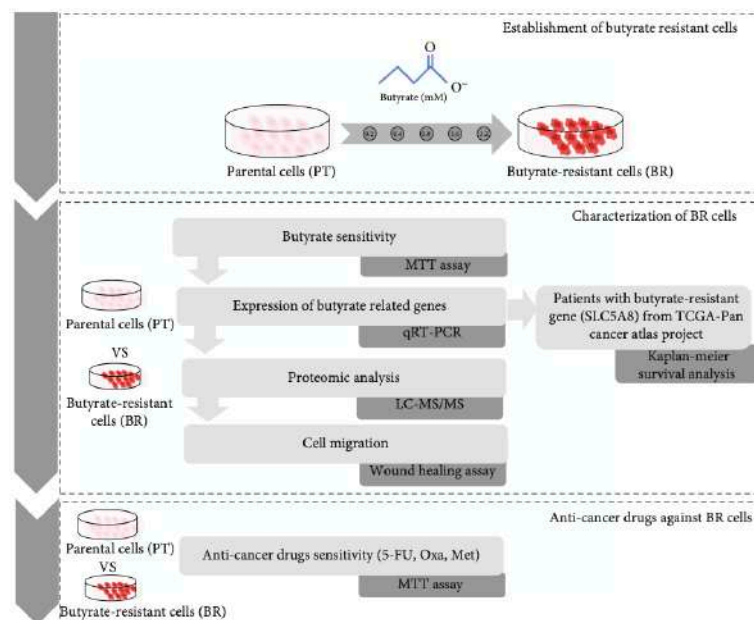
Figure 1: The experimental design of this study. The flow chart shows the workflow of our study.

used to treat diabetes mellitus (DM); however, its use is also associated with the reduction of cervical, endometrial, lung, and colon cancer risk in patients with type 2 DM [12–16]. Met inhibits mitochondrial respiration, leading to an imbalance in the AMP:ATP ratio, which is monitored by—or activates—AMP-activated protein kinase [17]. Decreased cellular invasion and increased adhesion to collagen are correlated with a reduction in cell motility in human astrocytoma (brain tumor) cell lines [18]. This information suggests the potential of Met as an anticancer drug that may kill cancer cells including butyrate-resistant (BR) CRC cells. However, currently, 90% of the chemotherapy failures occur due to the invasion and metastasis of cancer cells [19].

Butyrate, a short-chain fatty acid produced by the gut microbiota, plays a role in intestinal homeostasis by inducing the proliferation and differentiation of cells of the normal colonic epithelium. However, as an anticancer agent, butyrate inhibits the growth and induces the apoptosis of cancer cells [6, 20, 21]. Previous studies have shown that butyrate inhibits the growth of human endometrial and ovarian cancer cells [22] and induces the apoptosis of breast cancer cells [23]. However, recent microbiota studies have revealed a higher abundance of butyrate-producing bacteria in patients with CRC than in the non-CRC population [2, 24, 25]. Furthermore, a correlation exists between butyrate resistance and chemoresistance [26]. Acquired resistance to butyrate induces the development of a malignant phenotype,

such as the one that decreases cell death under glucose-deprivation conditions in BR colon adenocarcinomas [27, 28]. A study on a BR CRC (HCT-116/BR) cell line indicated that resistance to butyrate resulted in the development of resistance against chemotherapies, such as paclitaxel, 5-FU, and doxorubicin [26]. Moreover, stem cell markers, such as *OCT4* and ATP-binding cassette (ABC) transporter (*ABCG2*), are also highly expressed in the HCT-116/BR cell line [29]; this may result in treatment failure. Therefore, understanding the mechanisms underlying the regulation of butyrate resistance may enable us to develop better treatment strategies to eliminate cancer cells and/or improve the quality of life of patients with CRC.

In this study, we established a BR CRC cell line and subsequently evaluated the characteristics of the resistant cells, including cell morphology, butyrate sensitivity, and expression of butyrate- and drug efflux-related genes. Proteomic analyses were performed to determine the differences in parental (PT) and BR cells. Cell migration was used as an indicator of aggressiveness. Finally, anticancer drugs, including 5-FU, Oxa, and Met, were used to evaluate the cellular response. The experimental design is shown in Figure 1.

2. Materials and Methods

2.1. Cell Culture. The epithelial colorectal carcinoma cell lines, HCT-116 and PMF-K014, were grown in Dulbecco's
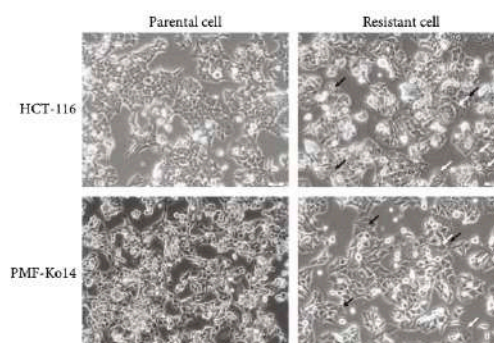
FIGURE 2: Micrographs of HCT-116 and PMF-K014 parental and butyrate-resistant subcell lines. Cell morphology was visualized using light microscopy. Increased vacuolization (black arrows) and cellular volume (white arrows) are indicated. Scale bar = 50 μm.
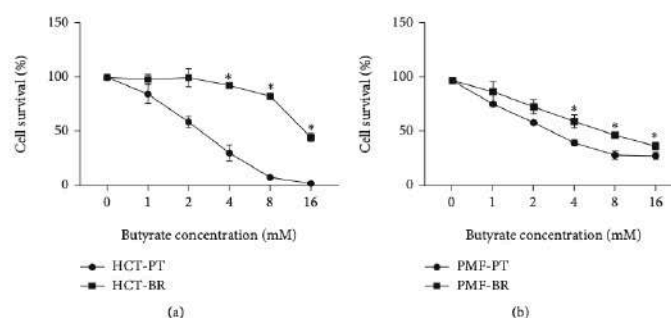

FIGURE 3: Cell survival determined using the 3-[4,5-dimethylthiazol-2-yl]-2,5-diphenyltetrazolium bromide (MTT) assay. Effects of butyrate on HCT-116 (a) and PMF-K014 (b) parental (PT) and butyrate-resistant (BR) cells. Dose-response curves of butyrate over 72 h. The data are expressed as means ± standard deviation (SD) of triplicate experiments. Statistically significant differences were determined using Student's t-test ($^*p$ value<0.05). Abbreviations: HCT-PT: HCT parental cells; HCT-BR: butyrate-resistant HCT cells; PMF-PT: PMF parental cells; PMF-BR: butyrate-resistant PMF cells.

Modified Eagle Medium (Gibco™ Thermo Fisher Scientific, Waltham, USA) supplemented with 10% heat-inactivated fetal bovine serum (Gibco™ Thermo Fisher Scientific) and 1% penicillin/streptomycin (Gibco™ Thermo Fisher Scientific) in a humidified incubator with an atmosphere of 5% CO_2 at 37°C.

2.2. Establishment of a BR CRC Cell Line.
HCT-116 and PMF-K014 cells were initially stimulated in complete-medium supplemented with 0.2 mM sodium butyrate (Sigma-Aldrich, St. Louis, USA). Butyrate treatment induced cancer cell death. However, some cells survived and continued to proliferate; these were considered BR. BR cells were subcultured till 80% confluent. Subsequently, the concentration of butyrate was increased twofold every three generations. After the concentration of butyrate reached 3.2 mM, BR cells were used in further experiments.

TABLE 1: IC_{50} values of butyrate according to the cells.

Cell lines	Butyrate (mM, mean ± SD)	Fold	p value (t-test)
HCT-PT	2.76 ± 0.05	5.38	>0.01
HCT-BR	14.85 ± 0.67		
PMF-PT	6.57 ± 0.80	3.00	>0.01
PMF-BR	19.72 ± 1.62		

2.3. Butyrate-Sensitivity Assay.
The cytotoxic effects of butyrate on the cells were determined using a tetrazolium bromide colorimetric assay (3-[4,5-dimethylthiazol-2-yl]-2,5-diphenyltetrazolium bromide; MTT). PT (HCT-PT and PMF-PT) and BR (HCT-BR and PMF-BR) cells were seeded in 96-well plates and incubated with various concentrations of butyrate (0–30 mM) for 72 h. After incubation, MTT was
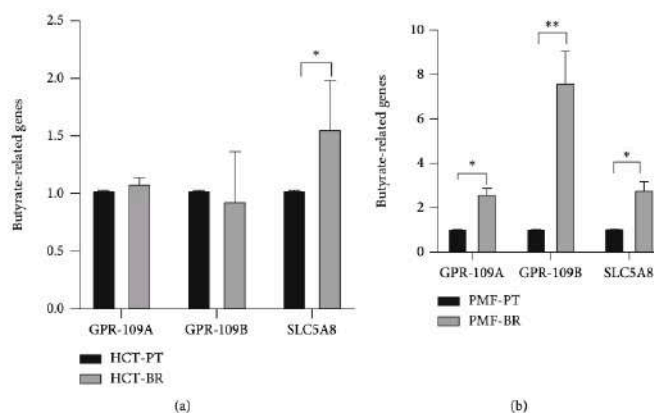
(a)   (b)

FIGURE 4: Relative expression of butyrate-related genes in HCT (a) and PMF (b) cells. Expression (*GPRI09A*, *GPRI09B*, and *SLC5A8*) is shown relative to that of *GAPDH*. Data are expressed as means ± SD of triplicate experiments. Significant differences were determined using Student's t-test (*p value<0.05, **p value<0.01).

added to the cells and incubated for 2 h. To determine the MTT results, dimethyl sulfoxide (DMSO; Sigma-Aldrich) was added to the cells and incubated for 30 min. The absorbance of formazan was recorded using a microplate spectrophotometer system (SpectraMax 190, Molecular Devices, San Jose, USA). The results were analyzed using the SoftMax Pro software (version 2.2.1) and presented as the percentage of cell survival compared with control values.

2.4. Evaluation of the Expression of Butyrate-Related Genes Using Quantitative Reverse-Transcription Polymerase Chain Reaction (qRT-PCR). To determine the expression of butyrate-related genes, total RNA was isolated from PT and BR cells using the TRIzol Reagent (Invitrogen, Waltham, USA) in accordance with the manufacturer's instructions. RNA was then quantified using absorbance measurements, 1.5% agarose gel electrophoresis, and a Nanodrop (Thermo Fisher Scientific). RNA samples (1 μg) of sufficient quality were reverse-transcribed into complementary DNA (cDNA) [30, 31] using an iScript™ cDNA synthesis kit (Bio-Rad Laboratories, Hercules, USA) in accordance with the manufacturer's instructions. *GAPDH* was used as the internal control. Differential expression of butyrate-related genes and *ABC* transporters was determined. The primer sequences are listed in Table S1. Quantitative reverse-transcription PCR (qRT-PCR) was performed in duplicates with three independent experiments. The delta-delta Ct ($2^{-(\Delta\Delta Ct)}$) method was used to calculate the relative gene expression levels.

2.5. Proteomic Analysis. Mass spectrometry was performed at the Functional Proteomics Technology Laboratory, National Center for Genetic Engineering and Biotechnology (BIOTEC), Thailand. The PT and BR proteins were reduced,

alkylated, digested with trypsin, and analyzed by liquid chromatography-mass spectrometry (MS) (Impact II, Bruker, Billerica, USA). Differentially expressed proteins were quantified and identified using the DeCyder MS differential analysis software 2.0 (GE Healthcare, Chicago, USA) and MASCOT search engine (Matrix Science, London, UK) based on the NCBI human protein database. Proteins differentially expressed among cell types were analyzed for pathway enrichment using Kyoto Encyclopedia of Genes and Genomes (KEGG) analysis by employing *R* (version 4.1.1; *R* Foundation for Statistical Computing, Vienna, Austria). Uniquely expressed proteins in each cell type were categorized using PANTHER (version 16.0) and UniProt.

2.6. Cell Migration Assay. To determine the migration of each cell, cell migration or wound healing assays were conducted as previously described [32]. Briefly, a 90–95% confluent cell monolayer was scratched using a pipette tip to generate a wound. Images were captured 0, 6, 12, and 24 h after wound scratching. The ImageJ (version 1.34) was then used to calculate the wound field.

2.7. Anticancer Drug Sensitivity Assay. The cytotoxic effects of anticancer drugs, including 5-FU, Oxa, and Met, were evaluated using the MTT assay. PT and BR cells were seeded in 96-well plates and incubated with various concentrations of the drugs for 72 h. After incubation, MTT was added to the cells and incubated for 2 h. To detect the MTT results, DMSO (Sigma-Aldrich) was added and incubated for 30 min. The absorbance of formazan was recorded using a microplate spectrophotometer system (SpectraMax190, Molecular Devices). The results were analyzed using Soft-MaxPro (version 2.2.1) and presented as the percentage of inhibition compared with control values.
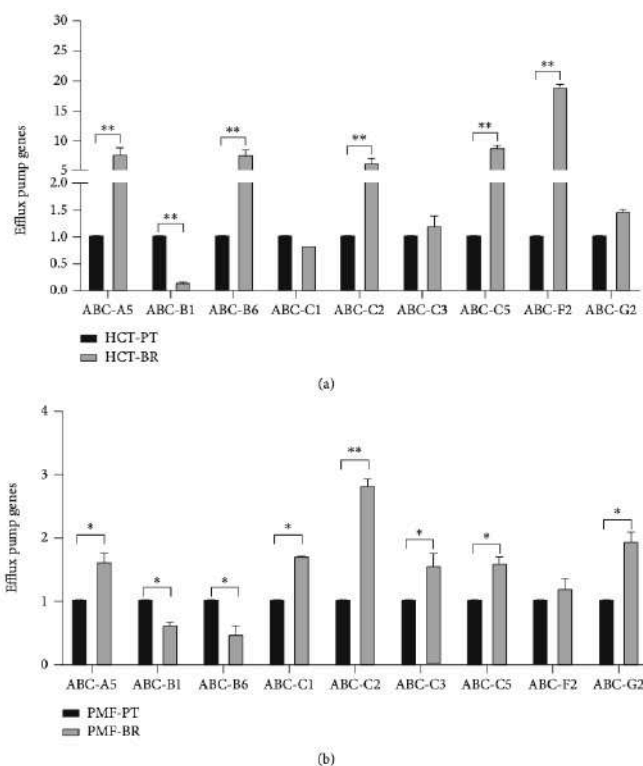
BioMed Research International

(a)

(b)

FIGURE 5: Relative expression of drug efflux genes in HCT (a) and PMF (b) cells. Expression is shown relative to *GAPDH* expression. Data are expressed as means ± SD of triplicate experiments. Significant differences were determined using Student's *t*-test (*p value<0.05).

2.8. Statistical Analysis. Data are presented as the mean ± standard deviation (SD) of at least three independent experiments. A Student's *t* -test (two-tailed, unpaired) was used to evaluate the statistical significance of results from all experiments.

3. Results

3.1. Cellular Morphology of BR Cells. Human colon cancer HCT-116 and PMF-K014cell lines were used to generate BR cells: HCT-BR and PMF-BR cells, respectively. To develop butyrate resistance, the cells were exposed to butyrate for three months. The morphology of the BR cells was altered slightly relative to that of the PT cells as shown in Figure 2. The HCT-116 PT cells displayed a sharp-pointed shape, while the HCT-BR cells were more rounded and expanded. The PMF-K014 PT cells displayed a polygonal epithelial structure indicating robust cell-cell interactions, while the BR cells showed a decrease in cell-cell interactions

compared to the PT cells. Vacuolization was also observed in BR cells (indicated by black arrows).

3.2. Butyrate Sensitivity. MTT assays were used to determine the 50% inhibitory concentration (IC_{50}) to evaluate the butyrate sensitivity of PT and BR cells. The viability of BR cells was significantly higher than that of their PT cells. Cell survival is shown in Figure 3, and the IC_{50} of each cell line is shown in Table 1. The IC_{50} value of the HCT-BR cells was 5.38-fold higher than that of the HCT-PT cells. For PMF-BR cells, the IC_{50} was 19.72, which was 3.00-fold higher than that of their PT cells.

3.3. Expression of Butyrate-Related Genes and Drug Efflux Pumps. The expression of butyrate-related genes was determined using GAPDH as an internal control. Figures 4 and 5 show the relative expression of butyrate-related genes and drug efflux pumps, respectively. Hydroxycarboxylic acid receptor 2 (GPR109A), which is a butyrate receptor, its
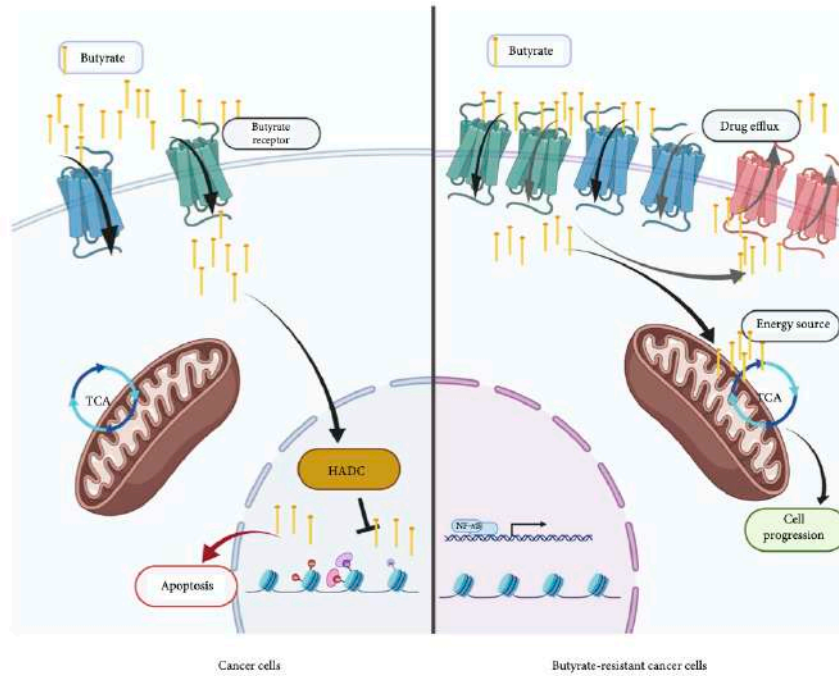
FIGURE 6: Schematic illustration of the proposed mechanism of butyrate resistance development. Abbreviations: HDAC: histone deacetylase; TCA: tricarboxylic acid cycle. The schematic was created https://usingbiorender.com/.
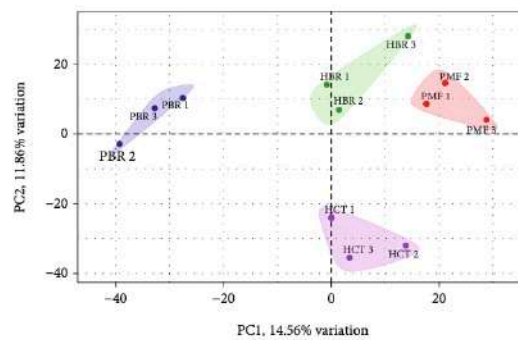
FIGURE 7: Principal component analysis (PCA) of the proteomic data in a 2-dimensionalgraph of PC1 and PC2. The biplot shows proteomic data (scores) as labeled dots and cell types as vectors for the parental (HCT and PMF) and butyrate-resistant (HBR and PBR) cells. Abbreviations: HCT: HCT parental cells; HBR: butyrate-resistant HCT cells; PMF: PMF parental cells; PBR: butyrate-resistant PMF cells.

FIGURE 8: Venn diagram illustrating the relationship between HCT (a) and PMF (b) annotated genes.

homolog GPR109B, and sodium-coupledmonocarboxylate transporter 1 (SLC5A8 or SMCT1) respond to the transport of bacterial metabolites, particularly butyrate, in intestinal cells. BR cells showed higher expression of these receptors than PT cells. SLC5A8 was significantly upregulated in HCT-BR cells, whereas all three receptors were significantly upregulated in PMF-BR cells. To evaluate the expression of the efflux pump, the expression of the ABC transporter, which plays an important role in drug transport in cancer cells, was evaluated. BR cells showed higher expression of this drug efflux gene than PT cells but showed different patterns of expression for the efflux genes. We found that the ABC-A5 and ABC-C5 were significantly upregulated in both BR cells compared with that in the corresponding PT cells. The expression of ABC-B1was low in both BR cell types. HCT-BR cells showed higher expression of ABC-B6, ABC-C2, ABC-C5, and ABC-F2 than HCT-PR cells. Simultaneously, PMF-BR cells showed higher expression of ABC-C1, ABC-C3, and ABC-G2 than PMF-PT cells. However, the expression of ABC-B6 was not clear. We proposed a mechanism for resistance in Figure 6.

3.4. Differential Protein Expression in PT and BR Cells. To investigate the characteristics of the PT and BR cells, principal component analysis (PCA) of the proteomic data was performed (Figure 7). The low dimensional variations (PC1 14.56% and PC2 11.86%) suggested that most proteins were identical among all cells, which maybe because the principal protein characteristics of all CRC cells are the same across cell types and resistance statuses. However, some unique proteins were identified in the PCA plot and used to distinguish clusters between PT and BR cells in both cell types (i.e., butyrate-resistant PMF cells [PBR] vs. PMF in PC1 and butyrate-resistant HCT cells [HBR] vs. HCT in PC2). Venn diagrams (Figure 8) confirmed this finding by showing that PT and BR cells shared 90% (2,644 proteins) and 80% (2,285 proteins) of the proteins in HCT and PMF cells, respectively. We analyzed the unique proteins according to cell type and resistance status and found that 3.84% (112 proteins) and 5.56% (162 proteins) were found in HCT-PT and HCT-BR cells, respectively. Unique proteins in PMF cells accounted for 11.10% (313 proteins) and 7.70% (217 proteins) in PT and BR cells, respectively. The

differential expression of proteins is shown in Figure 9, and the protein names are listed in Tables 2 and 3. We identified differential expression of proteins between the HCT and PMF cells, and 2,916 and 2,816 proteins were differentially expressed in HCT and PMF cells, respectively. Notably, the expression of coatomer complex subunit beta 2(COPB2), an essential protein required for Golgi budding and vesicular trafficking [33], was decreased in both HCT-BR and PMF-BR cells, compared with that in the corresponding PT cells. A pie chart showing the biological process annotations of the proteins in each cell type is shown in Figure 10. HCT-BR cells expressed more biological processes than their PT cells did, including localization, response to stimuli, signaling, biological adhesion, and locomotion. For the PMF cells, PMF-BR expressed fewer biological processes than their PT cells did, except the interspecies interaction between organisms, with PMF-PT cells expressing greater reproductive and multiorganism processes, reproduction, biological adhesion, and locomotion. We then used a bar graph to illustrate KEGG pathway enrichment (Figure 11). The pathways that were enriched in both PT cell lines were protein digestion and absorption, the phosphatidylinositol 3-kinase/Akt pathway, and pathways involved in cancers. For HCT-BR cells, pathways involved in homologous recombination and mismatch repair and signaling pathways were enriched. For PMF-BR cells, adherent junctions, cytokines, and receptors were enriched.

3.5. Cell Migration. To examine the migration capacity of PT and BR cells, we conducted wound healing assays. The field containing the wound area after 24 h is shown in Figure 12, and the percentage of migrated cells is shown in Figure 12(b)and Table S2. We found a significant difference between the migration rates of PT and BR cells. The migration rate in HCT-PT cells (45.81%) was higher than in BR cells(33.29%). However, the migration rate in PMF-BR cells (37.96%)was higher than in their PT cells (25.39%).

3.6. Anticancer Drug Sensitivity. To test the anticancer drug sensitivity of the cells, the MTT results were used to calculate the IC$_{50}$. The IC$_{50}$ of each cell was determined using data from three independent experiments and analyzed using

8
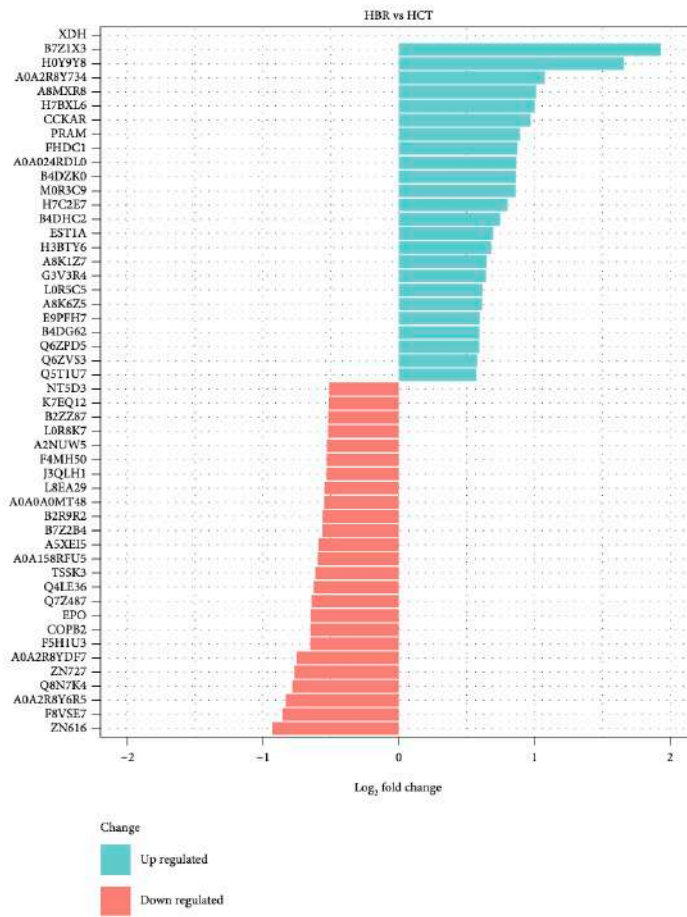
(a)

Figure 9: Continued.

65
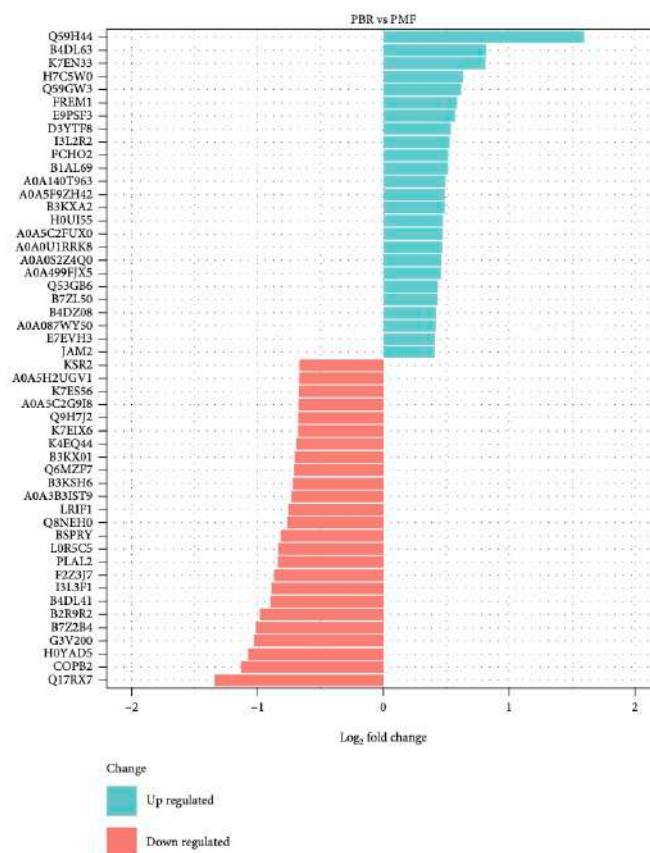
FIGURE 9: Top 10 differentially expressed proteins in HCT (a) and PMF (b) cells.

Student's t-test. The IC$_{50}$ values of PT and BR cells are listed in Table 4. We found crossresistance of chemotherapy agents in BR cells; HCT-BR cells showed crossresistance to Oxa at 28.67 μM (13.5-fold) and MET at 6.41 mM (3.66-fold). However, PMF-BR cells showed crossresistance to 5-FU at 26.18 μM (1.7-fold).

4. Discussion

Butyrate is an anticancer agent against which resistance has been reported in CRC cells. However, the mechanism underlying the development of butyrate resistance in CRC cells remains unclear. Investigation of the mechanism by which butyrate resistance develops in cells may help establish new therapeutic strategies for CRC. HCT-BR and PMF-BR cells

were established by continuously exposing the cells to butyrate. BR cells showed slight differences in morphology with respect to their PT cells based on the results of inverted light microscopy. Increasing vascularization and cellular volume were found in BR cells. This result is similar to that of previous studies in BCS-TC2. BR2 cells, a BR human colon adenocarcinoma cell line, showed an increase in vacuolization and cellular volume [27]. The butyrate sensitivity test revealed that BR cells had a higher survival rate than the PT cells in both cell lines. The IC$_{50}$ values were also higher in BR cells than in PT cells in both cell lines. These results confirm that the BR cells exhibit greater resistance to butyrate than PT cells.

Several mechanisms are involved in the resistance to butyrate, including alteration of the drug target and drug

TABLE 2: Top 10 upregulated and downregulated proteins in HCT cells.

HBR vs. HCT	Entry	Protein	Function
Up	XDH	Xanthine dehydrogenase/oxidase	Key enzyme in purine degradation
	B7Z1X3	Dynein regulatory complex subunit 4	Microtubule binding, small GTPase binding
	H0Y9Y8	RUN and FYVE domain-containing protein 1	Binds phospholipid vesicles containing phosphatidylinositol 3-phosphate and participates in early endosomal trafficking
	A0A2R8Y734	Thrombopoietin	Lineage-specific cytokine affecting the proliferation and maturation of megakaryocytes from their committed progenitor cells
	A8MXR8	PHD finger protein 20-like protein 1	Regulation of transcription, DNA-templated
	H7BXL6	Otogelin-like protein	Extracellular region
	CCKAR	Cholecystokinin receptor type A	Receptor for cholecystokinin. Mediates pancreatic growth and enzyme secretion, and smooth muscle contraction of the gall bladder and stomach.
	PRAM	PML-RARA-regulated adapter molecule 1	Lipid binding, protein kinase binding, and integrin-mediated signaling pathway
	FHDC1	FH2 domain-containing protein 1	Protein localization to plasma membrane
	A0A024RDL0	DNA-directed RNA polymerase III subunit RPC9	Microtubule-associated formin which regulates both actin and microtubule dynamics
Down	Q7Z487	Transforming growth factor beta 1	DNA-directed 5′-3′RNA polymerase activity and nucleotide binding
	EPO	Erythropoietin receptor	Growth factor activity
	COPB2	Coatomer subunit beta′	Receptor for erythropoietin mediates erythropoietin-induced erythroblast proliferation and differentiation. Upon EPO stimulation, EPOR dimerizes triggering the JAK2/STAT5 signaling cascade
	F5H1U3	Peptidylprolyl isomerase	The coatomer is a cytosolic protein complex that binds to dilysine motifs and reversibly associates with Golgi nonclathrin-coated vesicles, which further mediate biosynthetic protein transport from the ER, via the Golgi up to the trans Golgi network
	A0A2R8YDF7	Lysine-specific demethylase 4A	FK506 binding
	ZN727	Putative zinc finger protein 727	Heat shock protein binding
	Q8N7A4	cDNA FLJ25865 cis, clone CBR01927	Peptidyl-prolyl cis-transisomerase activity
	A0A2R8Y6R5	Caseinolytic peptidase B protein homolog	Histone demethylase that specifically demethylates "Lys-9" and "Lys-36" residues of histone H3, thereby playing a central role in the histone code
	F8VSE7	Transcription factor E2F7	DNA-binding transcription factor activity, RNA polymerase II-specific
	ZN616	Zinc finger protein 616	Uncharacterized protein

Abbreviations: HCT: HCT parental cells; HBR: butyrate-resistant HCT cells.

inactivation and efflux. To investigate the underlying mechanism in BR cells, we evaluated the expression of butyrate-related genes, including the butyrate receptors, GPR109A and GPR109B, and butyrate transporter, SLC5A8. We found different patterns of expression of butyrate-related genes in the two cell lines. HCT-BR cells showed an upregulation of SLC5A8, while PMF-BR cells showed an upregulation of GPR109A, GPR109B, and SLC5A8. In a previous study, the expression of butyrate-related genes was upregulated in BR mice compared with that in germ-free mice [34]. We also performed Kaplan–Meier survival analysis to evaluate the correlation between butyrate-related gene expression and

survival outcome of patients with cancer treated with 5-FU and/or Oxa using The Cancer Genome Atlas (TCGA) pan-cancer data portal. Interestingly, the Kaplan–Meier analysis showed that only patients with CRC with high SLC5A8 expression displayed significantly worse survival than patients with low expression (Figure S1). This finding suggests that high SLC5A8 expression found in BR cells represents a lower survival outcome in patients with CRC. We further investigated drug efflux gene expression. We found that the expression of ABC-B6, ABC-C5, and ABC-F2 was upregulated in HCT-BR cells, whereas that of ABC-C1, ABC-C3, and ABC-G2 was upregulated in PMF-BR

TABLE 3: Top 10 upregulated and downregulated proteins in PMF cells.

PBR vs. PMF	Entry	Protein	Function
Up	Q59H44	Lymphocyte antigen 75 variant	Integral component of membrane
	B4DL63	cDNA FLJ51231, highly similar to mitochondrial ornithine transporter 1	Integral component of membrane
	K7EN33	Notchless protein homolog 1	Plays a role in regulating notch activity. Plays a role in regulating the expression of CDKN1A and several members of the Wnt pathway, probably via its effects on notch activity
	H7C5W0	DnaJ homolog subfamily B member 5	Chaperone binding, unfolded protein binding
	Q59GW3	ST8 alpha-N-acetyl-neuraminide alpha-2,8-sialyltransferase 3 variant	Sialyltransferase activity, protein glycosylation
	FREM1	FRAS1-related extracellular matrix protein 1	Extracellular matrix protein that plays a role in epidermal differentiation and is required for epidermal adhesion during embryonic development
	E9PSF3	Bromodomain and PHD finger-containing protein 3	Metal ion binding
	D3YTF8	Thioredoxin-disulfide reductase	Protein has several cofactor binding sites
	I3L2R2	Protein PIMREG	During mitosis, may play a role in the control of metaphase-to-anaphase transition
	FCHO2	F-BAR domain only protein 2	Functions in an early step of clathrin-mediated endocytosis. Has both a membrane binding/bending activity and the ability to recruit proteins essential to the formation of functional clathrin-coated pits.
Down	PLAL2	Zinc finger protein PLAGL2	DNA-binding transcription activator activity, RNA polymerase II-specific, lipid metabolic process, positive regulation of intrinsic apoptotic signaling pathway
	F2Z3J7	Rab-like protein 2B	GTPase activity, GTP binding
	I3L3F1	Caspase recruitment domain-containing protein 14	Acts as a scaffolding protein that can activate the inflammatory transcription factor NF-kappa-B and p38/JNK MAP kinase signaling pathways
	B4DL41	cDNA FLJ57825, highly similar to DNA-dependent protein kinase catalytic subunit	Kinase activity, molecular function: kinase, transferase
	B2R9R2	cDNA, FLJ94517, highly similar to Homo sapiens baculoviral IAP repeat-containing 4 (BIRC4), mRNA	Metal ion binding
	B7Z2B4	cDNA FLJ53389, highly similar to Homo sapiens RAB GTPase activating protein 1 (RABGAP1), mRNA	GTPase activator activity
	G3V200	Liprin-alpha-2	Alters PTPRF cellular localization and induces PTPRF clustering. May regulate the disassembly of focal adhesions. May localize receptor-like tyrosine phosphatases type 2A at specific sites on the plasma membrane
	H0YAD5	Probable ATP-dependent RNA helicase DDX46	Protein predicted
	COPB2	Coatomer subunit beta 2	The coatomer is a cytosolic protein complex that binds to dilysine motifs and reversibly associates with Golgi nonclathrin-coated vesicles, which further mediate biosynthetic protein transport from the ER, via the Golgi up to the trans Golgi network.
	Q17RX7	Ras association (RalGDS/AF-6) domain family member 1	Intracellular signal transduction

Abbreviations: PMF: PMF parental cells; PBR: butyrate-resistant PMF cells.

cells. Moreover, *ABC-A5* and *ABC-C2* were upregulated in both BR cells. *ABC-C1* and *ABC-G2* are upregulated in Hep2-5-FU-resistant cells [35]. These two *ABC* transporters are considered chemoresistance-driving genes and play a role in the acquisition of chemoresistance. Additionally, *ABC-B6*, *ABC-C1*, *ABC-C3*, *ABC-C5*, *ABC-C10*, and *ABC-F2* are found in paclitaxel-resistant cells. Furthermore, doxorubicin resistance in breast cancer cells is induced by the overexpression of *ABC-C1* and *ABC-F2* [36, 37]. Lastly, cells expressing *ABC-A5* and *ABC-F2* show stem cell features [38]. We further evaluated the cytotoxicity of anticancer drugs including Met, 5-FU, and

HCT-PT

Total = 100%

☐ Developmental process (GO: 0032502)
☐ Cellular process (GO: 0009987)
☐ Multicellular organismal process (GO: 0032501)
☐ Metabolic process (GO: 0008152)
☐ Biological regulation (GO: 0065007)

(a)

HBR-PT

Total = 100%

☐ Cellular process (GO: 0009987)
☐ Localization (GO: 0051179)
☐ Biological regulation (GO: 0065007)
☐ Response to stimulus (GO: 0050896)
☐ Signaling (GO: 0023052)
☐ Developmental process (GO: 0032502)
☐ Biological adhesion (GO: 0022610)
☐ Locomotion (GO: 0040011)
☐ Multicellular organismal process (GO: 0032501)
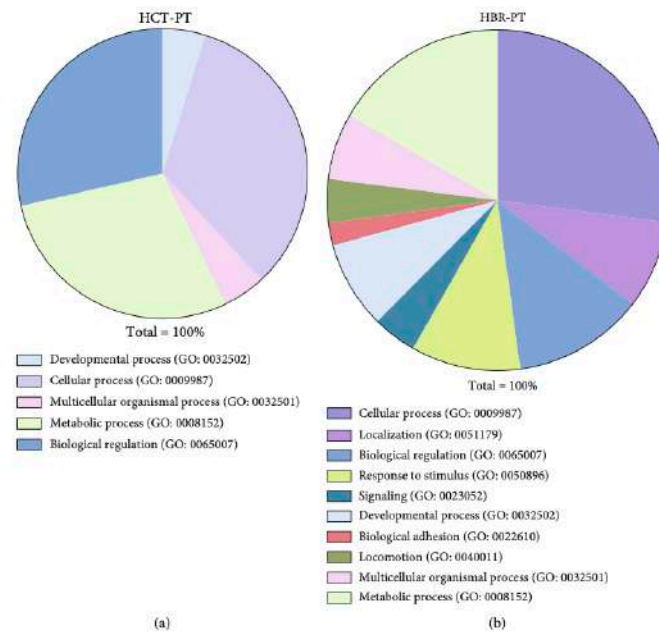☐ Metabolic process (GO: 0008152)
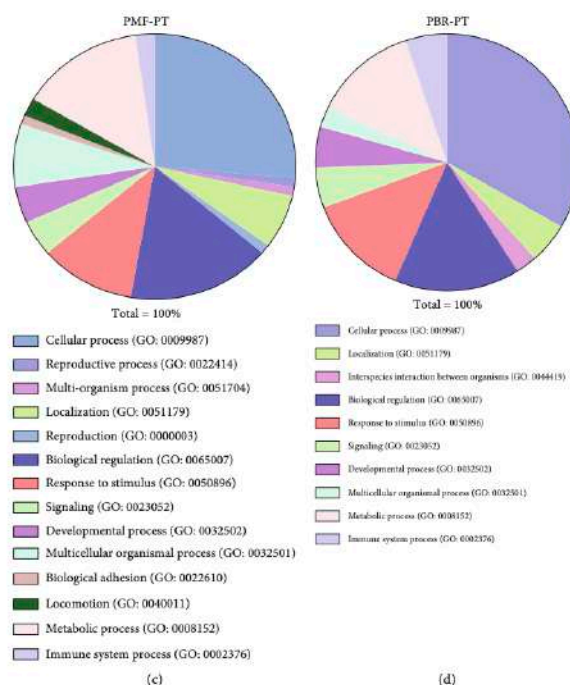
(b)

FIGURE 10: Continued.

FIGURE 10: Pie chart showing the biological processes of the HCT-PT (a), HCT-BR (b), PMF-PT (c), and PMF-BR (d) cells.

Oxa against PT and BR cells in both HCT and PMF cells. The results revealed different drug responses in different cells. HCT-BR showed a crossresistance toward Met and Oxa, while PMF-BR showed a crossresistance to 5-FU; similarly, our previous study demonstrated that PMF-BR spheroid cells were also crossresistant to 5-FU [39]. This crossresistance may be due to the upregulation of *ABC* transporters.

Proteomic analysis identified differential expression of proteins in HCT and PMF cells. PCA showed a difference between the BR and PT cell groups. A 14.56% variation in PC1 showed a shared dimension in HCT cells but presented a dissimilarity in PMF cells. Simultaneously, an 11.86% variation in PC2 showed a shared dimension in PMF cells whereas indicated a distinct feature of HCT cells. PCA indicated that there were some differences and similarities between PT and BR cells, and the Venn diagrams correlated with these results. The Venn diagram showed that several proteins were shared between the PT and BR cells; however, there were some unique proteins present in each cell, which resulted in differences in cell characteristics. We used the University of Alabama at Birmingham Cancer (UALCAN) data analysis portal (http://ualcan.path.uab.edu/index.html) to explore the relevant proteins enriched for the differen-

tially expressed genes. We found that the expression of COPB2 was decreased in both HCT-BR and PMF-BR cells. Regarding this unique finding in HCT-BR cells, we discovered two proteins from UALCAN that showed increased expression levels: xanthine dehydrogenase (XDH) and formin homology 2 domain-containing protein 1 (FHDC1). In the PMF-BR cells, the expression of FRAS1-related extracellular matrix 1 (FREM1) showed an increase. The COPB2 protein is related to a dilated endoplasmic reticulum (ER) with granular material, prominent rough ER, and vacuoles resulting in intracellular trafficking deficiency [33]. In cancer, COPB2 is highly expressed in glioblastomas and hepatocellular carcinomas, resulting in a worse overall survival [40, 41]. Additionally, studies on CRC cells have found that COPB2 plays an essential role in cancer cell proliferation and cell cycle progression [42]. The UALCAN database showed that the expression of COPB2 increases in CRC patients. However, the levels of the phosphorylated form of this protein were found to be decreased in every stage of CRC (Figure S2). The level and function of COPB2 across different cancers is controversial. Therefore, the function of COPB2 in BR-CRC requires further investigation. In HCT-BR cells, XDH exerts purine oxidation and electron acceptor functions and is highly expressed in uterine
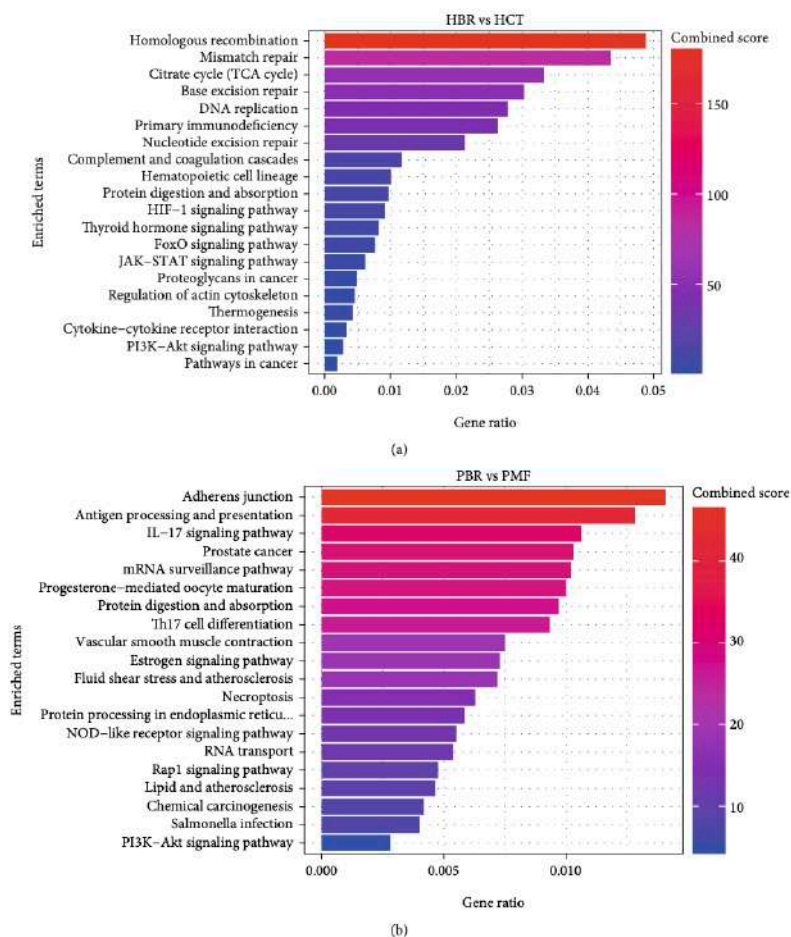
FIGURE 11: The top 20 KEGG enrichment pathways of the HCT (a) and PMF (b) cells.

corpus endometrial carcinoma and lung and pancreatic cancers(Figure S3). Furthermore, XDH is expressed at lower levels in colon adenocarcinoma tissue than in healthy tissue. Our study was performed in HCT cells which are derived from primary colorectal carcinoma [43]. Therefore, there may be a difference in the expression of XDH. A previous pan-cancer study showed that XDH is involved in proinflammatory and immune stimulation. Additionally, increases in XDH combined with adenine phosphoribosyl transferase, a key enzyme in the purine salvage pathway, result in increased sensitivity to 5-FU [44]. This finding requires further investigation to predict

the effects of 5-FU more effectively in patients with CRC and the BR phenotype. Another upregulated protein in HCT-BR cells was FHDC1, a microtubule-associated formin involved in regulating actin and microtubule dynamics. The expression of FHDC1 is increased in various cancers including CRC and at its highest level in stage 1 cancer (Figure S4). A study in lung adenocarcinoma reported that the high expression of FHDC1 was associated with significantly improved survival outcomes compared with that of low expression [45]. In PMF polygonal epithelial cells derived from the peritoneal dissemination of highly metastatic patients with CRC [46],
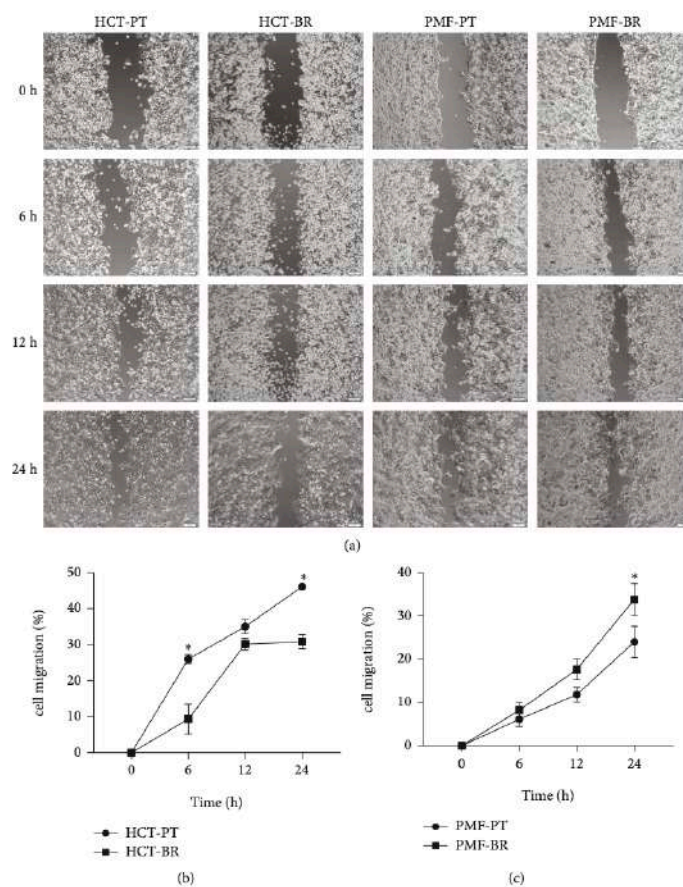
(a)

(b)

(c)

FIGURE 12: The capacity for cell migration (%) determined by wound healing assays. Parental and butyrate-resistant cells were incubated 24 h after wound field generation. (a) Wound fields were captured by inverted microscopy (×10 magnification). Scale bar = 100 μm. The line graph represents the percentage of migration of HCT (b) and PMF (c) cells. Significant differences were determined using Student's t-test ($^*p$ value <0.05).

we found the higher expression of FREM1 in CRC patients than in healthy patients, with the highest expression in stage 4 patients (Figure S5). FREM1 plays a role in epidermal differentiation and is required for epidermal adhesion during embryonic development. However, the function of FREM1 in cancer is not well understood. A study in breast cancer showed that the expression of FREM1 was dramatically decreased, which correlated with a lower overall and recurrence-free survival [47]. However, the expression of FREM1 in CRC differs from that in breast cancer. Moreover, FREM1 levels increased in the primary tumor and higher cancer stages. However, the

function of FREM1 in CRC remains unclear and requires investigation.

Cell migration was also investigated to evaluate the aggressiveness of BR and PT cells, and differences were found. HCT-BR showed a lower migration rate than HCT-PT. This may be due to the downregulation of the erythropoietin receptor, which is related to the downregulation of the JAK2/STAT5 signaling cascade [48, 49]. In contrast, the PMF-BR cells showed a higher migration rate than PMF-PT cells. The protein expression profile showed the upregulation of Notchless protein homolog 1 in PMF-BR cells. This protein plays a role in Notch activity which

TABLE 4: The cytotoxicity values (IC_{50}) of the anticancer agents against the HCT and PMF cell lines.

Cell lines	Metformin (mM, mean ± SD)	Fluorouracil (μM, mean ± SD)	Oxaliplatin (μM mean ± SD)
HCT-PT	1.75 ± 0.07	9.70 ± 0.09	2.13 ± 0.13
HCT-BR	$6.41 \pm 0.18^{**}$	9.45 ± 0.27	$28.76 \pm 3.43^{**}$
PMF-PT	1.67 ± 0.28	15.07 ± 1.74	28.15 ± 3.90
PMF-BR	1.58 ± 0.15	$26.18 \pm 4.37^{*}$	26.92 ± 4.82

*p value <0.05, **p value <0.01.

is known to promote cell migration and invasion in brain cancer [50].

Taken together, our findings suggest that 5-FU may be used as a potential anticancer agent in HCT-BR cells, representing primary tumor treatment. Meanwhile, Met and Oxa may be effective in PMF-BR cells, which represent metastatic tumors. However, further studies are needed to investigate the effects of Met.

5. Conclusions

Herein, we investigated the characteristics of butyrate resistance in CRC cells in both primary and metastatic conditions. The mechanisms underlying the development of butyrate resistance involve an increase in the expression levels of various efflux genes. The proteins expressed in the BR cells shared some parental characteristics, while unique proteins showed characteristic of resistance. Our study also confirmed that chemotherapy resistance arises from butyrate resistance in CRC cells. Moreover, Met showed a potential therapeutic effect against PMF-BR cells. Thus, further investigation of Metin, the molecular mechanism underlying butyrate resistance, is needed for its use in clinical settings to enhance the effectiveness of CRC therapies. Lastly, the effects of anticancer drugs on BR CRC cells requires further investigation in animal models.

Data Availability

The data that support the findings of this study are available from the corresponding author (Navakanitworakul, R), upon reasonable request (nraphatp@medicine.psu.ac.th).

Conflicts of Interest

The authors declare that there is no conflict of interest regarding the publication of this article.

Authors' Contributions

Conceptualization was contributed by R.N. and S.S. Methodology was contributed by K.N. Software was contributed by S.R. and K.L. Formal analysis was contributed by K.N. Investigation was contributed by K.N. Data curation was contributed by K.N. Writing-original draft preparation was contributed by K.N. Writing-review and editing was contributed by R.N. Supervision was contributed by R.N. All authors have read and agreed to the published version of the manuscript.

Acknowledgments

Supplementary Materials

Supplementary 1. Table S1: primer sequences used for butyrate receptors and drug efflux pumps. Supplementary 2. Table S2: the migration rate (%) of parental and butyrate-resistant cells. Figure S1: Kaplan–Meier survival analysis of cancer patients treated with 5-fluorouracil (5-FU), oxaliplatin (Oxa), or metformin (Met). (a)–(d) The survival probability curve related to SLC5A8 expression in various cancer types, such as colon adenocarcinoma (COAD) and rectal adenocarcinoma (READ) (a), stomach adenocarcinoma (STAD) (b), breast invasive carcinoma (BRCA) (c), and pancreatic adenocarcinoma (PAAD) (d). Abbreviations: TCGA: The Cancer Genome Atlas. Supplementary 4. Figure S2: the expression level of coatomer complex subunit beta (COPB2) in various types of cancers. (a) COPB2 showed higher expression in cancer patients than in healthy tissue. (b) Comparison between the expression of COPB2 in colorectal cancer in healthy and primary tumor tissues. (C) The expression of the phosphorylated form of COPB2 in each stage of cancer. Z values represent standard deviations from the median across samples for the given cancer type. Abbreviations: CPTAC: Clinical Proteomic Tumor Analysis Consortium; RCC: renal cell carcinoma; UCEC: uterine corpus endometrial carcinoma. Figure S2: expression of coatomer complex subunit beta 2 (COPB2) in various types of cancers. (a) COPB2 showed higher expression in cancer patients than in healthy individuals. (b) Comparison between the expression of COPB2 in colorectal cancer in healthy and primary tumor tissues. (c) Levels of the phosphorylated form of COPB2 in each stage of cancer. Z values represent standard deviations (SD) from the median across samples for the given cancer type. Abbreviations: CPTAC: Clinical Proteomic Tumor Analysis Consortium; RCC: renal cell carcinoma; UCEC: uterine corpus endometrial carcinoma. Figure S3: expression of xanthine dehydrogenase (XDH) in various types of cancers. (a) XDH showed higher expression in cancer patients than in normal healthy individuals. (b) Expression of XDH in colorectal cancer in normal healthy and primary tumor tissues. (c) Expression of XDH in each stage of cancer. Z values represent SD from the median across samples for the given cancer type. Figure S4: expression of formin homology 2 domain-containing protein 1

(FHDC1) in various types of cancers. (a) FHDC1 showed higher expression in cancer patients than in normal healthy individuals. (b) Expression of FHDC1 in colorectal cancer in normal healthy and primary tumor tissues. (c) Expression of FHDC1 in each stage of cancer. Log2 spectral count ratio values from CPTAC were first normalized within each sample profile and then normalized across samples. Figure S5: expression of FRAS1-related extracellular matrix 1 (FREM1) in various types of cancers. (a) FREM1 showed higher expression in cancer patients than in normal healthy individuals. (b) Expression of FREM1 in colorectal cancer in normal healthy and primary tumor tissues. (c) Expression of FREM1 in each stage of cancer. Log2 spectral count ratio values from CPTAC were first normalized within each sample profile and then normalized across samples. *(Supplementary Materials)*

References

[1] V. Lohsiriwat, N. Chaisomboon, J. Pattana-Arun, and For the Society of Colorectal Surgeons of Thailand, "Current colorectal cancer in Thailand," *Annals of Coloproctology*, vol. 36, no. 2, pp. 78–82, 2020.

[2] E. Saus, S. Iraola-Guzmán, J. R. Willis, A. Brunet-Vega, and T. Gabaldón, "Microbiome and colorectal cancer: roles in carcinogenesis and clinical potential," *Molecular Aspects of Medicine*, vol. 69, pp. 93–106, 2019.

[3] T. Armaghany, J. D. Wilson, Q. Chu, and G. Mills, "Genetic alterations in colorectal cancer," *Gastrointestinal Cancer Research*, vol. 5, no. 1, pp. 19–27, 2012.

[4] V. Namasivayam and S. Lim, "Recent advances in the link between physical activity, sedentary behavior, physical fitness, and colorectal cancer," *F1000Research*, vol. 6, p. 199, 2017.

[5] S. Jahani-Sherafat, M. Alebouyeh, S. Moghim, H. A. Amoli, and H. Ghasemian-Safaei, "Role of gut microbiota in the pathogenesis of colorectal cancer; a review article," *Gastroenterology and Hepatology from Bed to Bench*, vol. 11, no. 2, pp. 101–109, 2018.

[6] X. Wu, Y. Wu, L. He, L. Wu, X. Wang, and Z. Liu, "Effects of the intestinal microbial metabolite butyrate on the development of colorectal cancer," *Journal of Cancer*, vol. 9, no. 14, pp. 2510–2517, 2018.

[7] A. Koh, F. De Vadder, P. Kovatcheva-Datchary, and F. Bäckhed, "From dietary fiber to host physiology: short-chain fatty acids as key bacterial metabolites," *Cell*, vol. 165, no. 6, pp. 1332–1345, 2016.

[8] P. Louis, G. L. Hold, and H. J. Flint, "The gut microbiota, bacterial metabolites and colorectal cancer," *Nature Reviews Microbiology*, vol. 12, no. 10, pp. 661–672, 2014.

[9] N. Sermsri, T. Boonpipattanapong, P. Prechawittayakul, and S. Sangkhathat, "Influence of payer source on treatment and outcomes in colorectal cancer patients in a university hospital in Thailand," *Asian Pacific Journal of Cancer Prevention*, vol. 15, no. 20, pp. 9015–9019, 2014.

[10] B. Štabuc, "Systemic therapy for colorectal cancer," *Archives of Oncology*, vol. 11, no. 4, pp. 255–263, 2003.

[11] N. A. Dallas, L. Xia, F. Fan et al., "Chemoresistant colorectal cancer cells, the cancer stem cell phenotype, and increased sensitivity to insulin-like growth factor-I receptor inhibition," *Cancer Research*, vol. 69, no. 5, pp. 1951–1957, 2009.

[12] J. Hanprasertpong, I. Jiamset, A. Geater, T. Peerawong, W. Hemman, and S. Kornsilp, "The effect of metformin on oncological outcomes in patients with cervical cancer with type 2 diabetes mellitus," *International Journal of Gynecological Cancer*, vol. 27, no. 1, pp. 131–137, 2017.

[13] D. Chu, J. Wu, K. Wang et al., "Effect of metformin use on the risk and prognosis of endometrial cancer: a systematic review and meta-analysis," *BMC Cancer*, vol. 18, no. 1, pp. 1–11, 2018.

[14] N. Zhu, Y. Zhang, Y. Gong, J. He, and X. Chen, "Metformin and lung cancer risk of patients with type 2 diabetes mellitus: a meta-analysis," *Biomedical Reports*, vol. 3, no. 2, pp. 235–241, 2015.

[15] S. Gandini, M. Puntoni, B. M. Heckman-Stoddard et al., "Metformin and cancer risk and mortality: a systematic review and meta-analysis taking into account biases and confounders," *Cancer Prevention Research*, vol. 7, no. 9, pp. 867–885, 2014.

[16] Y. L. Tang, L. Y. Zhu, Y. Li et al., "Metformin use is associated with reduced incidence and improved survival of endometrial cancer: a meta-analysis," *Bio Med Research International*, vol. 2017, pp. 1–9, 2017.

[17] J. He, K. Wang, N. Zheng et al., "Metformin suppressed the proliferation of LoVo cells and induced a time- dependent metabolic and transcriptional alteration," *Scientific Reports*, vol. 5, no. 1, pp. 1–16, 2015.

[18] M. Al Hassan, I. Fakhoury, Z. El Masri et al., "Metformin treatment inhibits motility and invasion of glioblastoma cancer cells," *Analytical Cellular Pathology*, vol. 2018, Article ID 5917470, 2018.

[19] B. Mansoori, A. Mohammadi, S. Davudian, S. Shirjang, and B. Baradaran, "The different mechanisms of cancer drug resistance: a brief Review," *Pharmaceutical Bulletin*, vol. 7, no. 3, pp. 339–348, 2017.

[20] N. T. Baxter, A. W. Schmidt, A. Venkataraman, K. S. Kim, C. Waldron, and T. M. Schmidt, "Dynamics of human gut microbiota and short-chain fatty acids in response to dietary interventions with three fermentable fibers," *MBio*, vol. 10, no. 1, pp. e02518–e02566, 2019.

[21] M. Sun, W. Wu, Z. Liu, and Y. Cong, "Microbiota metabolite short chain fatty acids, GPCR, and inflammatory bowel diseases," *Journal of Gastroenterology*, vol. 52, no. 1, pp. 1–8, 2017.

[22] Y. Terao, J. I. Nishida, S. Horiuchi et al., "Sodium butyrate induces growth arrest and senescence-like phenotypes in gynecologic cancer cells," *International Journal of Cancer*, vol. 94, no. 2, pp. 257–267, 2001.

[23] Y. Wang, P. C. Hu, Y. B. Ma et al., "Sodium butyrate-induced apoptosis and ultrastructural changes in MCF-7 breast cancer cells," *Ultrastructural Pathology*, vol. 40, no. 4, pp. 200–204, 2016.

[24] M. Song and A. T. Chan, "Diet, gut microbiota, and colorectal cancer prevention: a review of potential mechanisms and promising targets for future research," *Current Colorectal Cancer Reports*, vol. 13, no. 6, pp. 429–439, 2017.

[25] S. H. Wong and J. Yu, "Gut microbiota in colorectal cancer: mechanisms of action and clinical applications," *Nature Reviews Gastroenterology & Hepatology*, vol. 16, no. 11, pp. 690–6704, 2019.

[26] H. R. Kang, H. G. Choi, C. K. Jeon, S. J. Lim, and S. H. Kim, "Butyrate-mediated acquisition of chemoresistance by human colon cancer cells," *Oncology Reports*, vol. 36, no. 2, pp. 1119–1126, 2016.

[27] I. L. De Silanes, N. Olmo, J. Turnay et al., "Acquisition of resistance to butyrate enhances survival after stress and induces malignancy of human colon carcinoma cells," *Cancer Research*, vol. 64, no. 13, pp. 4593–4600, 2004.

[28] N. Olmo, J. Turnay, E. Lecona et al., "Acquisition of resistance to butyrate induces resistance to luminal components and other types of stress in human colon adenocarcinoma cells," *Toxicology In Vitro*, vol. 21, no. 2, pp. 254–261, 2007.

[29] D. Surangkul, "Butyrate Selectively Enriches Stem-like Cells in Hct 116 Human," in *In Proceedings of the 43th Congress on Science and Technology of Thailand*, pp. 17–19, Bangkok, Thailand, October, 2017.

[30] T. D. Schmittgen and K. J. Livak, "Analyzing real-time PCR data by the comparative C_T method," *Nature Protocols*, vol. 3, no. 6, pp. 1101–1108, 2008.

[31] S. A. Bustin and R. Mueller, "Real-time reverse transcription PCR (qRT-PCR) and its potential use in clinical diagnosis," *Clinical Science*, vol. 109, no. 4, pp. 365–379, 2005.

[32] P. Friedl and K. Wolf, "Tumour-cell invasion and migration: diversity and escape mechanisms," *Nature Reviews Cancer*, vol. 3, no. 5, pp. 362–374, 2003.

[33] R. Marom, L. C. Burrage, R. Venditti et al., "*COPB2* loss of function causes a coatopathy with osteoporosis and developmental delay," *American Journal of Human Genetics*, vol. 108, no. 9, pp. 1710–1724, 2021.

[34] G. A. Cresci, M. Thangaraju, J. D. Mellinger, K. Liu, and V. Ganapathy, "Colonic gene expression in conventional and germ-free mice with a focus on the butyrate receptor GPR109A and the butyrate transporter SLC5A8," *Journal of Gastrointestinal Surgery*, vol. 14, no. 3, pp. 449–461, 2010.

[35] M. B. Duz and O. F. Karatas, "Expression profile of stem cell markers and ABC transporters in 5-fluorouracil resistant Hep-2 cells," *Molecular Biology Reports*, vol. 47, no. 7, pp. 5431–5438, 2020.

[36] J. P. Gillet, T. Efferth, D. Steinbach et al., "Microarray-based detection of multidrug resistance in human tumor cells by expression profiling of ATP-binding cassette transporter genes," *Cancer Research*, vol. 64, no. 24, pp. 8987–8993, 2004.

[37] C. F. Thorn, C. Oshiro, S. Marsh et al., "Doxorubicin pathways," *Pharmacogenetics and Genomics*, vol. 21, no. 7, pp. 440–446, 2011.

[38] M. B. Duz and O. F. Karatas, "Differential expression of ABCB1, ABCG2, and KLF4 as putative indicators for paclitaxel resistance in human epithelial type 2 cells," *Molecular Biology Reports*, vol. 48, no. 2, pp. 1393–1400, 2021.

[39] K. Nittayaboon, K. Leetanaporn, S. Sangkhathat, S. Roytrakul, and R. Navakanitworakul, "Cytotoxic effect of metformin on butyrate-resistant PMF-K014 colorectal cancer spheroid cells," *Biomedicine & Pharmacotherapy*, vol. 151, article 113214, 2022.

[40] Y. Zhou, X. Wang, X. Huang et al., "High expression of COPB2 predicts adverse outcomes: a potential therapeutic target for glioma," *CNS Neuroscience & Therapeutics*, vol. 26, no. 3, pp. 309–318, 2020.

[41] J. Zhang, X. Wang, G. Li et al., "COPB2: a novel prognostic biomarker that affects progression of HCC," *BioMed Research International*, vol. 2021, Article ID 6648078, 2021.

[42] Y. Wang, Z. Chai, M. Wang, Y. Jin, A. Yang, and M. Li, "COPB2 suppresses cell proliferation and induces cell cycle arrest in human colon cancer by regulating cell cycle-related proteins," *Experimental and Therapeutic Medicine*, vol. 15, no. 1, pp. 777–784, 2018.

[43] S. Chowdhury, M. Ongchin, E. Sharratt et al., "Intra-tumoral heterogeneity in metastatic potential and survival signaling between iso-clonal HCT116 and HCT116b human colon carcinoma cell lines," *PLoSOne*, vol. 8, no. 4, article e60299, 2013.

[44] Z. Saidak, C. Louandre, S. Dahmani et al., "A pan-cancer study of the transcriptional regulation of uricogenesis in human tumours: pathological and pharmacological correlates," *Bioscience Reports*, vol. 38, no. 5, article 20171716, 2018.

[45] R. Wang, H. Zhu, M. Yang, and C. Zhu, "DNA methylation profiling analysis identifies a DNA methylation signature for predicting prognosis and recurrence of lung adenocarcinoma," *Oncology Letters*, vol. 18, no. 6, pp. 5831–5842, 2019.

[46] K. Okazaki, Y. Nakayama, K. Shibao et al., "Establishment of a human colon cancer cell line (PMF-ko14) displaying highly metastatic activity," *International Journal of Oncology*, vol. 17, no. 1, pp. 39–45, 2000.

[47] H. N. Li, X. R. Li, Z. T. Lv, M. M. Cai, G. Wang, and Z. F. Yang, "Elevated expression of FREM1 in breast cancer indicates favorable prognosis and high-level immune infiltration status," *Cancer Medicine*, vol. 9, no. 24, pp. 9554–9570, 2020.

[48] J. S. Rawlings, K. M. Rosler, and D. A. Harrison, "The JAK/STAT signaling pathway," *Journal of Cell Science*, vol. 117, no. 8, pp. 1281–1283, 2004.

[49] J. C. Chang, "Cancer stem cells: role in tumor growth, recurrence, metastasis, and treatment resistance," *Medicine (Baltimore)*, vol. 95, no. 1S, pp. S20–S25, 2016.

[50] E. J. Allenspach, I. Maillard, J. C. Aster, and W. S. Pear, "Notch signaling in cancer," *Cancer Biology and Therapy*, vol. 1, no. 5, pp. 466–476, 2002.

REPRINT OF ARTICLES

Second article

Cytotoxic effect of metformin on butyrate-resistant PMF-K014 colorectal cancer

spheroid cells

Cytotoxic effect of metformin on butyrate-resistant PMF-K014 colorectal cancer spheroid cells

Kesara Nittayaboon [a], Kittinun Leetanaporn [a], Surasak Sangkhathat [a], Sittirak Roytrakul [b], Raphatphorn Navakanitworakul [a, *]

[a] *Department of Biomedical Sciences and Biomedical Engineering, Faculty of Medicine, Prince of Songkla University, Hat Yai, Songkhla 90110, Thailand*
[b] *National Center for Genetic Engineering and Biotechnology (BIOTEC), National Science and Technology Development Agency, Pathumthani 12120, Thailand*

ARTICLE INFO

ABSTRACT

Three-dimensional (3D) cell culture models are used in cancer research because they mimic physiological responses in vivo compared with two-dimensional (2D) culture systems. Recently, cross-resistance of butyrate-resistant (BR) cells and chemoresistance in colorectal cancer (CRC) cells have been reported; however, effective treatments for BR cells have not been identified. In this study, we investigated the cytotoxicity of metformin (MET), an anti-diabetic drug, on BR CRC cells in a 3D spheroid culture model. The results demonstrate that MET decreases spheroid size, migration, and spheroid viability, while it increases spheroid death. The molecular mechanism revealed that AMP-activated protein kinase (AMPK) and Akt serine/threonine kinase 1(Akt) were significantly upregulated, whereas the acetyl-CoA-carboxylase (ACC) and mammalian target of rapamycin (mTOR) were downregulated, which led to caspase activation and apoptosis. Our findings show the potential cytotoxicity of MET on CRC-BR cells. The combination of MET and conventional chemotherapeutic drugs should be addressed in further studies to reduce the side effects of standard chemotherapy for CRC.

1. Introduction

Based on the GLOBOCAN 2020 data, colorectal cancer (CRC) is the third most commonly diagnosed cancer and the second cause of cancer-related death in both men and women worldwide [1]. In Thailand, CRC is the third most common cancer. The incidence and mortality are increasing despite the existence of more effective screening programs and treatments [2,3]. Previous reports have demonstrated that butyrate, a bacterial metabolite present in the human colon, contributes to chronic inflammation and CRC development [4,5]. Butyrate normally inhibits the proliferation of cancer cells and induces apoptosis; however, long-term exposure can alter cancer cells to generate butyrate-resistant (BR) cells. BR cells exhibit various malignant phenotypes, including glucose deprivation survival, heat-shock tolerance, and increased tumorigenicity [6,7]. Previous reports have suggested that BR cells contribute to the chemoresistant phenotype, causing the treatments to fail[8]. Moreover, an AMP-activated protein kinase (AMPK)-activating compound exerted effects on BR cells, including proliferation inhibition and autophagy activation [9]. These AMPK activator drugs appear to sensitize BR cells.

Metformin (MET) is commonly used to treat diabetes mellitus (DM) but, surprisingly, it was also shown to reduce the risk of cervical, endometrial, lung, and colon cancers in type 2 DM patients [10–13]. MET acts by inhibiting mitochondrial respiration, resulting in an imbalance in the AMP:ATP ratio, which is regulated by AMPK [14,15]. Previous studies have shown that MET, which activates AMPK, is a candidate therapeutic agent against chemoresistant CRC cells when combined with 5-fluorouracil (5-FU) and oxaliplatin (Ox, FuOx) [13]. Moreover, a study of breast cancer cell lines revealed that MET pre-treatment reduces the doxorubicin-resistant phenotype [16]. Based on these findings, MET may exhibit therapeutic effects against drug-resistant cancer cells.

Three-dimensional (3D) spheroid culture is widely used in cancer research. Compared with two-dimensional (2D) or monolayer cultures, the 3D culture model can mimic the tumor environment in vivo [17,18]. Various reports have suggested that 3D CRC-primary cells could preserve the characteristic of their parental tumor tissue [19] and show a different response during irradiation and chemotherapy [20]. Previous

* Corresponding author.
E-mail addresses: kesara.nittayaboon@gmail.com (K. Nittayaboon), lkittinun1@gmail.com (K. Leetanaporn), s.sangkhathat@gmail.com (S. Sangkhathat), sittiruk@biotec.or.th (S. Roytrakul), nraphatp@medicine.psu.ac.th (R. Navakanitworakul).

studies conducted using a 3D breast cancer model revealed a different phenotype, including hypoxia in the bulk tumor and drug sensitivity, which was higher compared with that observed in the 2D system [21]. The 3D CRC cells also showed a reduction of cancer drug activity [22]. Moreover, the effects of drugs in a 3D cell culture model of BR cells have not been thoroughly investigated.

In this study, we characterized the formation of PMF-k014 cells-derived spheroids and determined the cytotoxic effect of MET on PMF-k014 BR spheroids. The drug response was evaluated in terms of cell viability, caspase3/7 activity, and spheroid migration. The underlying molecular mechanism was examined by Western blot analysis.

2. Materials and methods

2.1. Butyrate-resistant cell culture

PMF-k014 epithelial colorectal carcinoma——a polygonal epithelial derived from highly metastatic adenocarcinoma [23] (RBRC-RCB1426, RIKEN BRC, Japan)——cells were grown in Dulbecco's modified Eagle's medium (Gibco™ Thermo Fisher, USA) supplemented with 10 % heat-inactivated fetal bovine serum (Gibco™ Thermo Fisher scientific, USA) and 1 % penicillin/streptomycin (Gibco™ Thermo Fisher scientific, USA) in a humidified incubator with 5 % CO_2 and 95 % air at 37 °C. The butyrate-resistant PMF (PMF-BR) cells were previously established (unpublished data). Briefly, the cells were stimulated in a complete medium supplemented with 0.2 mM sodium butyrate (Sigma, USA). Butyrate treatments induced cancer cell death. However, some cells survived and continued to proliferate. BR cells were subcultured at 80 % confluency. Subsequently, the concentration of butyrate was increased by 2-fold every three generations. After the concentration of butyrate reached 3.2 mM, both the parental (PT) and BR cells were ready for further experiments.

2.2. Poly-HEMA-coated plate preparation and spheroid formation

A stock solution of poly-(2-hydroxyethyl methacrylate) (Poly-HEMA, Sigma, USA) was prepared at 120 mg/mL in 95 % ethanol by stirring with a sterile magnetic bar at room temperature overnight. A working solution was prepared (5 mg/mL) using the same procedure. Then, 20 μL of working solution was added to a 96-well U-bottom plate, and the plate was dried for 3 days in an incubator. The spheroids were generated by seeding PMF-PT and PMF-BR cells in the coated plate to generate 200–300 μm spheroid cells.

2.3. Characterization of spheroid formation

To detect the presence of CD44 surface marker, immunofluorescence assay was used. We fixed the spheroids in 4 % paraformaldehyde for 20 min. Then, fixed spheroids were incubated with antihuman CD44 (phycoerythrin [PE] conjugated; ImmunoTools, Germany) for 45 min. The nuclei were counterstained with 4′,6-Diamidine-2′-phenylindole dihydrochloride (DAPI) (Sigma, USA). The stained spheroids were imaged on a LionheartFX live cell imager (Biotek, USA).

To assess the genes expression, total RNA was isolated from the monolayer and spheroid cells using the Trizol reagent (Invitrogen, USA) as instructed by the manufacturer. RNA was then quantified using absorbance measurements by Nanodrop (Thermo Fisher). RNA samples (1 μg) with good quality were reverse-transcribed to complementary DNA (cDNA) using reverse transcriptase enzymes. An iScript™ cDNA synthesis kit (Bio-rad, USA) was used for cDNA synthesis according to the manufacturer's instructions. *GAPDH* was used as an internal control. Differential expression of stemness genes; *SOX2, OCT4, KLF4* and *CXCR4*, butyrate-related genes; *GPR-109A, GPR-109B, GPR-41* and *SLC5A8* and drug efflux genes; *ABCA5, ABCC1, ABCC2, ABCC3, ABCC5, ABCF2* and *ABCG2* were determined. The primer sequences are shown in Supplementary Table 1. The quantitative real time RT-PCR (RT-qPCR)

was carried out in duplicates with three independent experiments. The $2^{-\Delta Ct}$ method was used for calculating the relative gene expression levels.

2.4. Characterization of PMF-PT and PMF-BR spheroids by mass spectrometry

To examine the characteristics of PMF-PT and PMF-BR spheroids, mass spectrometry was performed at the Functional Proteomics Technology Laboratory, National Center for Genetic Engineering and Biotechnology (BIOTEC), Thailand. The spheroid cell lysates were reduced, alkylated, and digested with trypsin, and were analyzed by LC-MS/MS (Bruker Impact II, USA). Peptides were quantified and identified using the DeCyder MS differential analysis software 2.0 (GE Healthcare, USA) and the MASCOT search engine (Matrix Science, UK) based on the NCBI human protein databases. To display the list comparing PT and BR spheroids, the peptide data were used to generate Venn diagrams through jvenn, an interactive Venn diagram viewer (http://jvenn.toulouse.inra.fr/app/index.html). The functional enrichment analysis of the uniquely expressed proteins was performed using the PANTHER analysis tool (http://pantherdb.org/).

2.5. Butyrate sensitivity

Both the monolayer cells and spheroids generated on poly-HEMA-coated plates were treated with and without butyrate (Sigma, USA) at various concentrations (0–100 mM) for 72 h. After incubation, cell viability was measured using ApoLive-Glo™ Multiplex Assay (Promega, USA) following the manufacturer's instructions. Briefly, the fluorescent substrate (glycyl-phenylalanyl-amino fluorocoumarin; GF-AFC) was added to the treated spheroids. Live-cell protease was interacted with GF-AFC substrate. The fluorescent intensity was detected following a 400 nm excitation source and 505 nm emission filter, was then quantified using a Varioskan LUX multimode microplate reader (Thermo Fisher, USA), and was presented as the percentage of cell viability.

2.6. MET activity in butyrate-resistant spheroids

The spheroids generated on poly-HEMA coated plates were treated with and without MET at various concentrations for 72 h. After incubation, spheroid size, cell viability, and caspase activity were measured. The spheroid size was firstly determined using an inverted microscope and was analyzed using ImageJ analysis software. The LIVE/DEAD® Cell Imaging Kit (Thermo Fisher scientific, USA) was used for staining. The solution contained calcein AM and BOBO-3 iodide, which interacted with live and dead cells, respectively. The complete media of spheroids were removed until 100 μL was left in each well. Then, the mixed solution was added, and the plate was wrapped with aluminum foil to protect the contents from sunlight, and it was further incubated at 37 °C for 30 min. The images were obtained using a LionheartFX live cell imager. The ApoLive-Glo™ Multiplex Assay was used to detect viable cells as a marker of cytotoxicity, and caspase3/7 activation as a marker of apoptosis. The kit contains two assay components. Firstly, the activity of a protease marker of cell viability was measured. The protease activity of live cells was restricted to intact viable cells and was measured using a fluorogenic and cell-permeant peptide substrate (GF-AFC). The substrate entered intact cells where it was cleaved by the protease activity of live cells to generate a fluorescent signal proportional to the number of living cells, which was measured as relative fluorescence units using the following 400 nm excitation source and 505 nm emission filter. The protease of live cells is inactive as the cell membrane integrity is lost and leakage occurs into the culture medium. Secondly, the kit also contained the Caspase-Glo® assay which is used to detect caspase 3/7 activation. This assay provides a luminogenic caspase-3/7 substrate, which contains the tetrapeptide sequence DEVD, in a reagent optimized for caspase activity, luciferase activity, and cell lysis. Adding the Caspase-Glo®

3/7 reagent resulted in cell lysis, followed by caspase cleavage of the substrate and generation of a luminescent signal produced by luciferase. Luminescence is proportional to the amount of caspase activity present and was measured as relative luminescence units using the Caspase-Glo 3/7 assay system. Both assays were quantified with a Varioskan LUX multimode microplate reader. The means of three independent experiments were plotted as a dose response curve.

2.7. Spheroid migration

The migration properties of PMF-PT and PMF-BR spheroids were evaluated using a tumor spheroid-based migration assay. Briefly, PMF-PT and PMF-BR spheroids were generated by seeding the cells into 96-well U-bottom Poly-HEMA coated plates for 72 h, and were further incubated with MET at various concentrations for 72 h. Then, the spheroids were transferred to a new flat-bottom 96-well plate and further incubated for 72 h. After incubation, the spheroids were imaged using an inverted microscope (10x magnification). The migration areas were analyzed using ImageJ software.

2.8. Western blot analysis

Western blot analysis with spheroids was performed as previously described [24]. Briefly, spheroid pellets were lysed in RIPA buffer (Pierce Biotechnology, USA). Protein concentration was measured using the Bradford assay (Bio-Rad, USA). Protein extract with 30 µg was subjected to SDS-polyacrylamide gel electrophoresis (SDS-PAGE) followed by transfer to polyvinylidene difluoride (PVDF) membranes (Amersham Pharmacia Biotech, USA). The membranes were blocked in 5 % non-fat milk in Tris-buffer saline with 0.1 % (v/v) Tween-20 (TBS-T) for 1 h at room temperature. Then, they were washed twice with TBS-T for 10 min. Each membrane was incubated overnight at 4 °C, shaking continuously with primary antibodies (1:1000 diluted with 1 % non-fat milk in TBS-T) specific to AMPKα (cat. no. 5831; Cell Signaling Technology, Inc.), phospho-AMPKα (Thr172, cat. no. 2535; Cell Signaling Technology, Inc.), acetyl-CoA carboxylase (cat. no. 3676; Cell Signaling Technology, Inc.), phospho-acetyl-CoA carboxylase (Ser79; cat. no. 11818; Cell Signaling Technology, Inc.), Akt (cat. no. 4691; Cell Signaling Technology, Inc.), phospho-Akt (Ser473; cat. no. 4060; Cell Signaling Technology, Inc.), phospho-mTOR (Ser2448; cat. no. 5536; Cell Signaling Technology, Inc.), mTOR (cat. no. 2983; Cell Signaling Technology, Inc.), Raptor (cat. no. 2280; Cell Signaling Technology, Inc.), Rictor (cat. no. 2114; Cell Signaling Technology, Inc.), GβL (cat. no. 3274; Cell Signaling Technology, Inc.) and β-actin (cat. no. 4967; Cell Signaling Technology, Inc.) used as internal control. After incubation, the membranes were washed thrice (10 min/time) with TBS-T and were incubated with a secondary antibody (Anti-rabbit IgG horseradish peroxidase; cat. no. 7074; Cell Signaling Technology, Inc.) at 1:1000 diluted in 1 % non-fat milk in TBS-T for 2 h. Then, the membranes were washed again three times with TBS-T and the last washing was performed using TBS for 10 min. The protein expressions were visualized using an enhanced chemiluminescence reagent (Pierce™ ECL Western Blotting Substrate, Thermo Fisher scientific, USA). Densitometry was performed using a Chemiluminescence & Epi Fluorescence Alliance Q9 Advanced (Uvitec, UK) imager.

3. Results

3.1. PMF-PT and PMF-BR spheroid formation and characterization

We first evaluated the butyrate sensitivity on the butyrate-induced monolayer cells that were incubated with or without various concentrations of butyrate and determined the 50 % inhibitory concentration (IC$_{50}$). We found that the IC$_{50}$ value of PMF-BR cells was 3-fold higher than that of PMF-PT cells. Moreover, both PT and BR cells were treated with various concentrations of anticancer drugs such as 5-FU and MET

for 72 h. We found that butyrate-resistant cells were cross-resistant to 5-FU, whereas both PT and BR cells were sensitive to MET with an equal IC$_{50}$ value of MET (Supplementary Table 1).

Currently, several promising drug candidates tested using the 2D culture model have not proved successful in clinical practice. Therefore, we focused on the 3D culture model. PMF-PT and PMF-BR cells were grown on poly-HEMA-coated plates for 72 h to generate spheroids. Both cells formed spheroids with a round-shape structure, compact morphology, and smooth surface. The size of PMF-PT spheroids was slightly larger than that of PMF-BR spheroids (Fig. 1A). The average diameter of the PT spheroid was 208.29 ± 7.94 µm, whereas that of the BR spheroid was 196.41 ± 9.43 µm. We also characterized spheroid formation by detection of the presence of CD44 as cancer stem cell (CSC) marker on the surface of spheroids using immunofluorescence staining. CD44 was positively stained in the membrane of cells in spheroids in both spheroids (Fig. 1A). In addition, we investigated CSC enrichment in formed spheroids as compared to their 2D monolayers. The expression of key stemness genes including *SOX2*, *OCT4*, *KLF4* and *CXCR4* using RT-qPCR were assessed. We found that the expression of *SOX2* and *OCT4* genes were significantly upregulated in both PMF-PT and BR spheroids as compared to their 2D monolayers, while the expression of *KLF4* and *CXCR4* was not difference in both comparisons (Fig. 1B-C).

For butyrate sensitivity tests, both spheroids were incubated with various concentrations of butyrate, and IC$_{50}$ was then determined. The viability of PMF-BR spheroids was significantly higher than that of PMF-PT spheroids. The percentage of cell survival and the IC$_{50}$ of each spheroid cell are shown in Fig. 2A and B, respectively. The IC$_{50}$ value of PMF-BR spheroids was 2.7 times higher than that of PMF-PT spheroids. This result indicated that the BR spheroid still presents the trait of butyrate resistance. We also examined the response of the spheroids against 5-FU, which is normally used in clinical practice (Supplementary Figure 1). The IC$_{50}$ values of 5-FU in PMF-PT and PMF-BR spheroids were 78.50 ± 5.95 and 208.80 ± 4.77 µM, respectively. This result illustrated that the PMF-BR spheroids were also cross-resistant to 5-FU. Moreover, the expression of butyrate-related genes and drug efflux pumps was determined using *GAPDH* as an internal control. *GPR109A*-a butyrate receptor-its homolog *GPR109B*, *GPR-41* and sodium-couplet monocarboxylate transporter 1 (*SMCT1* or *SLC5A8*) are response to the transport of bacterial metabolites-particularly butyrate-in intestinal cells. PMF-BR spheroids showed significantly higher expression of *GPR-109A*, *GPR-109B* and *GPR-41* genes than that of PMF-PT spheroids, whereas *SLC5A8* was not difference in both spheroids (Fig. 2C). For evaluating the expression of the efflux pump, the expression of the ABC-binding cassette transporter genes, which plays an important role in drug transport in cancer cells, was elucidated. PMF-BR spheroids showed significantly higher expression of *ABC-C1*, *ABC-C2*, *ABC-C3*, *ABC-C5* and *ABC-G2* genes than PMF-PT spheroids. The expression of *ABC-A5* was significantly low in PMF-BR spheroids, whereas *ABC-F2* was not difference in both spheroids (Fig. 2D).

The protein expression profiles in both spheroid cell types were also identified by LC-MS/MS and then compared and visualized using a Venn's diagram (Fig. 2E). This demonstrated all the possible relations of protein expressions and the uniquely expressed proteins found in PMF-PT and PMF-BR spheroids. The names of the uniquely expressed proteins found only in PMF-PT and in PMF-BR spheroid cells are listed in Supplementary Table 3 and Supplementary Table 4, respectively. These uniquely expressed proteins were subsequently subjected to functional enrichment analysis using PANTHER based on their pathway. We found that the unique proteins involved in the metabolic pathway and signal reception and transduction were enriched in PMF-BR spheroids rather than in PMF-PT spheroids. In addition, proteins related to apoptosis and stress response, transcriptional and posttranscriptional process, cell cycle control and proliferation, and DNA replication and repair were enriched only in PMF-BR spheroids. However, the unique proteins involved in the cytoskeleton structure and cell–matrix interactions were found in only PMF-PT spheroids (Fig. 2F).
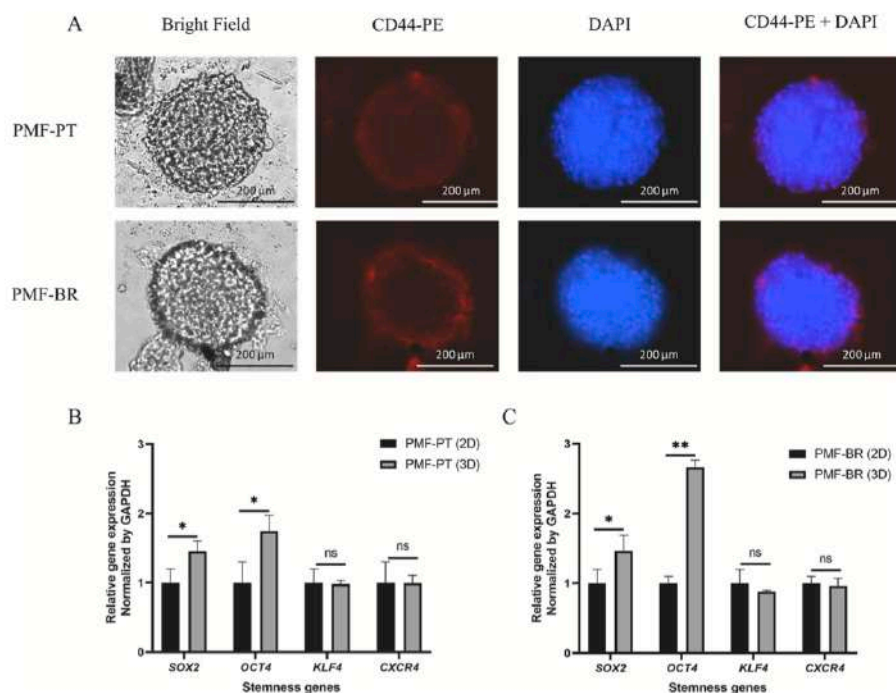
Fig. 1. Morphology of PMF-PT and PMF-BR spheroids and their characteristics. Spheroids were formed by seeding the cells on poly-HEMA coated plates for 72 h and stained with CD44-PE (red) and DAPI (blue). Their images were obtained using an inverted microscope with 10x magnification (scale bar = 100 μm) (A). Relative expression of stemness genes in PMF-PT (B) and PMF-BR (C) was performed using RT-qPCR. Gene expression levels are shown relative to those of GAPDH. Data are shown as mean ± standard deviation (SD) of triplicate experiments (* p-$value$ < 0.05 and ** p-$value$ < 0.01; the mean difference is significant at the 0.05 and 0.01 level, respectively compared between 2D and 3D via Student's t-test. Abbreviations: PMF-PT, PMF parental cells; PMF-BR, butyrate-resistant PMF cells; DAPI, 4′,6-Diamidine-2′-phenylindole dihydrochloride.

3.2. MET effect on PMF-PT and PMF-BR spheroids

3.2.1. MET reduces the size of PMF-PT and PMF-BR spheroids

The spheroid size was determined upon treatment (Day 0) and after 72 h (Day 3). Spheroid diameter was measured using ImageJ analysis software. Briefly, the scale bar was calibrated in a micrometer unit. Then, the spheroid diameter was measured by a linear line across the edge. The software then converted the pixels of the linear line into micrometer. Fig. 3 shows decreasing spheroid size in a dose-dependent manner. However, spheroid size increased at 100 mM, possibly due to cell death and disaggregation.

3.2.2. MET induces PMF-PT and PMF-BR spheroid death

After 72 h of treatment with MET, the viability of the spheroids was determined using the LIVE/DEAD staining kit. The kit distinguishes live and dead cells using two probes, namely calcein AM for intracellular esterase activity and BOBO-3 iodide for plasma membrane integrity. The results indicated that MET-induced spheroid death as evidenced by a red fluorescent signal in the treatment group, whereas viable cells showed a green fluorescent signal in the control (Fig. 4).

3.2.3. MET reduces cell viability and induces caspase activity in PMF-PT and PMF-BR spheroids

To investigate the mode of cell death, we used the ApoLive-Glo assay to measure enzyme activity as a marker for viable cells, and caspase-3/7 activity as an indication of apoptosis. We found that MET decreased cell viability and increased caspase-3/7 activity in the treatment group (Fig. 5). The caspase-3/7 activity of PMF-BR spheroids at all concentrations was higher than that of PMF-PT, even though the percentage of cell viability was equal in both spheroid cell types. These results suggested that PMF-BR spheroids are sensitive to MET, resulting in apoptosis.

3.2.4. MET reduces spheroid migration in PMF-PT and PMF-BR cells

The anti-migration of MET on PT and BR spheroids was evaluated using a tumor spheroid-based migration assay [25]. After MET treatment for 72 h, the spheroids were transferred to a new flat-bottom plate containing fresh complete media and were further incubated for 72 h. Then, the migration area of the spheroids was measured and calculated as the percentage of spheroid migration. The results showed a significant decrease in migration at 25- and 50-mM MET for PMF-PT and at 50 mM for PMF-BR spheroids (Fig. 6). This indicated that MET may have anti-migration properties in both spheroid cell types, with even significant effects on PMF-PT spheroids.
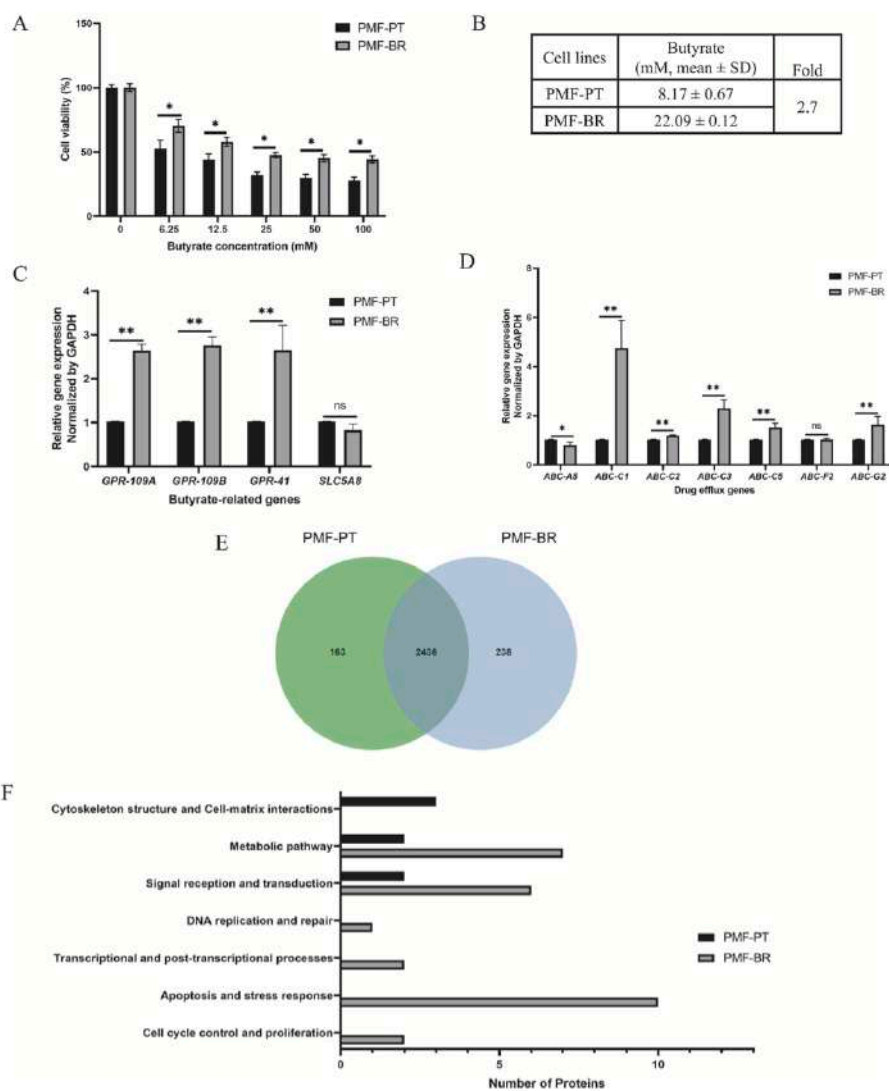
Fig. 2. Characterization of butyrate resistance spheroids. Effect of butyrate on PMF-PT and PMF-BR spheroids for 72 h represented as percentage of cell viability (A). The IC_{50} value of butyrate after the 72-h treatment was estimated from dose response curves (B). Relative expression of butyrate-related genes (B) and drug efflux genes (C) in the spheroids was perform using RT-qPCR. Gene expression levels are shown relative to those of GAPDH. Data are shown as mean ± standard deviation (SD) of triplicate experiments (* *p-value* < 0.05 and ** *p-value* < 0.01; the mean difference is significant at the 0.05 and 0.01 level compared between PMF-PT and PMF-BR spheroids via Student's *t*-test. Proteomic analysis of PMF-PT and PMF-BR spheroids. The Venn's diagram illustrates the overlapping and uniquely expressed proteins of the spheroids (E). Functional enrichment analysis of the uniquely expressed proteins in terms of the pathways found in PMF-PT and PMF-BR spheroids (F). Abbreviations: PMF-PT, PMF parental cell; PMF-BR, butyrate-resistant PMF cell.
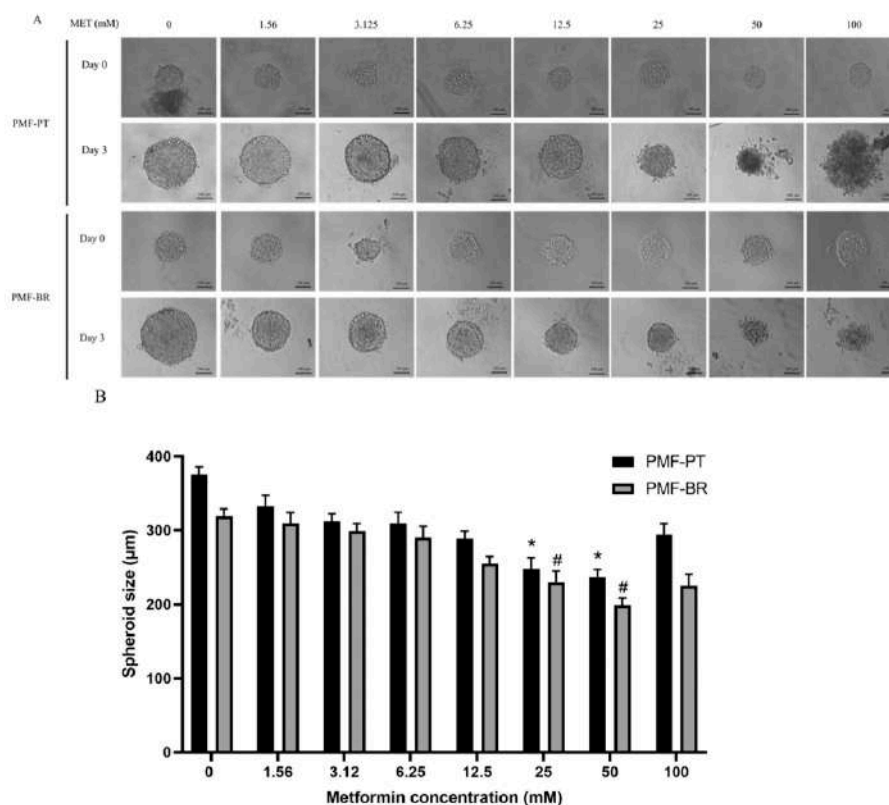
Fig. 3. Effect of MET on the size of PMF-PT and PMF-BR spheroids. The spheroids were incubated with various concentrations of MET for 72 h. Spheroids were imaged by inverted microscopy (10x magnification) (A). The bar graphs show the size of the spheroids. Scale bar= 100 µm. Significance: * p-value < 0.05 compared with PMF-PT control; MET 0 mM, # p-value < 0.05 compared with PMF-BR control; MET 0 mM. Abbreviations: PMF-PT, parental cell; PMF-BR, butyrate-resistant cell.

3.3. Molecular mechanism of MET in PMF-PT and PMF-BR spheroids

The primary mechanism associated with the activity of MET is the activation of the AMPK pathway and inhibition of the mTOR pathway. These two pathways are involved in the inhibition of proliferation and induction of apoptosis in many cancer cells. Therefore, the proteins related to them were examined. The expression of the proteins of interest in PMF-PT and PMF-BR spheroids following MET treatment was determined by Western blot analysis. Phospho-AMPK and p-Akt were significantly upregulated in the MET-treated group in both PT and BR spheroids. In addition, acetyl-CoA-carboxylase (ACC) was significantly reduced in the MET-treated group. We also found that p-mTOR exhibited lower expression in the MET-treated group; however, we found no significant difference in ratio of mTOR/p-mTOR expression. We also examined other molecules in the mTOR pathway. The expression of Raptor and Rictor were not different. The binding molecule of mTOR, Raptor, and Rictor is GβL. We found a significant decrease in GβL expression following MET treatment. Finally, c-Raf showed a significant decrease in MET-treated BR spheroids (Fig. 7). Altogether, these results

suggested that MET could inhibit the cell viability of both PMF-PT and PMF-BR spheroids by activating the AMPK and Akt pathways and caspase activity and inhibiting the ACC and mTOR pathways.

4. Discussion

BR cells have been considered on the one of cancer-related chemo-resistant and leading to treatment failure [8]. In this study, we induced the PMF-k014 cells with butyrate at the maximum concentration of 3.2 mM, whereas previous studies have used a lower butyrate concentration of 1.6 mM in CRC cell lines, including HCT-116, SW480, and HT29 cells, to induce as BR cells [8,26]. Unlike previous studies, we used PMF-k014 derived from metastatic colon adenocarcinoma, which is less responsive to anticancer drugs [27]. Moreover, previous studies have investigated several anticancer drugs tested in the 2D cell culture model, which is not adequately successful in clinical practice, whereas in vivo-like models such as the 3D culture are currently attracting significant attention. The present study is the first report to establish a butyrate-resistant PMF spheroid and its parental cell with a
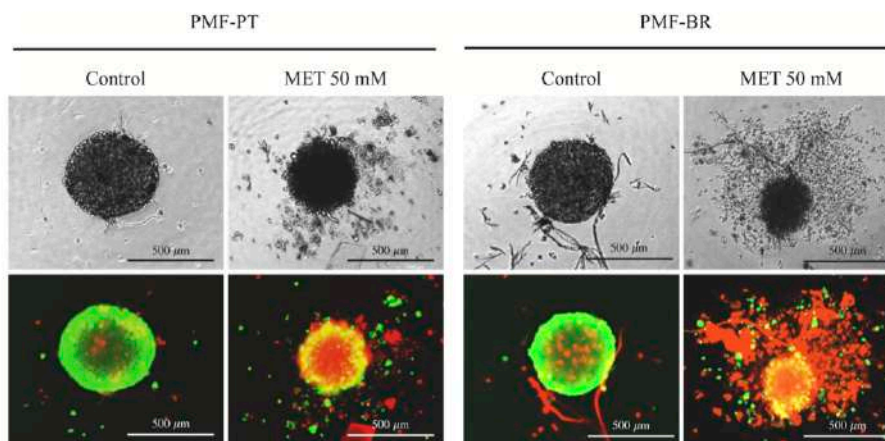
Fig. 4. Cytotoxic effect of MET on PMF-PT and PMF-BR spheroids. After being treated with MET at 50 mM for 72 h, the live/dead staining (live = green and dead = red) of the spheroids was imaged with a LionheartFX live cell imager (10x magnification). Scale bar = 500 μm. Abbreviations: PMF-PT, parental cell; PMF-BR, butyrate-resistant cell; MET 50 mM, MET treatment at 50 mM.
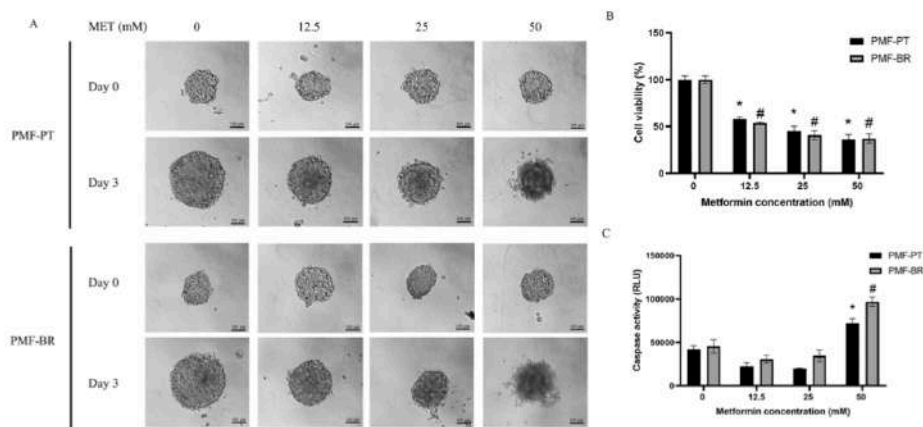

Fig. 5. MET-induced apoptosis in PMF-PT and PMF-BR spheroids. The morphology of the spheroids treated with and without MET at 0, 12.5, 25, and 50 mM for 72 h was visualized using an inverted microscope (10x magnification) (A). Scale bar = 100 μm. The ApoLive-Glo assay was used to detect cell viability (B) and caspase-3/7 activity (C). Statistical analysis was performed using the Student's t-test. Significance: * p-value < 0.05 compared with PMF-PT control; MET 0 mM, # p-value < 0.05 compared with PMF-BR control; MET 0 mM. Abbreviations: PMF-PT, parental cell; PMF-BR, butyrate-resistant cell.

round-shaped structure, compact morphology, and smooth surface, which is consistent with published results on CRC BCS-TC2, BR2 spheroids [28]. Numerous studies reported that 3D tumor spheroids including CRC, have enriched with CSC-like phenotype [29,30]. For example, the key stemness markers such as CD44 protein and *SOX2*, *OCT4*, *KLF4* genes were significantly higher expression in CRC HT-29 and Caco-2 spheroids than their 2D monolayers. This is in line with our study that both PMF-PT and PMF-BR spheroids showed the presence of CD44 on the membrane of cells in the spheroids. Moreover, *SOX2* and *OCT4* genes were also significantly high expression in PMF-PT and

PMF-BR spheroids compared to their 2D monolayers.

Previous studies have also demonstrated that BR cells present a highly malignant phenotype, which includes traits such as survival in glucose depletion, inhibition of apoptosis, and resistance to anticancer drugs [6,7,31]; similarly, our findings demonstrated that PMF-BR spheroids were also cross-resistant to 5-FU. Several mechanisms are involved in the resistance to butyrate, including alteration of the drug target and, drug inactivation and efflux expression. To investigate the underlying mechanism in BR spheroids, we evaluated the expression of butyrate-related genes, including butyrate receptors, *GPR109A*,
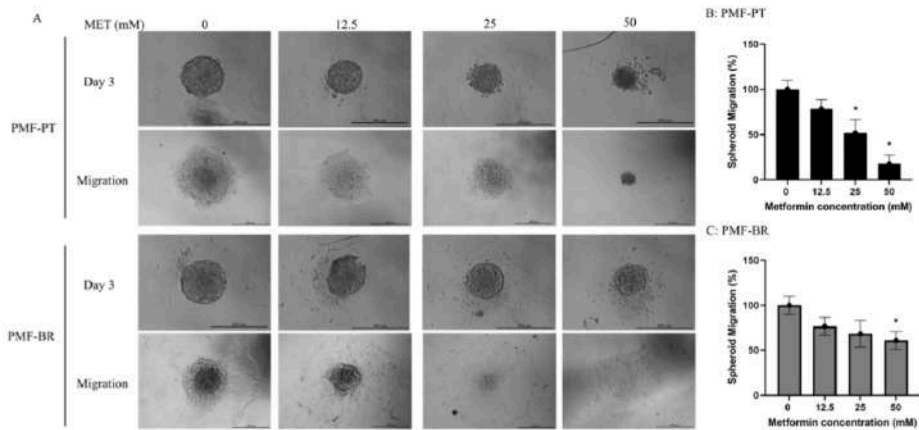
Fig. 6. Effect of MET on the cell migration of PMF-PT and PMF-BR spheroids. After the two spheroid cell types were treated with 0, 12.5, 25, and 50 mM of MET for 72 h, they were transferred to a flat-bottom plate and were further incubated for 72 h; their representative images were visualized using an inverted microscopy (10x magnification) (A). The bar graphs show the average percentage of the migration of PMF-PT (B) and PMF-BR (C) spheroids compared with the control value obtained from three independent experiments + SD (n = 3). Scale bar = 400 μm. Statistical analysis was performed using the Student's t-test. Significance: * p-value < 0.05 compared with the control; MET 0 mM. Abbreviations: PMF-PT, PT, parental cell; PMF-BR, BR, butyrate-resistant cell; MET, metformin treatment.
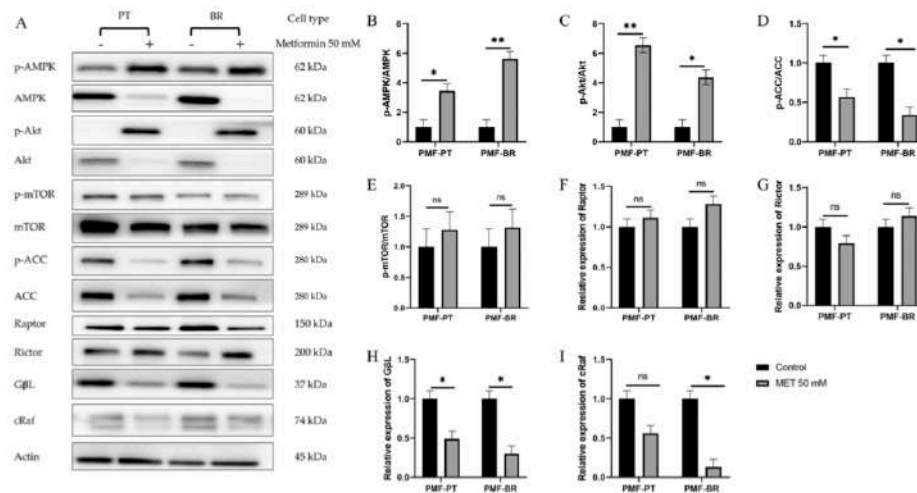

Fig. 7. Effect of MET on the AMPK/ACC/mTOR pathway and its binding proteins. Both PMF-PT and PMF-BR spheroids were treated with and without MET (50 mM) for 72 h. After incubation, the spheroids were collected and lysed by RIPA buffer. The total proteins were loaded on SDS-PAGE, and those of interest were examined by Western blot analysis. Actin was used as internal control (A). The quantitative proteins of interest, including p-AMPK/AMPK (B), p-Akt/Akt (C), p-ACC/ACC (D), p-mTOR/mTOR (E), Raptor (F), Rictor (G), GβL (H), and c-Raf (I), were normalized to actin band intensity. Data are shown as the mean ± SD of triplicate experiments. Statistical analysis was performed using Student's t-test. Significance: * p-value < 0.05 compared with the control; MET 0 mM. ** p-value < 0.01 compared with the control; MET 0 mM. Abbreviations: PMF-PT, PT, parental cell; PMF-BR, BR, butyrate-resistant cell; ns, non-significant; MET 50 mM, metformin treatment 50 mM.

GPR109B and GPR-41, and butyrate transporter, SLC5A8. PMF-BR spheroids showed an upregulation of GPR109A, GPR109B, and GPR-41. In a previous study, the expression of butyrate-related genes was upregulated in butyrate resistant mice (compared to germ-free mice) [32]. We further investigated the drug efflux gene expression. We found the expression of ABC-C1, ABC-C2, ABC-C3, ABC-C5 and

ABC-G2 was upregulated in PMF-BR spheroids, whereas that of *ABC-A5* was upregulated in PMF-PT spheroids. Our finding is in line with the previous reports that have shown the upregulation of *ABC-C1* and *ABC-G2* in Hep2–5-FU-resistant cells [33]. These two ABC transporters are considered chemoresistance driven genes and play a role in the acquisition of chemoresistance. This finding would be the reason that PMF-BR spheroids were cross-resistant to 5-FU. Additionally, *ABC-C1*, *ABC-C3*, *ABC-C5* and *ABC-F2* are found in paclitaxel-resistant cells. Furthermore, doxorubicin resistance in breast cancer cells is induced by the overexpression of *ABC-C1* and *ABC-F2* [34,35]. In addition, cells expressing *ABC-A5* and *ABC-F2* are demonstrated to show stem cell features [36]. Moreover, we characterized the protein patterns between PT and BR spheroids. The proteins related to metabolic pathway and signal reception and transduction were found in PMF-BR greater than PMF-PT spheroids. For example, the proteins related to metabolic pathway in PMF-BR spheroids composed of proteins involved in glycolysis, gluconeogenesis, fructose, galactose, and pyruvate metabolism which are consistent with the previous research that showed upregulation of proteins in glycolysis/gluconeogenesis related to the higher rate of metabolism in rapid growing tumor cells [37]. While the proteins involved in glycolysis and TCA cycle were found lesser quantities in PMF-PT spheroids. Our finding indicated that many proteins related to metabolism process found in BR cells may help the cells to grow and survive in butyrate exposure condition. However, the molecular mechanism of butyrate resistance related to a cross-resistance of anti-cancer drugs should be addressed in further study. Moreover, the proteins related to apoptosis and stress response, DNA replication and repair, transcriptional and posttranscription process, and cell cycle control and proliferation were uniquely expressed in PMF-BR cells. The upregulation of the stress/apoptosis-related gene in particular proteins plays a role in the elimination of cytotoxic agents during chemotherapy for colon cancer [31].

Previous studies have attempted to overcome BR cells by targeting the AMPK pathway [9], which is a key pathway to balance the energy of cells and maintain homeostasis in various types of cancers [38]. The acquisition of butyrate resistance is associated with chemotherapeutic drug resistance, as mentioned above. The proposed mechanism of butyrate resistance included an increased p-Akt leading to decreased p-AMPK and p-ACC, resulting in the suppression of fatty-acid synthesis and apoptosis resistance [9]. To circumvent butyrate resistance in CRC cells, the activation of the AMPK pathway represents a promising strategy, as it would inhibit cell proliferation and coordinate metabolic reprogramming in drug-resistant cells [9]. MET, an anti-diabetic compound and AMPK activator drug, has been investigated as a cytotoxic drug in the tumoral cells of numerous cancer types, such as breast [39], cervical [38], and colorectal [40] cancers. MET primarily inhibits the mitochondrial respiratory chain complex I leading to AMPK activation [12,15]. MET is inexpensive and safe for diabetes patients, but its use is still controversial in cancer patients. However, retrospective studies of various cancer types showed the correlation between MET and lower cancer incidence, higher disease-free survival, and reduced cancer mortality [10,11,41,42]. Therefore, MET is a candidate for potential drug repurposing in cancer. Moreover, the combination of MET with conventional chemotherapy drugs showed a better anticancer effect compared to the use of chemotherapy alone [38,43,44]. MET also prevents doxorubicin resistance in breast cancer [16] and re-sensitizes the colorectal chemoresistant cancer cells [13]. Based on the above, MET may represent an effective treatment strategy for BR CRC cells. However, its effects on BR CRC cells using the 3D model have not been reported yet.

The present study demonstrated that the cytotoxic effect of MET on PMF-BR spheroids was dose-dependent. The spheroid morphology changed from a compact aggregation to a disaggregated state after MET treatment. We also detected an increase of caspase 3/7 activity following MET treatment, which resulted in apoptosis induction. The results are consistent with those reported in previous studies using the

2D culture model in breast, cervical, and CRC cells [38,39,45]. MET also inhibits PMF spheroid migration. However, it is necessary to further elucidate the anti-migration properties of MET in this cell type. Migration is a primary step for cell invasion and metastasis [46,47]. Previous studies have shown that MET inhibits cell migration in breast, pancreatic, and CRCs [13,46,47]. The molecular mechanism behind this inhibitory effect has also been previously elucidated. The inhibition of Akt/mTOR signaling was shown to reduce migration in squamous cell carcinoma [48], whereas the activation of AMPK/p53 with the inhibition of PI3K/Akt decreased migration in cervical cancer [49]. Further studies on the effect of MET on invasion should be conducted to the potential for use in cancer [50]. Cell invasion is one of the metastatic processes important for cancer cell distribution [51]. The inhibition of cell invasion by MET may be useful in cancer treatment.

The molecular mechanism of MET in PMF spheroids was determined by Western blot analysis. We found a significant upregulation of p-AMPK in the MET treatment group, and AMPK activation resulted in mTOR inhibition; however, we found no significant differences in the expression of mTOR-related molecules such as mTOR, p-mTOR, Raptor, and Rictor. Nevertheless, we observed a significant decrease in GβL, a binding factor of mTOR and its complex. The results suggested that AMPK activation reduces mTOR signaling by reducing the level of the binding molecules in PMF-BR spheroid cells. ACC, a key enzyme in fatty-acid synthesis, also significantly decreased, resulting in lipid synthesis inhibition and in the activation of fatty-acid oxidation. A previous study of head and neck cancer cells found that a higher ACC leads to an increased cell proliferation, whereas a lower level of this enzyme produces the opposite effect [52]. We observed upregulation of p-Akt in MET-treated spheroids. The overexpression of Akt and p-Akt occurs frequently in cancer cells. Because of its key role in cell survival, angiogenesis, and tumor formation, Akt is considered a hallmark of cancer [53]. Previous studies of human mesenchymal stem cells showed a significant activation of Akt, but not of AMPK, which resulted in cell survival following MET exposure [43]. In the present study, we also found a significant decrease of c-Raf in BR spheroids. This molecule plays an important role in apoptosis signaling and normally binds to the Bcl-2 protein, resulting in anti-apoptotic activity [54]. Decreased c-Raf levels result in the binding of Bcl-2 and BAD, leading to apoptosis.

Based on the overall results of this study, a proposed mechanism of MET action is presented in Fig. 8. It is concluded that the effect of MET is dependent on different regulatory pathways in the cells. MET activates AMPK which leads to mTOR pathway inhibition, a reduction in GβL expression, and cell cycle arrest. AMPK activation also leads to ACC inactivation, which results in a reduction of fatty-acid synthesis. Akt activation and c-Raf reduction result in the activation of caspase activity and apoptosis.

Altogether, our result demonstrated a potential cytotoxicity of MET on metastatic CRC cells at high concentration. However, it is necessary to evaluate the combination of MET and chemotherapeutic drugs to reduce the concentration of drugs and test in in vivo conditions before applying in clinical practice with low dose of MET.

5. Conclusions

In summary, MET shows potential therapeutic effects in PMF-BR spheroids through the activation of AMPK and Akt pathways and inhibition of the ACC and mTOR pathways leading to cell apoptosis. These findings suggest that MET is an effective treatment for drug-resistant CRC cells. Moreover, MET combined with chemotherapy should be further investigated as a strategy to treat CRC to improve the treatment and reduce the side effects of chemotherapy.
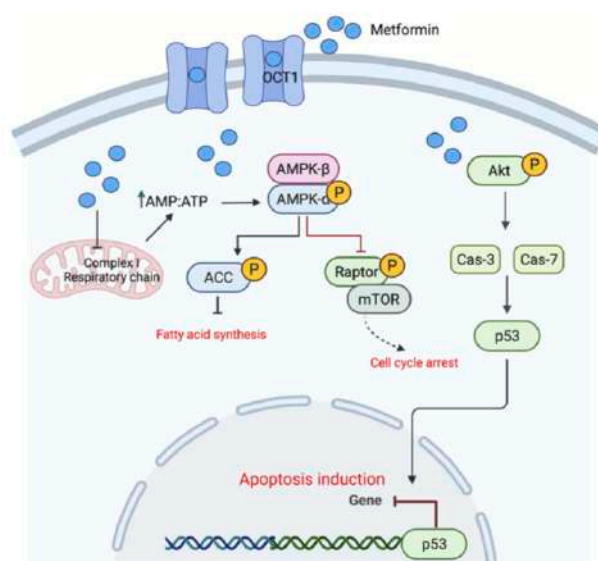
Funding

Fig. 8. Proposed mechanism of MET action through the AMPK/ACC/mTOR pathway in PMF-BR spheroids. Abbreviations: ACC, acetyl-CoA-carboxylase; Akt, RAC-alpha serine/threonine-protein kinase; AMPK, AMP-activated protein kinase; Cas, caspase; p53, mTOR, mammalian target of ra-pamycin; Protein 53; P, phosphorylation; OCT1, organic cation transporters 1; → means activation; ⊥ means inhibition.

Control in Thailand (MEDRC59036), and Graduate scholarship, Faculty of Medicine, Prince of Songkla University.

CRediT authorship contribution statement

Kesara Nittayaboon: Conceptualization, Methodology, Investigation, Data curation, Writing – original draft. **Kittinun Leetanaporn:** Software. **Surasak Sangkhathat:** Conceptualization. **Sittirak Roytrakul:** Software. **Raphatphorn Navakanitworakul:** Conceptualization, Writing – review & editing. All authors have read and agreed to the published version of the manuscript.

Conflicts of interest statement

The authors declare that there are no conflicts of interest.

Acknowledgments

Institutional review board statement

Not applicable.v

Appendix A. Supporting information

Supplementary data associated with this article can be found in the online version at doi:10.1016/j.biopha.2022.113214.

References

[1] H. Sung, J. Ferlay, R.L. Siegel, M. Laversanne, I. Soerjomataram, A. Jemal, F. Bray, Global cancer statistics 2020: GLOBOCAN estimates of incidence and mortality worldwide for 36 cancers in 185 countries, CA Cancer J. Clin. 71 (3) (2021) 209–249, https://doi.org/10.3322/caac.21660.

[2] V. Lohsiriwat, N. Chaisomboon, J. Pattana-Arun, Current colorectal cancer in Thailand, Ann. Coloproctol. 36 (2) (2020) 78–82. (https://pubmed.ncbi.nlm.nih.gov/32054248).

[3] K. Tiankanon, S. Aniwan, R. Rerknimitr, Current status of colorectal cancer and its public health burden in Thailand, Clin. Endosc. 54 (4) (2021) 499, https://doi.org/10.5946/ce.2020.245-IDEN.

[4] X. Wu, Y. Wu, L. He, L. Wu, X. Wang, Z. Liu, Effects of the intestinal microbial metabolite butyrate on the development of colorectal cancer, J. Cancer 9 (14) (2018) 2510–2517, https://doi.org/10.7150/jca.25324.

[5] M. Song, A.T. Chan, Diet, Gut microbiota, and colorectal cancer prevention: a review of potential mechanisms and promising targets for future research, Curr. Colorectal Cancer Rep. 13 (6) (2017) 429–439, https://doi.org/10.1007/s11888-017-0389-y.

[6] L.L. De Silanes, N. Olmo, J. Turnay, G. González De Buitrago, P. Pérez-Ramos, A. Guzmán-Aránguez, M. García-Díez, E. Lecona, M. Gorospe, M.A. Lizarbe, Acquisition of resistance to butyrate enhances survival after stress and induces malignancy of human colon carcinoma cells, Cancer Res. 64 (13) (2004) 4593–4600, https://doi.org/10.1158/0008-5472.CAN-04-0711.

[7] J.M. Mariadason, A. Velcich, A.J. Wilson, L.H. Augenlicht, P.R. Gibson, Resistance to butyrate-induced cell differentiation and apoptosis during spontaneous Caco-2 cell differentiation, Gastroenterology 120 (4) (2001) 889–899, https://doi.org/10.1053/gast.2001.22472.

[8] H.R. Kang, H.G. Choi, C.K. Jeon, S.J. Lim, S.H. Kim, Butyrate-mediated acquisition of chemoresistance by human colon cancer cells, Oncol. Rep. 36 (2) (2016) 1119–1126, https://doi.org/10.3892/or.2016.4838.

[9] H.Y. Yoo, S.Y. Park, S.-Y. Chang, S.H. Kim, Regulation of butyrate-induced resistance through AMPK signaling pathway in human colon cancer cells, Biomedicines Vol. 9 (2021), https://doi.org/10.3390/biomedicines9111604.

[10] J. Hanprasertpong, I. Jiamset, A. Geater, T. Peerawong, W. Hemman, S. Kornsilp, The Effect of metformin on oncological outcomes in patients with cervical cancer with type 2 diabetes mellitus, Int. J. Gynecol. Cancer 27 (1) (2017) 131–137, https://doi.org/10.1097/IGC.0000000000000855.

[11] Y.-L. Tang, L.-Y. Zhu, Y. Li, J. Yu, J. Wang, X.-X. Zeng, K.-X. Hu, J.-Y. Liu, J.-X. Xu, Metformin use is associated with reduced incidence and improved survival of endometrial cancer: a meta-analysis, Biomed. Res. Int. 2017 (2017) 1–9, https://doi.org/10.1155/2017/5905384.

[12] A. Fatehi Hassanabad, K.T. MacQueen, Molecular mechanisms underlining the role of metformin as a therapeutic agent in lung cancer, Cell Oncol. 44 (1) (2021) 1–18, https://doi.org/10.1007/s13402-020-00570-0.

[13] P. Nangia-Makker, Y. Yu, A. Vasudevan, L. Farhana, S.G. Rajendra, E. Levi, A.P. N. Majumdar, Metformin: a potential therapeutic agent for recurrent colon cancer, PLoS One 9 (1) (2014) 1–10, https://doi.org/10.1371/journal.pone.0084369.

[14] B. Viollet, B. Guigas, N. Sanz Garcia, J. Leclerc, M. Foretz, F. Andreelli, Cellular and molecular mechanisms of metformin: an overview, Clin. Sci. 122 (6) (2012) 253–270. (https://www.ncbi.nlm.nih.gov/pubmed/22117616).

[15] T.E. LaMoia, G.I. Shulman, Cellular and molecular mechanisms of metformin action, Endocr. Rev. 42 (1) (2021) 77–96, https://doi.org/10.1210/endrev/bnaa023.

[16] P.C. Marinello, C. Panis, T.N.X. Silva, R. Binato, E. Abdelhay, J.A. Rodrigues, A. L. Mencalha, N.M.D. Lopes, R.C. Luiz, R. Cecchini, A.L. Cecchini, Metformin prevention of doxorubicin resistance in MCF-7 and MDA-MB-231 involves oxidative stress generation and modulation of cell adaptation genes, Sci. Rep. 9 (1) (2019) 1–11, https://doi.org/10.1038/s41598-019-42357-w.

[17] M. Vinci, S. Gowan, F. Boxall, L. Patterson, M. Zimmermann, W. Court, C. Lomas, M. Mendiola, D. Hardisson, S.A. Eccles, Advances in establishment and analysis of three-dimensional tumor spheroid-based functional assays for target validation and drug evaluation, BMC Biol. (2012), https://doi.org/10.1186/1741-7007-10-29.

[18] S. Breslin, L. O'Driscoll, Three-dimensional cell culture: the missing link in drug discovery, Drug Discov. Today 18 (5–6) (2013) 240–249, https://doi.org/10.1016/j.drudis.2012.10.003.

[19] S. Lee, J. Hwa, H. Ki, J. Seok, B. Kim, J. Lee, J. Yun, G. Suk, M. Inoue, G. Choi, Colorectal cancer-derived tumor spheroids retain the characteristics of original tumors, Cancer Lett. (2015), https://doi.org/j.canlet.2015.06.024.

[20] J. Koch, D. Mönch, A. Maaß, C. Gromoll, T. Hehr, T. Leibold, H.J. Schlitt, M.-H. Dahlke, P. Renner, Three dimensional cultivation increases chemo- and radioresistance of colorectal cancer cell lines, PLoS One 16 (1) (2021), e0244513. (https://europepmc.org/articles/PMC7781370).

[21] Y. Imamura, T. Mukohara, Y. Shimono, Y. Funakoshi, N. Chayahara, M. Toyoda, N. Kiyota, S. Takao, S. Kono, T. Nakatsura, H. Minami, Comparison of 2D- and 3D-culture models as drug-testing platforms in breast cancer, Oncol. Rep. 33 (4) (2015) 1837–1843, https://doi.org/10.3892/or.2015.3767.

[22] H. Karlsson, M. Fryknäs, R. Larsson, P. Nygren, Loss of cancer drug activity in colon cancer HCT-116 cells during spheroid formation in a new 3-D spheroid cell culture system, Exp. Cell Res. 318 (13) (2012) 1577–1585. (https://www.sciencedirect.com/science/article/pii/S0014482712001620).

[23] K. Okazaki, Y. Nakayama, K. Shibao, K. Hirata, T. Sako, N. Nagata, Y. Kuroda, H. Itoh, Establishment of a human colon cancer cell line (PMF-ko14) displaying highly metastatic activity, Int. J. Oncol. 17 (1) (2000) 39–45, https://doi.org/10.3892/ijo.17.1.39.

[24] S. Hirano, Western Blot Analysis. Nanotoxicity, Springer, 2012, pp. 87–97, https://doi.org/10.1007/978-1-62703-002-1.6.

[25] M. Vinci, C. Box, M. Zimmermann, S.A. Eccles, Tumor Spheroid-based Migration Assays for Evaluation of Therapeutic Agents. Target identification and validation in drug discovery, Springer, 2013, pp. 253–266, https://doi.org/10.1007/978-1-62703-311-4_16.

[26] H.Y. Yoo, S.Y. Park, S.-Y. Chang, S.H. Kim, Regulation of butyrate-induced resistance through AMPK signaling pathway in human colon cancer cells, Biomedicines 9 (11) (2021). (https://www.mdpi.com/2227-9059/9/11/1604).

[27] Y. Okada, T. Kimura, T. Nakagawa, K. Okamoto, A. Fukuya, T. Goji, S. Fujimoto, M. Sogabe, H. Miyamoto, N. Muguruma, EGFR downregulation after anti-EGFR therapy predicts the antitumor effect in colorectal cancer, Mol. Cancer Res. 15 (10) (2017) 1445–1454, https://doi.org/10.1158/1541-7786.MCR-16-0383.

[28] N. Olmo, J. Turnay, P. Perez-Ramos, E. Lecona, J.I. Barrasa, I.L. de Silanes, M. A. Lizarbe, In vitro models for the study of the effect of butyrate on human colon adenocarcinoma cells, Toxicol. Vitr. 21 (2) (2007) 262–270, https://doi.org/10.1016/j.tiv.2006.09.011.

[29] F.M. Robertson, M.A. Ogasawara, Z. Ye, K. Chu, R. Pickei, B.G. Debeb, W. A. Woodward, W.N. Hittelman, M. Cristofanilli, S.H. Barsky, Imaging and analysis of 3D tumor spheroids enriched for a cancer stem cell phenotype, J. Biomol. Screen 15 (7) (2010) 820–829, https://doi.org/10.1177/1087057110376541.

[30] E. Gheytanchi, M. Naseri, F. Karimi-Busheri, F. Atyabi, E.S. Mirsharif, M. Bozorgmehr, R. Ghods, Z. Madjd, Morphological and molecular characteristics of spheroid formation in HT-29 and Caco-2 colorectal cancer cell lines, Cancer Cell Int. 21 (1) (2021) 1–16, https://doi.org/10.1186/s12935-021-01898-9.

[31] N. Olmo, J. Turnay, E. Lecona, M. García-Díez, B. Llorente, A. Santiago-Gómez, M. A. Lizarbe, Acquisition of resistance to butyrate induces resistance to luminal components and other types of stress in human colon adenocarcinoma cells, Toxicol. Vitr. 21 (2) (2007) 254–261, https://doi.org/10.1016/j.tiv.2006.09.010.

[32] G.A. Cresci, M. Thangaraju, J.D. Mellinger, K. Liu, V. Ganapathy, Colonic gene expression in conventional and germ-free mice with a focus on the butyrate receptor GPR109A and the butyrate transporter SLC5A8, J. Gastrointest. Surg. 14 (3) (2010) 449–461, https://doi.org/10.1007/s11605-009-1045-x.

[33] M.B. Duz, O.F. Karatas, Expression profile of stem cell markers and ABC transporters in 5-fluorouracil resistant Hep-2 cells, Mol. Biol. Rep. 47 (7) (2020) 5431–5438, https://doi.org/10.1007/s11033-020-05633-x.

[34] J.P. Gillet, T. Efferth, D. Daniel Steinbach, J. Hamels, F. De Longueville, V. Bertholet, J. Remacle, Microarray-based detection of multidrug resistance in human tumor cells by expression profiling of ATP-binding cassette transporter genes, Cancer Res. 64 (2004) 8987–8993, https://doi.org/10.1158/0008-5472.CAN-04-1978.

[35] C.F. Thorn, C. Oshiro, S. Marsh, T. Hernandez-Boussard, H. McLeod, T.E. Klein, R. B. Altman, Doxorubicin pathways, Pharm. Genom. 21 (7) (2011) 440–446.

[36] M.B. Duz, O.F. Karatas, Differential expression of ABCB1, ABCG2, and KLF4 as putative indicators for paclitaxel resistance in human epithelial type 2 cells, Mol. Biol. Rep. 48 (2) (2021) 1393–1400.

[37] M.N. Song, P.G. Moon, J.E. Lee, M. Na, W. Kang, Y.S. Chae, J.Y. Park, H. Park, M. C. Baek, Proteomic analysis of breast cancer tissues to identify biomarker candidates by gel-assisted digestion and label-free quantification methods using LC-MS/MS, Arch. Pharm. Res. 35 (10) (2012) 1839–1847, https://doi.org/10.1097/FPC.0b013e32833ffb56.

[38] H.T. Kwan, D.W. Chan, P.C.H. Cai, C.S.L. Mak, M.M.H. Yung, T.H.Y. Leung, O.G. W. Wong, A.N.Y. Cheung, H.Y.S. Ngan, AMPK activators suppress cervical cancer cell growth through inhibition of DVL3 mediated Wnt/β-catenin signaling activity, PLoS One 8 (1) (2013) 1–10, https://doi.org/10.1371/journal.pone.0053597.

[39] I.N. Alimova, B. Liu, Z. Fan, S.M. Edgerton, T. Dillon, S.E. Lind, A.D. Thor, Metformin inhibits breast cancer cell growth, colony formation and induces cell cycle arrest in vitro, Cell Cycle 8 (6) (2009) 909–915, https://doi.org/10.4161/cc.8.6.7933.

[40] S.J. Koh, J.M. Kim, I.K. Kim, S.H. Ko, J.S. Kim, Anti-inflammatory mechanism of metformin and its effects in intestinal inflammation and colitis-associated colon cancer, J. Gastroenterol. Hepatol. 29 (3) (2014) 502–510, https://doi.org/10.1111/jgh.12435.

[41] A. DeCensi, M. Puntoni, P. Goodwin, M. Cazzaniga, A. Gennari, B. Bonanni, S. Gandini, Metformin and cancer risk in diabetic patients: a systematic review and meta-analysis, Cancer Prev. Res. 3 (11) (2010) 1451–1461, https://doi.org/10.1158/1940-6207.CAPR-10-0157.

[42] S. Gandini, M. Puntoni, B.M. Heckman-Stoddard, B.K. Dunn, L. Ford, A. DeCensi, E. Szabo, Metformin and cancer risk and mortality: a systematic review and meta-analysis taking into account biases and confounders, Cancer Prev. Res. 7 (9) (2014) 867–885, https://doi.org/10.1158/1940-6207.CAPR-13-0424.

[43] R. Würth, A. Pattarozzi, M. Gatti, A. Bajetto, A. Corsaro, A. Parodi, R. Sirito, M. Massollo, C. Marini, G. Zona, D. Fenoglio, G. Sambuceti, G. Filaci, A. Daga, F. Barbieri, T. Florio, Metformin selectively affects human glioblastoma tumor-initiating cell viability, Cell Cycle 12 (1) (2013) 145–156, https://doi.org/10.4161/cc.23050.

[44] H.A. Hirsch, D. Iliopoulos, K. Struhl, Metformin inhibits the inflammatory response associated with cellular transformation and cancer stem cell growth, Proc. Natl. Acad. Sci. 110 (3) (2013) 972–977. (https://www.pnas.org/content/110/3/972).

[45] J. He, K. Wang, N. Zheng, Y. Qiu, G. Xie, M. Su, W. Jia, H. Li, Metformin suppressed the proliferation of LoVo cells and induced a time-dependent metabolic and transcriptional alteration, Sci. Rep. 5 (October) (2015) 1–16, https://doi.org/10.1038/srep17423.

[46] B. Bao, Z. Wang, S. Ali, A. Ahmad, A.S. Azmi, S.H. Sarkar, S. Banerjee, D. Kong, Y. Li, S. Thakur, F.H. Sarkar, Metformin inhibits cell proliferation, migration and invasion by attenuating CSC function mediated by deregulating miRNAs in pancreatic cancer cells, Cancer Prev. Res. 5 (3) (2012) 355–364, https://doi.org/10.1158/1940-6207.CAPR-11-0299.

[47] C. Schexnayder, K. Broussard, D. Onuaguluchi, A. Poché, M. Ismail, L. McAtee, S. Llopis, A. Keizerweerd, H. McFerrin, C. Williams, Metformin inhibits migration and invasion by suppressing ROS production and COX2 expression in MDA-MB-231 breast cancer cells, Int. J. Mol. Sci. 19 (11) (2018) 3692, https://doi.org/10.3390/ijms19113692.

[48] C. Harsha, K. Banik, H.L. Ang, S. Girisa, R. Vikkurthi, D. Parama, V. Rana, B. Shabnam, E. Khatoon, A.P. Kumar, A.B. Kunnumakkara, Targeting AKT/mTOR in oral cancer: mechanisms and advances in clinical trials, Int. J. Mol. Sci. Vol. 21 (2020), https://doi.org/10.3390/ijms21093285.

[49] Y.-H. Chen, P.-H. Wang, P.-N. Chen, S.-F. Yang, Y.-H. Hsiao, Molecular and cellular mechanisms of metformin in cervical cancer, Cancers Vol. 13 (2021), https://doi.org/10.3390/cancers13112545.

[50] F. Weiss, D. Lauffenburger, P. Friedl, Towards targeting of shared mechanisms of cancer metastasis and therapy resistance, Nat. Rev. Cancer 22 (3) (2022) 157–173, https://doi.org/10.1038/s41568-021-00427-0.

[51] N.H. Ha, F. Faraji, K.W. Hunter, Mechanisms of metastasis, Cancer Target Drug Deliv. Elus. Dream. 9781461478 (2013) 435–458.

[52] Li K., Chen L., Lin Z., Zhu J., Fang Y., Du J., Shen B., Wu K., Liu Y., 2020. Role of the AMPK/ACC Signaling Pathway in TRPP2-Mediated Head and Neck Cancer Cell Proliferation. Saponaro G., editor. Biomed Res Int. 2020;2020:4375075. https://doi.org/10.1155/2020/4375075.

[53] J.R. Testa, A. Bellacosa, AKT plays a central role in tumorigenesis, Proc. Natl. Acad. Sci. 98 (20) (2001) 10983–10985. (https://pubmed.ncbi.nlm.nih.gov/11572954).

[54] U.R. Rapp, U. Rennefahrt, J. Troppmair, Bcl-2 proteins: master switches at the intersection of death signaling and the survival control by Raf kinases, Biochim. Biophys. Acta - Mol. Cell Res. 1644 (2) (2004) 149–158. (https://www.sciencedirect.com/science/article/pii/S0167488903001812).
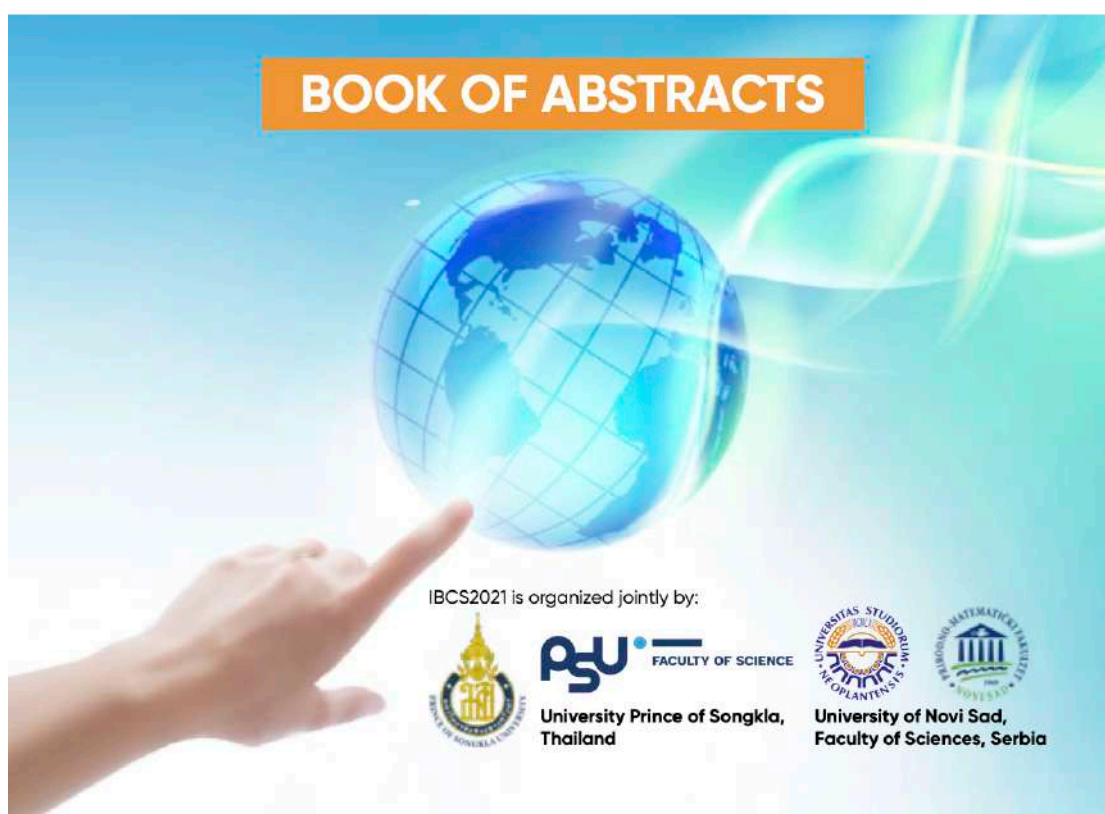
Oral presentation

Effect of Metformin on AMPK/AKT/MTOR Pathway Against Butyrate-Resistant Colorectal Cancer Spheroid Cells.

antimicrobial activity against *S. aureus* with MIC values of 0.03, 0.06, and 0.06 mg/mL, respectively. On *P. aeruginosa* PAO1, defense secretions did not show antimicrobial activity even at the highest tested concentration of 1 mg/mL for MUN while for PHU and CBO the MIC was 1 mg/mL, which is most likely due to the high resistance of this bacterial strain. The antibiofilm effect was observed in all tested defense secretions and was more pronounced against *S. aureus* than against *P. aeruginosa* PAO1. The strongest biofilm inhibition of *S. aureus* was at the highest tested concentrations (2 × MIC) with percentages of inhibition of CBO: 88.6%, PHU: 73.7%, and MUN: 67.2%. Degradation of already formed *S. aureus* biofilm was shown at lower tested defensive secretions concentrations (MIC/4), about 40% of biofilm degradation for MUN and PHU and about 30% for CBO. The strongest inhibition of *P. aeruginosa* PAO1 biofilm formation was observed at the highest tested concentrations of defensive secretions, 1 and 0.5 mg/mL for PHU (82 and 54%), and CBO (64.3 and 38.5%) while MUN had the strongest activity at the lowest tested concentration of 0.06 mg/mL (34.3%). All examined defense secretions had similar degradation activity of *P. aeruginosa* PAO1 biofilm with stronger activity at lower tested concentrations (about 30%). Defensive secretions of MUN and PHU extracted in DMSO solvent showed a stronger antibiofilm effect compared to the same ethanol extracts.

CONCLUSIONS:

The defense secretions of MBO, PHU, and CBO show a good basis for further investigations of their use as antimicrobial agents, especially against *S. aureus*.

T3-P-20 Effect of metformin on AMPK/Akt/mTOR pathway against butyrate-resistant colorectal cancer spheroid cells

Kesara Nittayaboon, Surasak Sangkhathat, Raphatphorn Navakanitworakul[73]

KEYWORDS: Metformin; Butyrate-resistant cells; Colorectal cancer; Spheroid cells.

INTRODUCTION: Metformin, the anti-diabetic drug, has been studied as anti-cancer drug in various types of cancer, such as cervical, breast, prostate, and colorectal cancer. The meta-analysis study has been shown that metformin is associated with decreasing cancer incidence and mortality rate. However, there is no study on the effect of metformin on butyrate-resistant colorectal cancer cells. Normally, butyrate is an anti-cancer agent produced by colonic microbiota. However, the microbiota study reveals that *F. nucleatum*, a butyrate producing and inflammatory stimulator bacteria, was increased in colorectal cancer patients. The resistant-to-butyrate cell show a chemotherapy resistant phenotype which related to treatment failure and cancer recurrence.

OBJECTIVES: The aim of this study was evaluated the effect of metformin on butyrate-resistant colorectal cancer spheroid cells.

METHOD / DESIGN: HCT-116, and PMFko-14 colorectal cancer cells were induced with butyrate reagent at the final concentration of 3.2 mM. The resistant properties were determined by cell viability at IC50 of parental and resistant cells. Influx and efflux transporters were evaluated by qRT-PCR. The spheroids of parental and resistant cell were generated, then the effect of metformin was studied. Live/dead and caspase assays were used to examine the inhibitory effect of metformin on spheroid cells. Finally, molecular mechanisms of metformin were investigated by Immunoblotting analysis.

73   Department of Biomedical Sciences and Biomedical Engineering, Faculty of Medicine, Prince of Songkla University, Hat Yai, Songkhla, Thailand, 90110.
Corresponding author: n_ruxapon@yahoo.com

RESULTS: After treatment of butyrate, butyrate-resistant (BR) cells showed higher cell viability than parental (PT) cells. The influx and efflux transporter genes were increased in BR cells. Both PT and BR cells could form spherical shape in a Poly-HE-MA coating plate. Metformin shows an inhibition effect on spheroid cells in a dose-dependent manner by increase of dead cells and caspase activity. The results indicated that metformin could induce apoptosis of spheroid cells. Finally, metformin's actions on BR cells were induced through AMPK/Akt phosphorylation, resulting in mTOR and ACC inhibition leading to apoptosis.

CONCLUSIONS: Our findings can demonstrate that metformin showed a potential therapeutic utility by apoptotic induction on BR spheroid cells. This information may be used as alternative approach in colorectal cancer therapy improvement.

T3-P-21 Evaluating the potential effect of ethanol treatment on whey proteins digestibility

Charikleia Kyrkou, Konstantina Tentzidou, Asterios Stamkopoulos, Foteini Tsakoumaki, Garyfalia Charitou, Thomas Moschakis, Costas G. Biliaderis, Alexandra-Maria Michaelidou[74]

KEYWORDS: *In vitro* digestion, Whey protein isolates, Ethanol treatment, SDS-PAGE

INTRODUCTION:
Whey proteins (WP), although exhibiting high nutritional and functional attributes, demonstrate significant resistance to hydrolysis phenomena due to their globular structure (Sanchón et al., 2018; Hussein et al., 2020). Studies have indicated that, in comparison with the traditional heat treatment, ethanol can irreversibly and more effectively denature proteins and change their secondary structures (Nikolaidis and Moschakis 2018; Feng et al., 2021). However, to the best of our knowledge, data regarding the effect of ethanol on WP digestibility is scarce.

OBJECTIVES:
This study focuses on the comparison of the degradation pattern and evaluation of differences in digestibility of whey proteins under four different conditions, namely: in native WP isolates aqueous solution (N-WPI), in water-ethanol WP solutions with different ethanol concentrations (i.e., 10% and 50% w/v, E-10 WPI, and E-50 WPI, respectively) and in WP aqueous solution obtained after heating at 90°C for 10 min (H-WPI).

METHOD / DESIGN:
The protein content was measured with the Kjeldahl method according to ISO 8968-3:2007/IDF 20-3: 2007 (ISO 8968-3, 2007). To simulate the physiological digestion process (i.e., the oral (OP), gastric (GP), and intestinal phases (IP)), all substrates were subjected to the INFOGEST static *in vitro* digestion protocol (Brodkorb et al., 2019). The enzyme activities (pepsin and trypsin) were quantified prior to the implementation of the INFOGEST protocol as proposed by Minekus et al., (2014). A discontinuous polyacrylamide gel electrophoresis (disc-PAGE) was initially applied on the samples obtained from the *in vitro* digestion (4 treatments x 3 phases) (Andrews,1983). Furthermore, Sodium Dodecyl Sulphate PAGE (SDS–PAGE) was carried out following the method of Laemmli (1970) with some modifications. All experiments were conducted in triplicates and on a protein-equivalent basis.

74 Department of Food Science and Technology, School of Agriculture, Faculty of Agriculture, Forestry and Natural Environment, Aristotle University of Thessaloniki, Thessaloniki 541 24, Greece. Corresponding author: amichail@agro.auth.gr

VITAE

Name   Miss Kesara Nittayaboon

Student ID   6110330017

Educational Attainment

Degree	Name of Institution	Year of Graduation
Bachelor of Science (Biotechnology)	Prince of Songkla University	2012
Master of Science (Biomedical Sciences)	Prince of Songkla University	2016

Scholarship Awards during Enrolment

1. Postgraduate Scholarship from Faculty of Medicine, Prince of Songkla University

List of Publication and Proceeding

1. **Nittayaboon K**, Sangkhathat S, and Navakanitworakul R. Effect of Metformin on AMPK/AKT/MTOR Pathway Against Butyrate-Resistant Colorectal Cancer Spheroid Cells. IBSC2021. November 25-26, 2021. Novi Sad, Serbia.

2. **Nittayaboon K**, Leetanaporn K, Sangkhathat S, Roytrakul S, Navakanitworakul R. Characterization of Butyrate-Resistant Colorectal Cancer Cell Lines and the Cytotoxicity of Anticancer Drugs against These Cells., BioMed Res. Int. 2022.

3. **Nittayaboon K**, Leetanaporn K, Sangkhathat S, Roytrakul S, Navakanitworakul R. Cytotoxic effect of metformin on butyrate-resistant PMF-K014 colorectal cancer spheroid cells. Biomed. Pharmacother. 2022(151).

4. Gottschlich A, Nuntadusit T, Zarins KR, Hada M, Chooson N, Bilheem S, et al. Barriers to cervical cancer screening and acceptability of HPV self-

testing: A cross-sectional comparison between ethnic groups in southern Thailand. BMJ Open. 2019;9(11).

5. Chothiphirat A, **Nittayaboon K**, Kanokwiroon K, Srisawat T, Navakanitworakul R. Anticancer potential of fruit extracts from vatica diospyroides symington type SS and their effect on program cell death of cervical cancer cell lines. The Scientific World Journal. 2019;2019:1–9.